Calhoun
Institutional Archive of the Naval Postgraduate School

Calhoun: The NPS Institutional Archive

DSpace Repository

Theses and Dissertations | 1. Thesis and Dissertation Collection, all items

1974-06

Projectile thrust-drag optimization with external burning

Smithey, William John Henry

Monterey, California. Naval Postgraduate School

http://hdl.handle.net/10945/17185

This publication is a work of the U.S. Government as defined in Title 17, United States Code, Section 101. Copyright protection is not available for this work in the United States.

Downloaded from NPS Archive: Calhoun

http://www.nps.edu/library

Calhoun is the Naval Postgraduate School's public access digital repository for research materials and institutional publications created by the NPS community. Calhoun is named for Professor of Mathematics Guy K. Calhoun, NPS's first appointed -- and published -- scholarly author.

Dudley Knox Library / Naval Postgraduate School
411 Dyer Road / 1 University Circle
Monterey, California USA 93943

PROJECTILE THRUST-DRAG OPTIMIZATION WITH EXTERNAL BURNING

William John Henry Smithey

DUDLEY KNOX LIBRARY
NAVAL POSTGRADUATE SCHOOL
MONTEREY, CALIFORNIA 93940

NAVAL POSTGRADUATE SCHOOL
Monterey, California

THESIS

PROJECTILE THRUST-DRAG OPTIMIZATION
WITH EXTERNAL BURNING

by

William John Henry Smithey

June 1974

Thesis Advisor: Allen E. Fuhs

Approved for public release; distribution unlimited.

T 162 S64

REPORT DOCUMENTATION PAGE		READ INSTRUCTIONS BEFORE COMPLETING FORM
1. REPORT NUMBER	2. GOVT ACCESSION NO.	3. RECIPIENT'S CATALOG NUMBER
4. TITLE (and Subtitle) Projectile Thrust - Drag Optimization With External Burning		5. TYPE OF REPORT & PERIOD COVERED Doctor's Thesis; June 1974 6. PERFORMING ORG. REPORT NUMBER
7. AUTHOR(s) William John Henry Smithey		8. CONTRACT OR GRANT NUMBER(s)
9. PERFORMING ORGANIZATION NAME AND ADDRESS Naval Postgraduate School Monterey, California 93940		10. PROGRAM ELEMENT, PROJECT, TASK AREA & WORK UNIT NUMBERS
11. CONTROLLING OFFICE NAME AND ADDRESS Naval Postgraduate School Monterey, California 93940		12. REPORT DATE June 1974 13. NUMBER OF PAGES 130
14. MONITORING AGENCY NAME & ADDRESS(if different from Controlling Office) Naval Postgraduate School Monterey, California 93940		15. SECURITY CLASS. (of this report) UNCLASSIFIED 15a. DECLASSIFICATION/DOWNGRADING SCHEDULE

16. DISTRIBUTION STATEMENT (of this Report)

Approved for public release; distribution unlimited.

17. DISTRIBUTION STATEMENT (of the abstract entered in Block 20, if different from Report)

18. SUPPLEMENTARY NOTES

19. KEY WORDS (Continue on reverse side if necessary and identify by block number)

Base Drag Reduction
Axisymmetric Heat Addition
External Heat Addition
Method of Characteristics With Heat Addition

20. ABSTRACT (Continue on reverse side if necessary and identify by block number)

External burning increases base pressure. The characteristic and linearized equations with heat addition are discussed, and the condition for maintaining irrotationality with heat addition is derived. A transition model, which extends the Crocco-Lees base flow model, and a spin model are discussed. Computed results are compared with experiment. The optimum location for supersonic external burning is given.

Block #19 continued

Base Flow
Base Drag

Projectile Thrust-Drag Optimization

With External Burning

by

William John Henry Smithey
Commander, United States Navy
B.M.E., University of Virginia, 1957
B.S., Naval Postgraduate School, 1963
A.E., California Institute of Technology, 1964

Submitted in partial fulfillment of the
requirements for the degree of

DOCTOR OF PHILOSOPHY

from the
NAVAL POSTGRADUATE SCHOOL
June 1974

MONTEREY, CALIFORNIA 93940

ABSTRACT

External burning increases base pressure. The characteristic and linearized equations with heat addition are discussed, and the condition for maintaining irrotationality with heat addition is derived. A transition model, which extends the Crocco-Lees base flow model, and a spin model are discussed. Computed results are compared with experiment. The optimum location for supersonic external burning is given.

TABLE OF CONTENTS

I. INTRODUCTION..... 12

II. THEORY..... 18

III. EXPERIMENTAL INVESTIGATION..... 37

IV. NUMERICAL INVESTIGATION..... 48

V. DISCUSSION OF RESULTS..... 54

VI. CONCLUSIONS..... 73

APPENDIX A: DERIVATION OF THE CHARACTERISTIC EQUATIONS WITH HEAT ADDITION..... 75

APPENDIX B: DERIVATION OF CONDITION FOR IRROTATIONALITY WITH HEAT ADDITION..... 79

APPENDIX C: BRIEF DEVELOPMENT OF CROCCO-LEES BASE FLOW FORMULATION..... 83

APPENDIX D: CALCULATION OF BOUNDARY LAYER MASS FLUX AT THE BASE..... 87

APPENDIX E: MASS FLUX CALCULATION ALONG THE SHEAR LAYER..... 90

APPENDIX F: CALCULATION OF BOUNDARY LAYER THICKNESS AND MIXING COEFFICIENT..... 92

APPENDIX G: DERIVATION OF LINEARIZED STEADY FLOW EQUATION WITH HEAT ADDITION..... 96

APPENDIX H: DETERMINATION OF THE MACH ANGLE..... 98

APPENDIX I: SPINNING CYLINDER DESIGN..... 101

APPENDIX J: COMPUTER PROGRAM..... 103

COMPUTER PROGRAM..... 107

LIST OF REFERENCES..... 124

INITIAL DISTRIBUTION LIST..... 128

LIST OF TABLES

I. Base Pressure Ratio and Specific Impulse with Simulated Heat Addition..... 46

II. Comparison of Calculated Base Pressure Ratio with External Heat Addition, Two Dimensional Planar Flow and Mach Number of 2.3..... 60

LIST OF FIGURES

1. External Burning Projectile..... 13

2. Base Pressure Ratio and Flow Angle..... 15

3. Natural and Characteristic Coordinate Systems..... 19

4. Conceptual Diagram Depicting Shear Layer Pressures, P_{SL}, Which Straddle the Critical Point..... 26

5. Transition Model..... 27

6. Transition of Shear Layer Mixing Coefficient..... 31

7. Momentum Control Volume Depicting Shear Layer Mixing..... 32

8. Sensitivity of Base Pressure Ratio..... 34

9. Computed Values of p_b/p_∞ vs. Reynolds Number, Mach 2.0, No Heat Addition..... 35

10. Heat Zone Simulation with Nozzle Wall..... 38

11. Photograph of Free Jet Experimental Facility..... 39

12. Schematic Diagram of Free Jet Experimental Facility..... 40

13. Coaxial Epoxy Nozzle. Insert Showing Spacers..... 42

14. Schlieren Photographs at Mach 2.0 Showing Uniform Flow and Flow with Compression..... 44

15. Characteristic Mesh..... 49

16. Integration in the F - w_e Plane..... 51

17. Computed Values of p_b/p_∞, Transition Points and Critical Point..... 55

18. Experimental Values of p_b/p_∞ vs. Reynolds Number Without Heat Addition, from Ref. 32..... 56

19. Experimental Values of p_b/p_∞ vs. Reynolds Number Without Heat Addition..... 57

20. Comparison of Experimental and Computed Values of Base Pressure Ratio vs. Reynolds Number at Mach 2.0 Without and With Simulated Heat Addition..... 62

21. Comparison of Experimental [Ref. 26] and Computed Values of Base Pressure Ratio vs. Reynolds Number With Spin..... 64

22. Computed Values of Base Pressure Ratio at a Mach Number of 2.0 With External Burning..... 66

23. Comparison of Calculated Base Flow With And Without Heat Addition at Mach 2.0..... 68

24. Schematic Diagram of Resulting Base Flow When an External Shock Wave Impinges on the Shear Layer... 71

1I. Disassembled View of Spinning Cylinder.....102

1J. Simplified Flow Diagram for External Burning Assisted Projectile (EBAP) Computer Program.....105

NOTATION

English

a	speed of sound, feet/second
C_f	skin friction coefficient, dimensionless
c_p	specific heat at constant pressure, foot-pounds/slug-degree Rankine
F	dimensionless ratio of various boundary layer thicknesses
h	specific enthalpy, foot-pounds/slug
k	shear layer mixing coefficient, dimensionless
L	body length, feet
M	Mach number, dimensionless
$\bar{m}$	mass flux, slugs/second-square foot
n	normal coordinate, feet; also velocity profile integer
p	static pressure, pounds/square-foot
Q	heat added per unit mass, foot-pounds/slug; also dimensionless heat addition rate of Eqn. (12)
q	heat addition rate, foot-pounds/slug-second
R	universal gas constant, foot-pounds/slug-degree Rankine
Re	Reynolds number, dimensionless
r	radial coordinate, feet
S	specific entropy, foot-pounds/slug-degree Rankine
s	streamline coordinate, feet
T	static temperature, degrees Rankine
$\bar{U}$	velocity vector, feet/second
U,u	speed, feet/second

w speed along streamline, feet/second; also nondimensionalized by stagnation speed of sound, a_s

w/r dimensionless heat zone length

z/r dimensionless position on body or shear layer, measured from base

Greek

α flow field type, dimensionless

β $(M^2 - 1)^{\frac{1}{2}}$

γ ratio of specific heats, dimensionless

δ boundary layer thickness, feet

δ^* boundary layer displacement thickness, feet

δ^{**} boundary layer momentum thickness, feet

ε dimensionless small quantity, $0 < \varepsilon << 1$

η left running characteristic coordinate, feet; also dimensionless heating parameter of Ref. 7

θ flow angle, radians

κ dimensionless ratio of average internal to external speed

μ Mach angle, radians

ν Prandtl-Meyer angle, radians

ξ right running characteristic coordinate, feet

ρ density, slugs/cubic foot

ϕ perturbation velocity potential, square feet/second

$\overline{\Omega}$ curl $\overline{U}$, radians/second

ω angular velocity, radians/second

Superscripts

$( )'$ dimensionless perturbation quantity

Subscripts

1	average condition
∞	freestream condition
b	base condition
e	condition at edge of shear layer
L	laminar
o,s	total or stagnation condition
T	turbulent
tr	laminar transition point
trt	turbulent transition point

I. INTRODUCTION

Projectiles in supersonic flight experience drag. One source of drag is due to the pressure acting on the base (rear surface) of the projectile, which, under normal circumstances, is below ambient pressure. The base drag force is equal to the base surface area normal to the direction of flight multiplied by the mean difference between the ambient and base pressures.

External burning has been studied by many authors [Ref. 1] to determine its ability to reduce the drag of a body or even to produce thrust. The basic objective of external burning in a supersonic flow, Fig. 1, is to create compression waves which impinge on the base flow region and increase the static pressure within the recirculation zone, thereby increasing the pressure acting on the base of the body to reduce base drag or produce thrust.

Other methods of reducing base drag or producing thrust are available. The rocket assisted projectile provides thrust from combustion of self-contained fuel and oxidizer. With external burning, additional fuel can replace some of this oxidizer since oxygen is used from the atmosphere for burning the excess fuel. The ram jet assisted projectile delivers excellent performance but does require air inlets and has additional hardware costs. The method of base burning offers advantages similar to external burning, but has not proven its ability to create thrust.

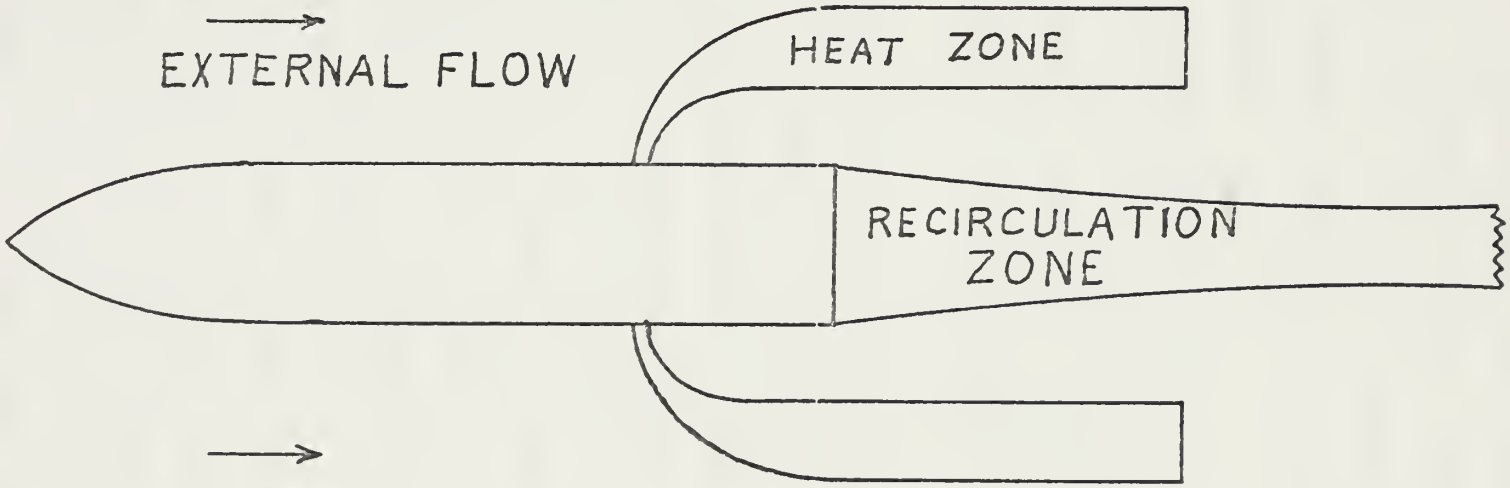

Figure 1. External Burning Projectile

The external burning assisted projectile provides a 50% increase in range when fuel rich propellant is substituted for one third of the conventional projectile payload. In addition to an increase in range, external burning can be used to decrease the projectile flight time to the target, increase its kinetic energy at the target and provide a flatter trajectory.

The base pressure ratio, p_b/p_∞, is a measure of the effectiveness of the external burning process. As shown in Fig. 2, the behavior and effect of this ratio can be related to the flow angle, θ, of the boundary layer streamline at the base.

For purposes of analysis, the external burning process may be described thermodynamically as a heat addition term in the energy equation, bearing in mind that numerous other factors must be considered with actual combustion, such as the effect of pressure on combustion rate. The linearized problem involving two dimensional planar uniform flow with unit heat addition has been solved by Tsienand Beilock in closed form [Ref. 2,3]. In supersonic flow it was shown that a pressure perturbation, due to the heat source, is transmitted along a characteristic. Further study of the linearized flow equations by Rues has shown that there is an equivalence between heat, force and mass sources [Ref. 4]. These unit sources were given an integral formulation by Fuhs to determine the flow field perturbation resulting from a source zone [Ref. 5]. It is the study of these linearized

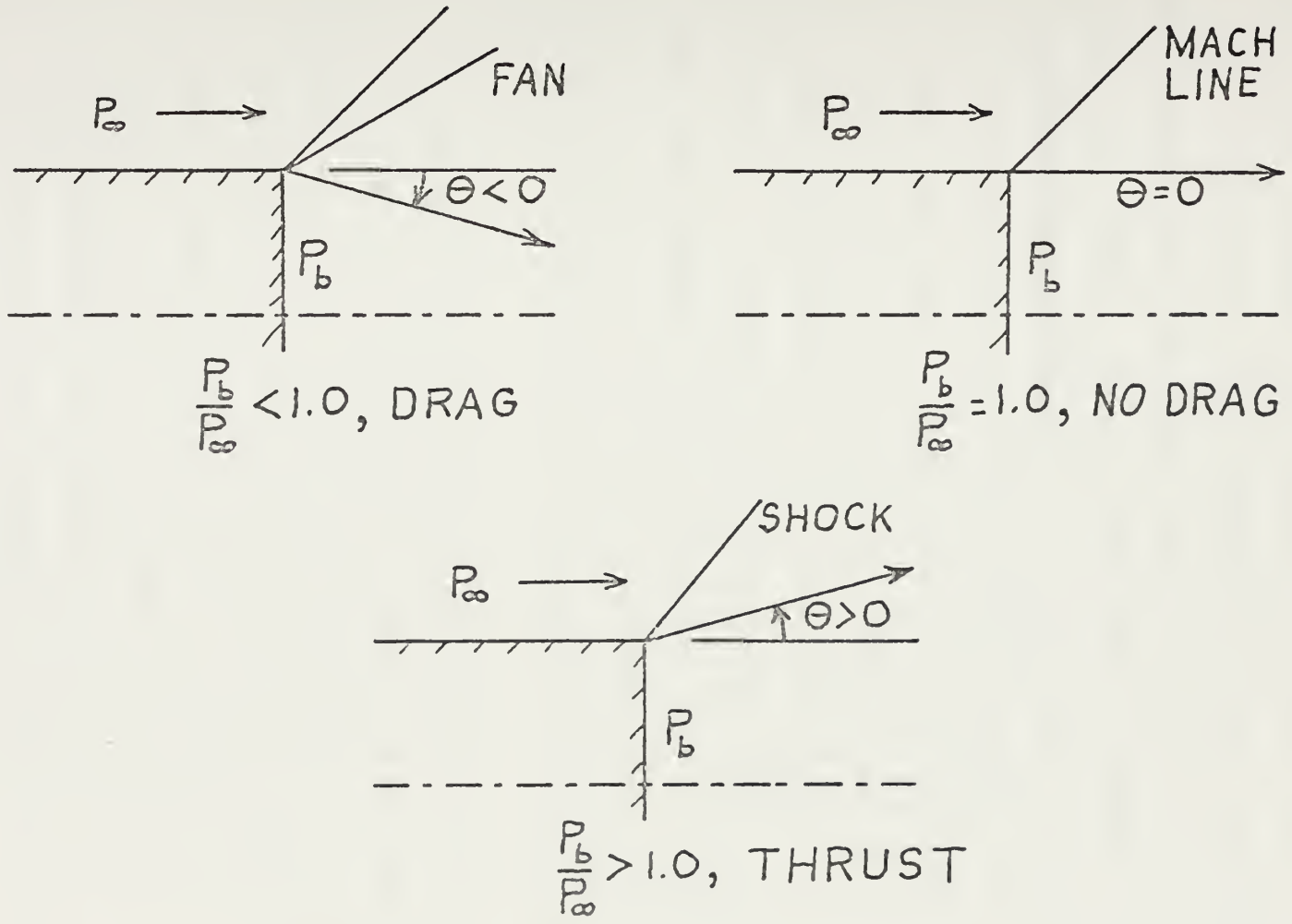

Figure 2. Base Pressure Ratio and Flow Angle

results which suggested that for experimental investigation the external burning process may be simulated by supersonic nozzle wall contours which generate identical characteristics.

Heat addition in a two dimensional planar supersonic flow was investigated by Strahle, using one dimensional and linearized heat addition theory, and shown to reduce base drag or produce thrust [Ref. 6,7]. In this study, the base flow was described by the Crocco-Lees [Ref. 8] model, and the resulting base pressure ratio was determined for heat addition zones of different intensity, location and extent. Experimental investigation [Ref. 9-11] has demonstrated the feasibility of external burning and shown that it can increase base pressure. Heat addition in an axisymmetric supersonic flow has been studied by Hosack and O'Leary using the method of characteristics and the Korst base flow model [Ref. 11].

The object of the present investigation was to study base pressure in two dimensional planar and axisymmetric supersonic flow with external heat addition using the method of characteristics and the Crocco-Lees base flow model. The effects of varying Reynolds number, including boundary layer transition, and projectile spin have been included. A concurrent experimental investigation studied the effect on base pressure of various axisymmetric nozzle contours which simulated the external burning process.

It should be mentioned that several combinations of external heat addition analysis and base flow models have not

been investigated theoretically. These include two dimensional planar method of characteristics and linearized theory with the Chapman-Korst base flow model, and linearized axisymmetric flow with both the Chapman-Korst and Crocco-Lees base flow models. The linearized axisymmetric flow problem will be discussed later.

II. THEORY

The theory employed for this investigation must describe the steady flow in two entirely different flow regimes, Fig. 1. The external flow is supersonic and can be accurately treated by the method of characteristics. The internal viscous flow, or recirculation zone, is dissipative and difficult to describe. As in the two dimensional case, it was assumed that the Crocco-Lees model [Ref. 1,12-15] adequately describes the axisymmetric internal flow. Boundary layer type (laminar or turbulent), thickness and transition were included as a function of Reynolds numer since these effects profoundly influence the base flow behavior.

The characteristic equations have been derived for flow with heat addition [Ref. 16,17]. In vector notation the steady equations for flow without viscosity, heat conduction or body forces are

$$\nabla\cdot(\rho\bar{U}) = 0 \tag{1}$$

$$\rho\bar{U}\cdot\nabla\bar{U} + \nabla p = 0 \tag{2}$$

$$\bar{U}\cdot\nabla(h + \tfrac{1}{2}\bar{U}\cdot\bar{U}) = q \tag{3}$$

$$p = \rho RT \tag{4}$$

where ρ is density, $\bar{U}$ is velocity, p is static pressure, h is enthalpy, q is the time rate of heat addition per unit mass, R is the universal gas constant and T is static temperature. Using a natural coordinate system [Ref. 18], Fig. 3, the characteristic equations were derived from the above equations

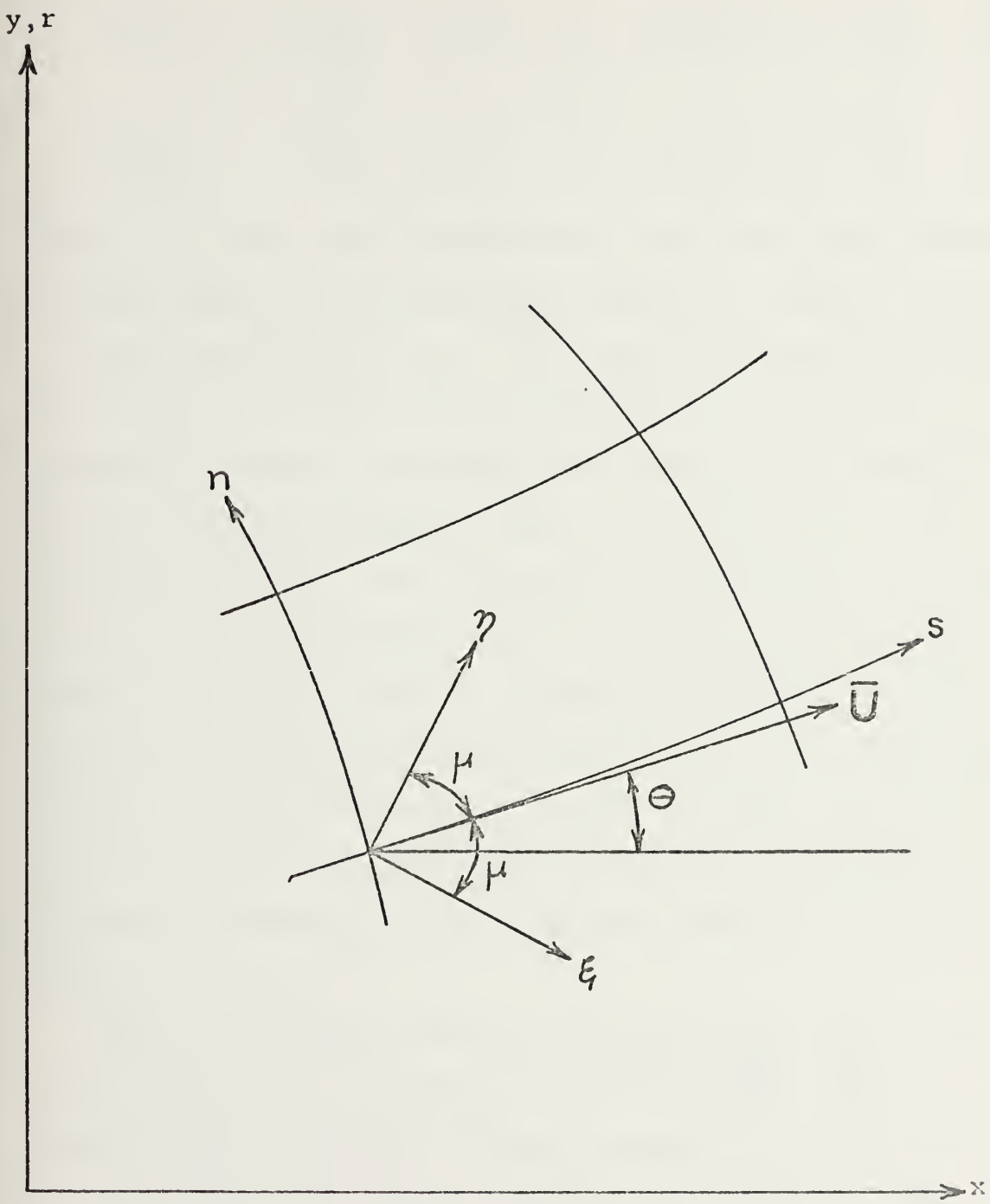

Figure 3. Natural and Characteristic Coordinate Systems

in the following convenient form (Appendix A)

$$\frac{\partial(\nu-\theta)}{\partial\eta} = \left(\frac{\alpha\sin\theta}{r/r_b} - \frac{r_b q}{Uc_p T} \right) \sin\mu - \frac{\cos\mu}{U^2}\left(T\frac{\partial S}{\partial n} - \frac{\partial h_0}{\partial n}\right) \qquad (5)$$

$$\frac{\partial(\nu+\theta)}{\partial\xi} = \left(\frac{\alpha\sin\theta}{r/r_b} - \frac{r_b q}{Uc_p T} \right) \sin\mu + \frac{\cos\mu}{U^2}\left(T\frac{\partial S}{\partial n} - \frac{\partial h_0}{\partial n}\right) \qquad (6)$$

where θ, ν and μ are respectively the flow, Prandtl-Meyer and Mach angles, U is speed, S is specific entropy and h_0 is total enthalpy, $h_0 = h + \frac{1}{2}U^2$. The left and right running characteristics are η and ξ respectively. The natural coordinates, s and n, are along and normal to the streamline. For two dimensional planar flow, α is 0, and α is 1 for axisymmetric flow. The characteristic equations, (5) and (6), have been multiplied by the characteristic length of base radius, r_b, to obtain a dimensionless form. Therefore, in contrast to the dimensional coordinates η, ξ and n used in Fig. 3, the coordinates η, ξ and n in Eqns. (5) and (6) are understood to be dimensionless. Also, the specific heat at constant pressure, c_p, was assumed constant in the enthalpy relation $h = c_p T$.

The characteristic computations with Eqns. (5) and (6) were simplified by neglecting the term $\frac{1}{U}\left(T\frac{\partial S}{\partial n} - \frac{\partial h_0}{\partial n}\right)/r_b$, which is the vorticity. One may assume the external flow to be irrotational before heat addition and then determine the restrictions on heat addition which preserve irrotationality. Crocco's theorem for steady flow may be written (Appendix B)

$$T\nabla S + \bar{U}\times\bar{\Omega} = \nabla h_0 \qquad (7)$$

where $\bar{\Omega} = \nabla\times\bar{U}$. Taking the curl of Eqn. (7)

$$\dot{\bar{U}}\cdot\nabla\bar{\Omega} = \bar{\Omega}\cdot\nabla\bar{U} - \bar{\Omega}\nabla\cdot\bar{U} + \nabla T X \nabla S. \tag{8}$$

Assume $\bar{\Omega} = 0$ before and during heat addition. Then, from Eqn. (8), the condition which preserves irrotationality is

$$\nabla T X \nabla S = 0. \tag{9}$$

If one redefines the heat addition and has uniform upstream conditions at infinity [Ref. 19], then

$$\nabla(h_0 - Q) = 0 \tag{10}$$

where Q is the heat per unit mass which has been supplied to the fluid element. Using Eqn. (7), with $\bar{\Omega} = 0$, Eqns. (9) and (10) yield the following result

$$\nabla Q X \nabla(\tfrac{1}{2}U^2) = 0 \tag{11}$$

which is the condition preserving irrotationality; that is, the gradients of kinetic energy and heat added must be parallel. If Q is a small perturbation, $(Q/h_\infty) = \varepsilon$, then Eqn. (11) is of order ε^2 and the irrotationality condition is automatically satisfied to order ε. To neglect the vorticity term in Eqns. (5) and (6), one must insure

$$\frac{r_b q}{U c_p T} = r_b \frac{\bar{U}\cdot\nabla Q}{U c_p T} = \varepsilon << 1. \tag{12}$$

In the computations discussed in Section V, the quantity of Eqn. (12), $(r_b q)/(U c_p T)$, was assigned a constant value independent of local pressure, within the heat zone and was taken as zero outside the heat zone. Thus, within the heat zone, ∇Q was approximately parallel to the gradient of kinetic energy and the irrotationality condition of Eqn. (11) was

satisfied. This condition was not satisfied along the inner and outer streamlines of the heat zone, since a jump in Q existed normal to the streamlines. However, by assigning a value for Eqn. (12), $(r_b q)/(Uc_p T) \leq 0.2 << 1$, the irrotationality condition was satisfied to order epsilon along the streamline boundaries of the heat zone.

Equations (1) through (4) may be combined to give

$$\nabla\cdot\bar{U} - \frac{1}{a^2}\bar{U}\cdot\nabla(\tfrac{1}{2}\bar{U}\cdot\bar{U}) = \frac{q}{c_p T} \tag{13}$$

where a is the speed of sound. Assuming small perturbation, Eqn. (13) may be linearized (Appendix G)

$$\nabla^2\phi - M_\infty^2 \frac{\partial^2\phi}{\partial x^2} = q' \tag{14}$$

where M_∞ is the Mach number at infinity, q' is the heat addition, $q = h_\infty q'$, ϕ is the perturbation velocity potential, $\bar{U} = \bar{i}U_\infty + \bar{U}'$, $\bar{U}' = \nabla\phi$ and $T = T_\infty(1+T')$. In Cartesian coordinates, Eqn. (14) may be written

$$-\beta^2\phi_{xx} + \phi_{yy} + \phi_{zz} = q' \tag{15}$$

where $\beta^2 = M_\infty^2 - 1$. For supersonic flow, the solution of Eqn. (15) is found by integrating the sources in the forecone volume, V_f [Ref. 20],

$$\phi = -\frac{1}{2\pi}\int_{V_f} \frac{q'dx_1dy_1dz_1}{((x-x_1)^2 - \beta^2((y-y_1)^2 + (z-z_1)^2))^{\frac{1}{2}}}. \tag{16}$$

Although the linearized theory was not pursued further, it should be noted that this theory could be used instead of the method of characteristics to establish the effect of

external burning at the base flow shear layer. Studies of linearized supersonic flow through ducts have provided solutions for an annular source distribution [Ref. 21-23], which could be used in conjunction with centerline sources and sinks [Ref. 18] to describe the axisymmetric external flow with burning.

The two dimensional planar Crocco-Lees theory [Ref. 8] considers the base flow as a separated boundary layer merging into a free jet profile and derives integral equations to describe the mean values of the flow quantities (Appendix C). From the integrals of the conservation equations, a single ordinary differential equation is derived. This ordinary differential equation has a saddle point singularity; existence of the singularity is a key feature of the Crocco-Lees model. The behavior of this equation is partly determined by an empirical F - κ relation and by the nature of the shear layer mixing. κ is the ratio of average internal base flow velocity to the external velocity, u_1/u_e. F is a ratio formed by using the various boundary layer thicknesses. The turbulent shear layer mixing coefficient, k_T, was assigned the constant value, 0.03, by Crocco-Lees. The laminar value used for this investigation was 0.0033, about 1/9 the turbulent value.

F is conceptually a profile form factor; when the velocity profile changes shape, the value of F changes. As discussed in reference 8, the F - κ functional relationship is based on many known viscous flows. For example the Blasius

solution is represented by a point in the F - κ plane. Falkner-Skan boundary layer solutions, which involve either favorable or adverse pressure gradients, become a curve in the F - κ plane. The velocity profiles of jets under certain conditions are described by the error function; these jets become a point in the F - κ plane. Likewise the Howarth boundary layer solutions for flows in pressure gradients are a curve in the F - κ plane.

The F - κ curve corresponds to viscous flow near walls, i.e. boundary layers, as well as free jets. Furthermore, adverse, zero or favorable pressure gradients are represented by positions on the F - κ curve. Heat addition in a supersonic flow generates compression waves. When $z/r < 0$, the compression waves impinge ahead of the base; the boundary layer on the body and the shear layer experience an adverse pressure gradient. When $z/r > 0$, the compression waves impinge downstream of the base and only the shear layer flows into the adverse pressure gradient established by the external burning. Since the F - κ curve incorporates pressure gradients, the presence of an adverse pressure gradient due to heat addition should not alter its validity. As stated in reference 8, the F - κ curve needs additional experimental verification; this applies to the case with external burning. Further discussion of the F - κ curve may be found in references 6, 12, 13, 14 and 15.

The reformulation of the Crocco-Lees theory for axisymmetric flow [Ref. 1,12-14] resulted in the same single ordinary

differential equation which had been derived for planar flow. In two dimensional planar flow this equation is numerically integrated by starting at the singularity, or so called critical point, and working toward the base, using the Prandtl-Meyer relation to obtain flow angle for various Mach numbers. With external heat addition, one may no longer use the Prandtl-Meyer relation for flow angle at the shear layer, since the heat addition, described by either linearized or one dimensional flow, introduces a correction term [Ref. 6,7].

This procedure cannot be used for the axisymmetric problem without heat addition due to the 1/r term arising in the continuity equation; thus, one must start at the base and integrate toward the critical point. As was anticipated, attempts to numerically integrate through this saddle point singularity were unsuccessful; however, by repeated integration one may determine two Mach numbers on the downstream side of the expansion fam which straddle the saddle point singularity, thus establishing the base pressure within the limits given by the two Mach numbers, Fig. 4. This technique was used with Eqns. (5) and (6) for both axisymmetric and two dimensional planar flow.

To incorporate the effects of various boundary layers on the body (laminar, transitional, turbulent) and shear layer transition, it was necessary to formulate a transition model, Fig. 5. While this model treats the boundary layer mass flux differently, it is not a departure from the existing Crocco-Lees theory. In fact, this transition model extends the Crocco-Lees base flow model.

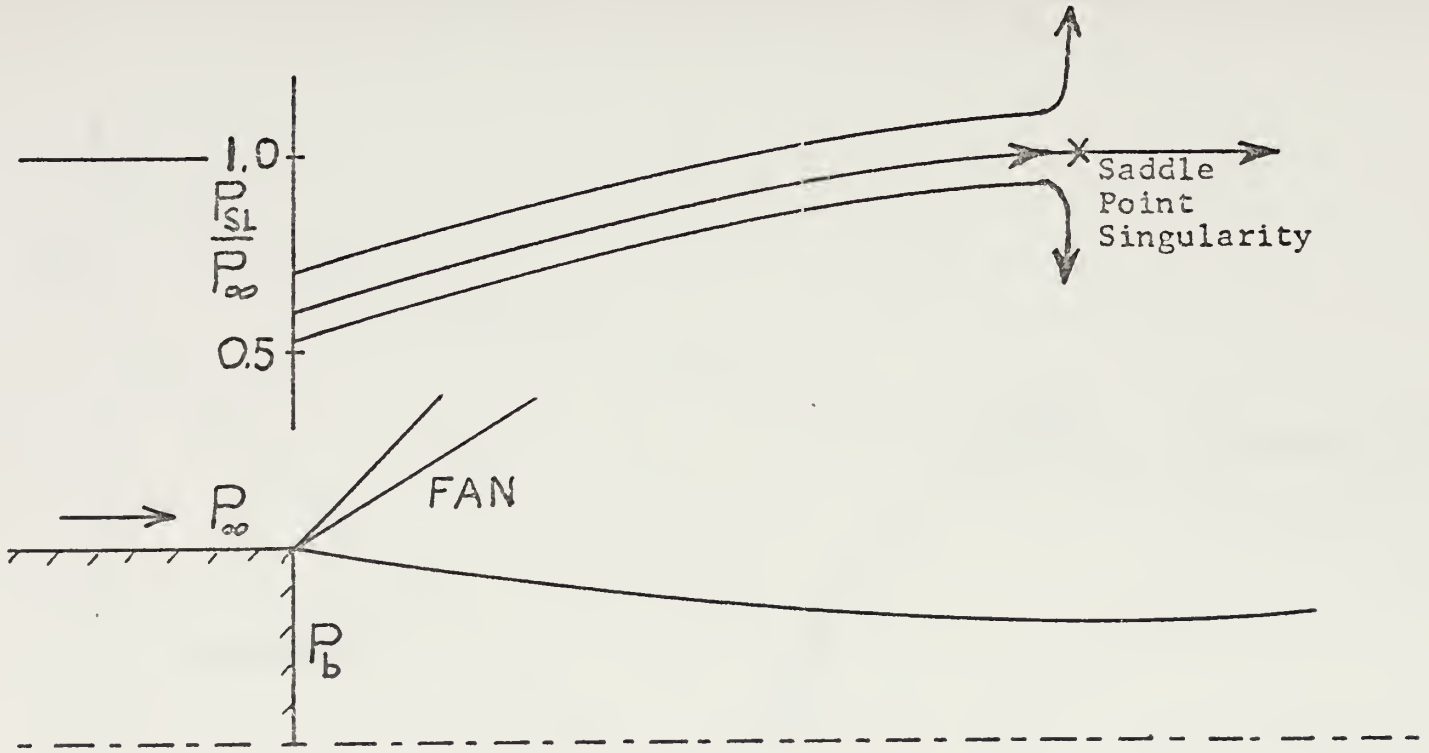

Figure 4. Conceptual Diagram Depicting Shear Layer Pressures, P_{SL}, Which Straddle the Critical Point

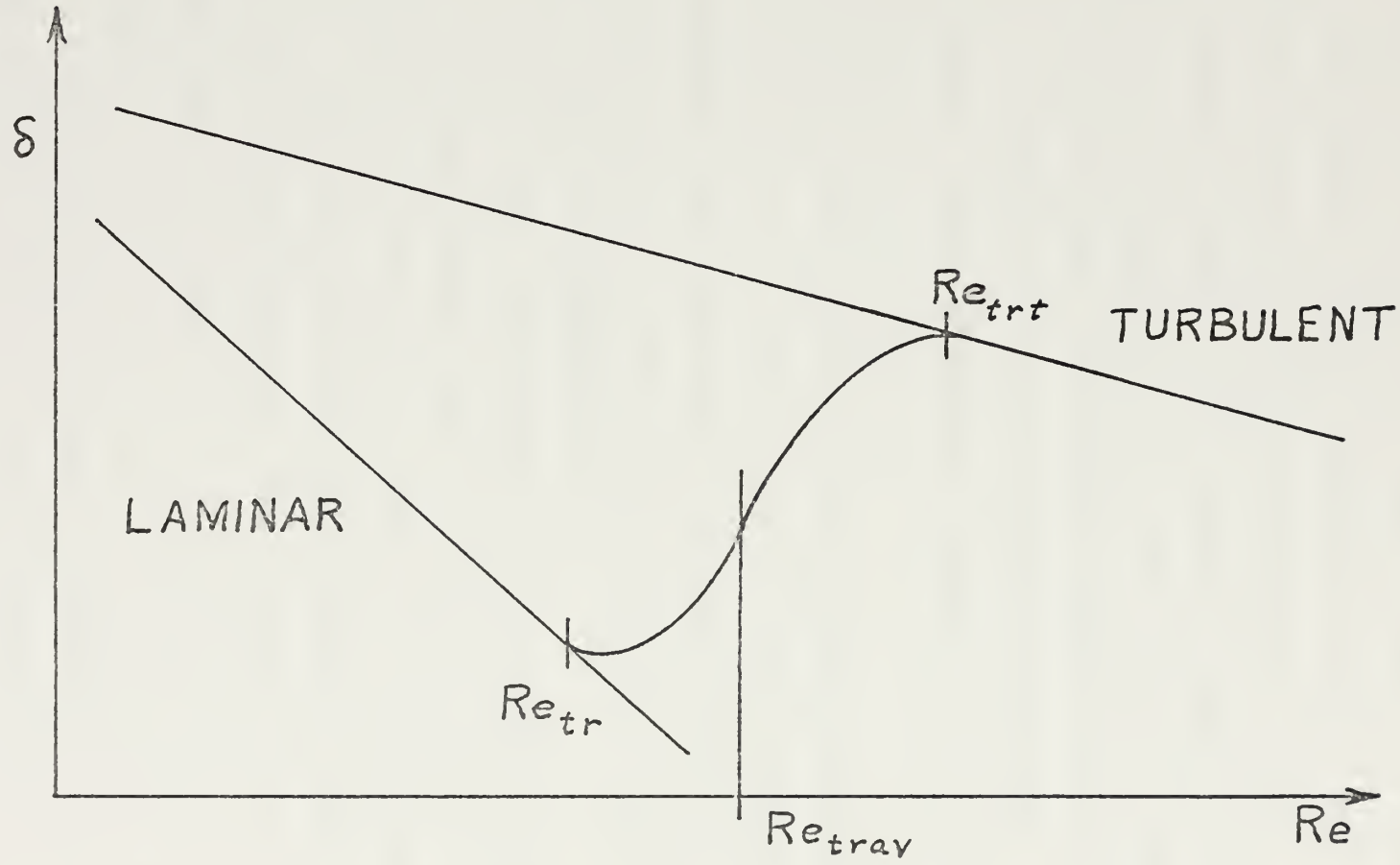

Figure 5. Transition Model

Since the transition from laminar to turbulent flow is more or less probabilistic in nature and, depending on the Reynolds number, may occur on the body or along the shear layer, it was assumed that the transition process could be described by an integrated normal distribution and two transition Reynolds numbers. The transition Reynolds numbers identified the start and end of the transition process, and the integrated normal distribution ranged from 0.02 to 0.98 in the span between the two specified transition Reynolds numbers. This assumption replaces the previously assumed transition curves [Ref. 8].

The transition model must provide several parameters which are required in the Crocco-Lees base flow formulation. It must establish the values for the mixing coefficient, k, along the shear layer and the boundary layer mass flux at the base to permit determination of F.

The boundary layer was assumed to be at constant static pressure and total enthalpy, and the velocity profile was assumed to have a 1/n dependence, where n is an integer, $1 \leq n \leq 7$. This formulation may be integrated (Appendix D) for both planar and axisymmetric flows to give the boundary layer mass flux at the base as an explicit function of velocity profile, 1/n, base radius, r_b, and boundary layer thickness, δ. If the flow over the body is completely laminar, δ is given by the compressible Blasius solution [Ref. 8], $\delta_L = (5.0+1.2(\gamma-1)M^2)L/(Re_b)^{\frac{1}{2}}$, and the value of n = 1 is used for the velocity profile [Ref. 24]. If the boundary layer is

completely turbulent, the n is taken as 7 and δ is computed from the compressible one-seventh power solution [Ref 8], $\delta_T = (0.037L/Re_b)^{1/5})(C_{f_M}/C_{f_i})(\delta/\delta^{**})$. The term (C_{fM}/C_{fi}) is a ratio of skin friction coefficients for compressible and incompressible turbulent flow [Ref. 24]. It was recognized that the boundary layer thickness computed for planar flow will be different from the axisymmetric thickness. This difference will be small if δ/r_b and radial velocity, v/U, are of order ε. The dimensional term $\rho v/r$ from the axisymmetric continuity equation will be of order ε^2 upon nondimensionalizing with δ and U. Thus, the governing equations and their solutions are identical to order ε in both cases.

The first transition Reynolds number, Re_{tr}, is where the laminar flow starts transition to turbulent. The second transition Reynolds number, Re_{trt}, is where the flow must be completely turbulent ($Re_{trt} \doteq 4Re_{tr}$). As one changes values of base Reynolds number from Re_{tr} to Re_{trt}, the values for n and δ, which determine the boundary layer mass flux at the base, must vary from 1 to 7 and δ_L to δ_T, respectively. This transition was computed by the error function, erf, since it is readily available in FORTRAN and can be directly related to the integral of the normal distribution. A numerical span, S, of 4, which takes the value of erf from -0.96 to 0.96, was used to normalize the difference $(Re_{trt} - Re_{tr})$. Let $Re_{tra} = \frac{1}{2}(Re_{tr} + Re_{trt})$. Then

$$ERF_B = \tfrac{1}{2}erf(\frac{S}{2^{\frac{1}{2}}}(Re_{tra} - Re_b)/(Re_{trt} - Re_{tr})). \qquad (17)$$

So, when $Re_b > Re_{tr}$

$$\delta_{BASE} = \delta_L(\tfrac{1}{2} + ERF_B) + \delta_T(\tfrac{1}{2} - ERF_B) \quad (18)$$

and

$$n_{BASE} = 1(\tfrac{1}{2} + ERF_B) + 7(\tfrac{1}{2} - ERF_B) \quad (19)$$

were the values used to compute the boundary layer mass flux at the base (Appendix F).

When transition from laminar to turbulent flow occurred on the shear layer, the value for the mixing coefficient, k, at a particular point was computed in a similar fashion using the error function to transition from laminar mixing, k_L, to turbulent mixing, k_T, Fig. 6.

The effect of shear layer mixing on base pressure is shown schematically in the momentum control volume of Fig. 7. The axial pressure on surfaces cd and de, and momentum flux leaving the volume, de, must be balanced by the pressure on surfaces ab and bc and momentum flux entering the volume, abcd. Thus, to maintain this balance, an increase of momentum flux along cd due to mixing requires a corresponding decrease of base pressure, p_b, along ab.

One additional assumption was necessary to obtain good agreement with experimental data. At low Reynolds numbers and completely laminar flow, it was necessary to increase the value of the laminar mixing coefficient, k_L, in direct proportion to the increase of the thickness of the boundary layer at the base. This assumption may be expressed as

$$k_L = k(Re_{tr}/Re_b)^{\frac{1}{2}} \quad (20)$$

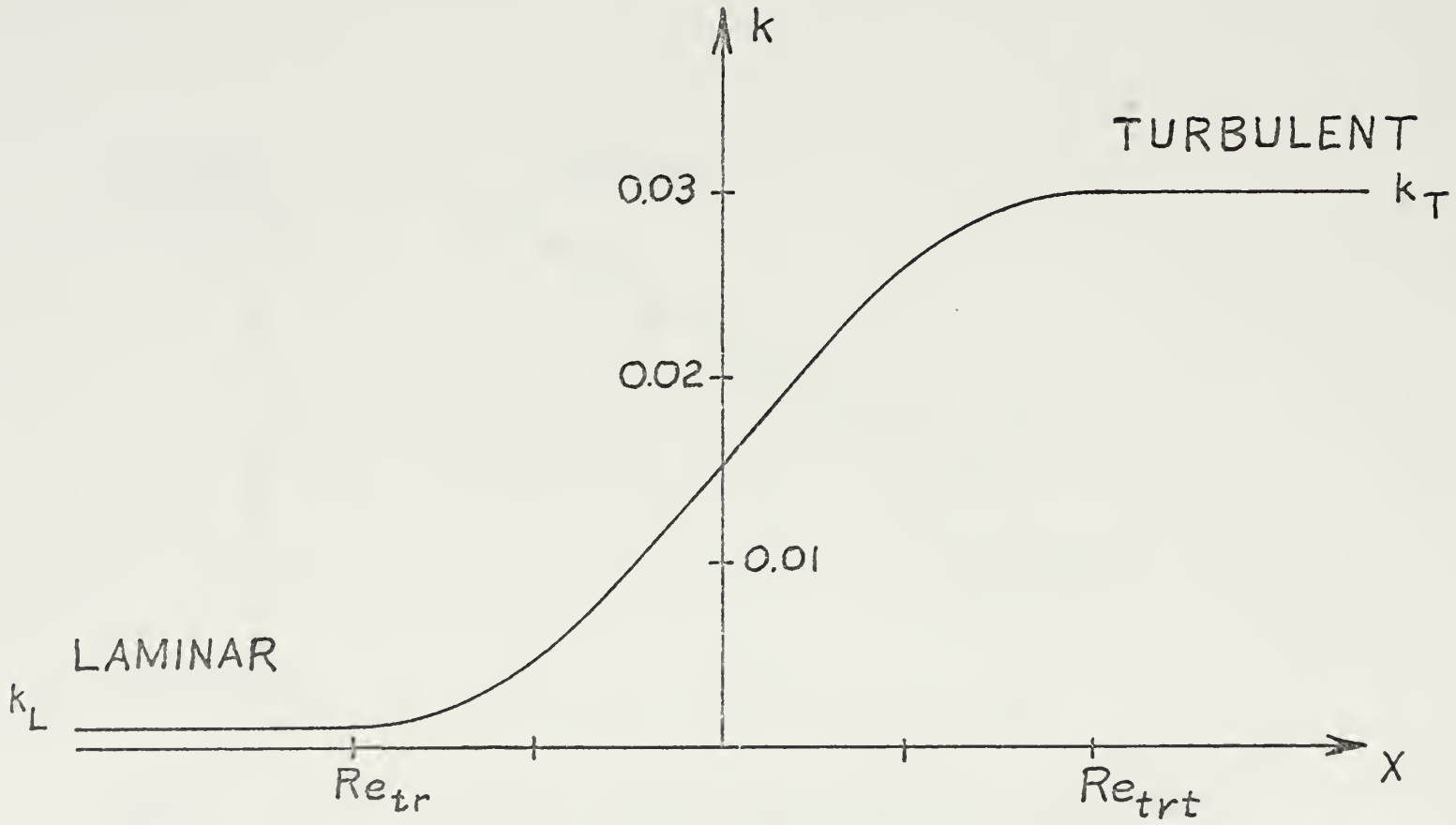

Figure 6. Transition of Shear Layer Mixing Coefficient

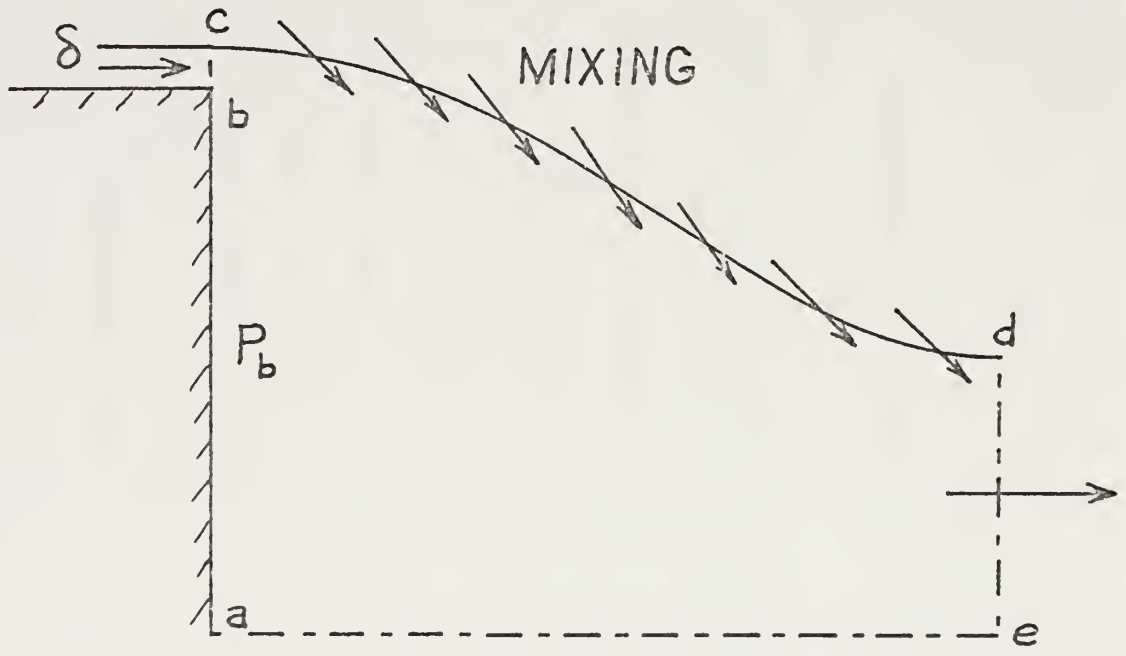

Figure 7. Momentum Control Volume Depicting Shear Layer Mixing

where Re_{tr} is the transition Reynolds number, Re_b is the Reynolds number of the body, based on length or chord, L, and k is the laminar mixing coefficient when $Re_{tr} = Re_b$. Some justification may be provided for Eqn. (20) by considering the Blasius boundary layer solution where the mass flux, $\bar{m}$, is given by $3.28\rho ux/(Re)^{\frac{1}{2}}$ and the Crocco-Lees theory where $k\rho u$ is taken equal to $d\bar{m}/dx$. If one forms the derivative of $3.28\rho ux/(Re)^{\frac{1}{2}}$, $d\bar{m}/dx$ is found to vary as $1/(Re)^{\frac{1}{2}}$, thereby suggesting the form assumed in Eqn. (20). Although k_T was held constant at 0.03 for all calculations, a similar analysis using the incompressible turbulent solution suggests that k_T might vary as $1/(Re)^{1/5}$.

It has been suggested that the effect of projectile spin could be included in the mixing coefficient [Ref. 15], k, by using $k_{spin} = k(1+r\omega/U)$, where $r\omega/U$ is the spin number. However, since k_{spin} always increased with an increase in spin number, and, since it has been determined through numerical experiments with the Crocco-Lees theory, Fig. 8, that increasing k decreases the base pressure, this simple hypothesis contradicts experiment [Ref. 25,26] where, in some cases, increasing the spin number increased the base pressure. In Fig. 9 it is clear that at certain values of Reynolds number, Re_b, an increase of Reynolds number resulted in an increase in base pressure. This fact suggests that the spin number could be used to shift the p_b/p_∞ versus Re_b curve, Fig. 9, instead of increasing the mixing coefficient. Several methods were attempted at this point, such as increasing

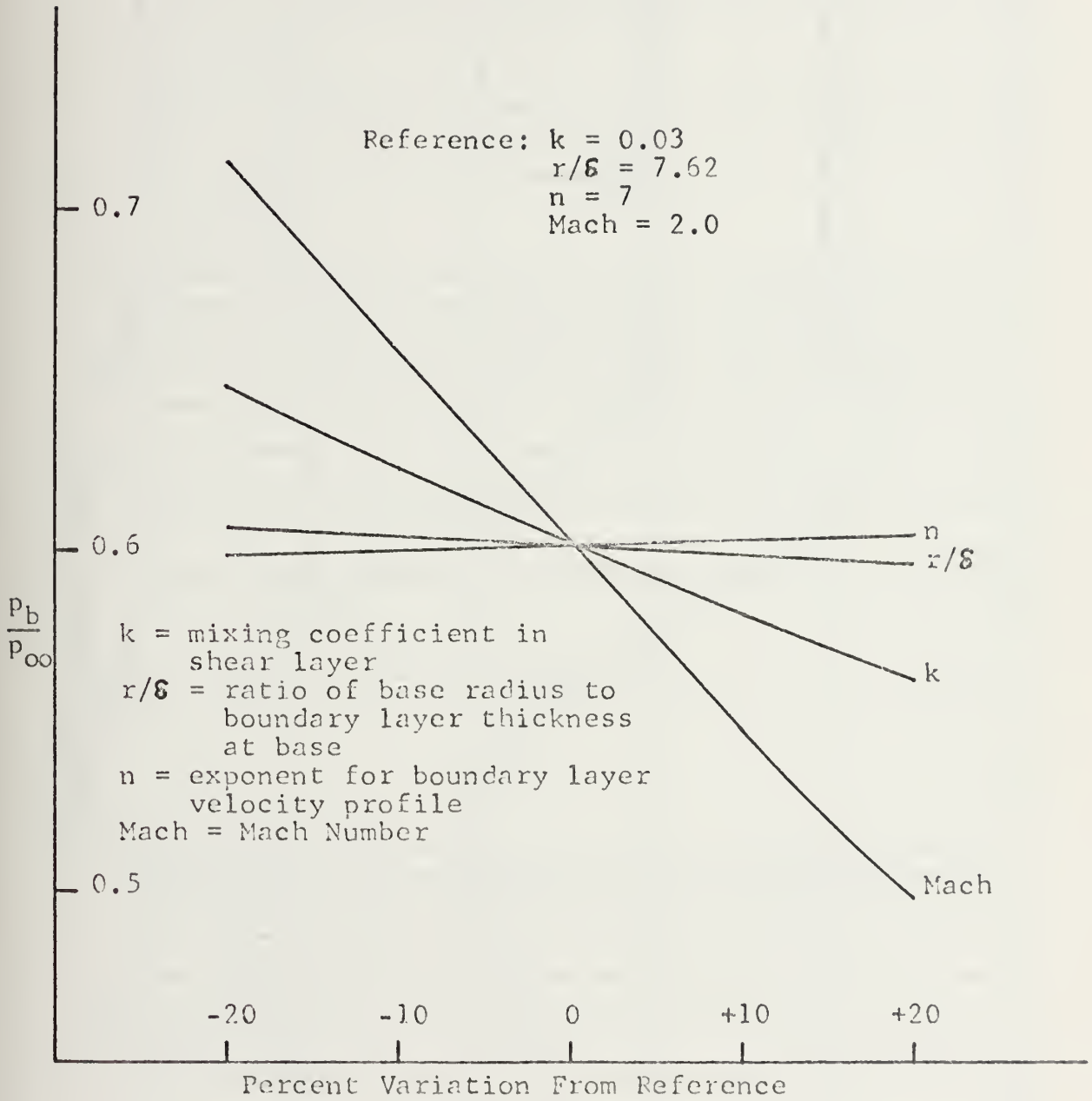

Figure 8. Sensitivity of Base Pressure Ratio

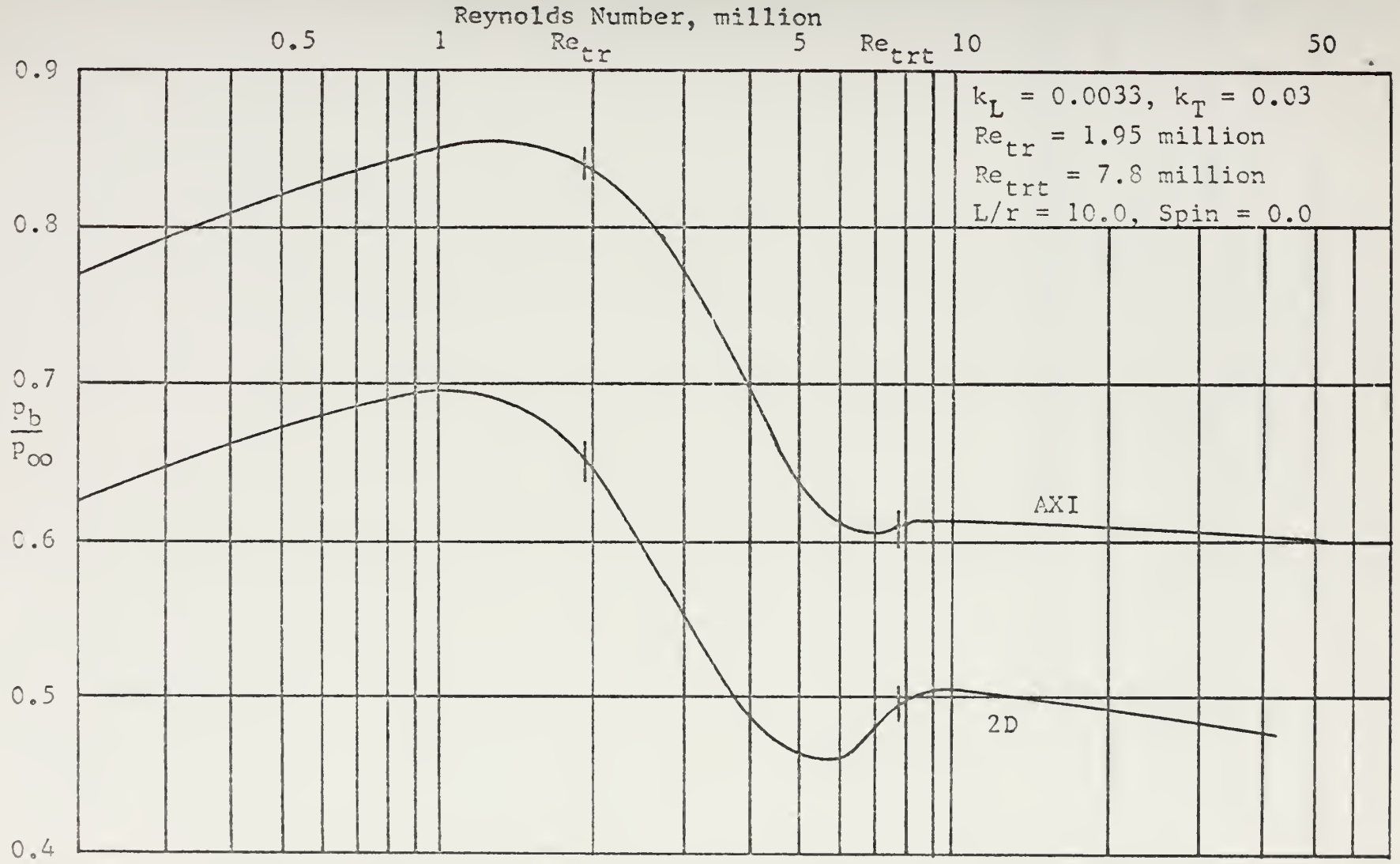

Figure 9. Computed Values of p_b/p_∞ vs. Reynolds Number, Mach 2.0, No Heat Addition

Re_b by [Ref. 27] $(1+(\frac{r\omega}{U})^2)^{\frac{1}{2}}$ or $(1+(\frac{r\omega}{U})^2)$, but the method which provided the best correlation was to simply decrease the transition Reynolds numbers. The spin transition Reynolds numbers used to compute p_b/p_∞ versus Re_b were formed by dividing the corresponding no spin transition Reynolds numbers by $(1+(\frac{r\omega}{U}))$. Interpretation of base pressure data for a spinning projectile is given in Section V.

III. EXPERIMENTAL INVESTIGATION

To carry out experiments related to the five inch projectile, the mid point of a maximum range trajectory was selected. This flight condition established an altitude of 23,000 feet and a Mach number of 2.0 for determining similarity parameters. For the five inch projectile, this gave a body Reynolds number of 15.7×10^6, a radius Reynolds number of 1.51×10^6, and a turbulent boundary layer thickness to radius, δ/r, of 0.1313. The spin at 23,000 feet was assumed to be the same as the muzzle spin, 250 revolutions per second, which gave a spin number, $r\omega/U$, of 0.1595. Using these nomial values, it was found that all similarity parameters could be matched with a free jet Mach 2.0 coaxial nozzle exhausting at room pressure if the center cylinder had a radius of 0.641 inches, δ of 0.084 inches, and a spin of 800 revolutions per second. As stated in the introduction, the actual combustion process was simulated with various nozzle contours which duplicated the compression waves generated by the external burning.

The simulation process is depicted in Fig. 10 where the streamline deflected by the presence of a heat zone can be replaced by a nozzle wall to generate an identical flow field.

The free jet experimental facility, Figs. 11 and 12, was conventional in most respects and has been previously reported [Ref. 28,29]. The use of cast aluminum filled epoxy

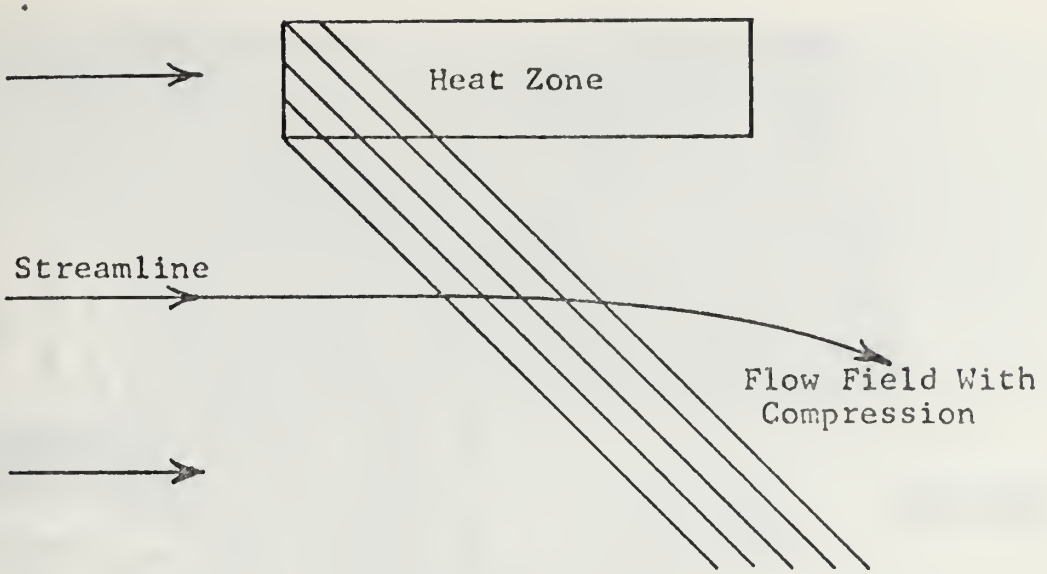

(a) Heat Zone in Supersonic Flow

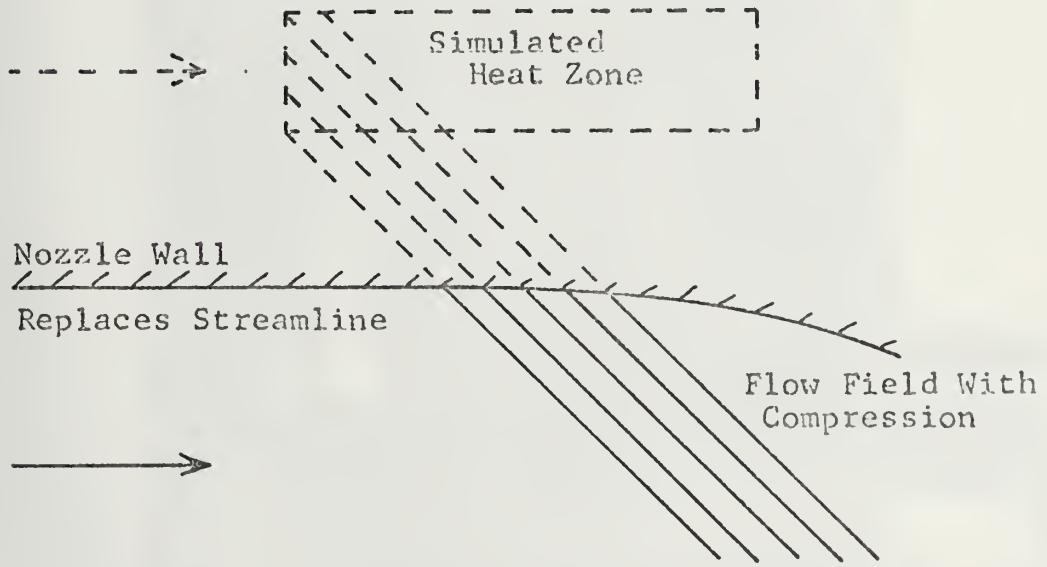

(b) Identical Flow Field With Compression Generated by Nozzle Wall to Simulate Heat Zone

Figure 10. Heat Zone Simulation With Nozzle Wall

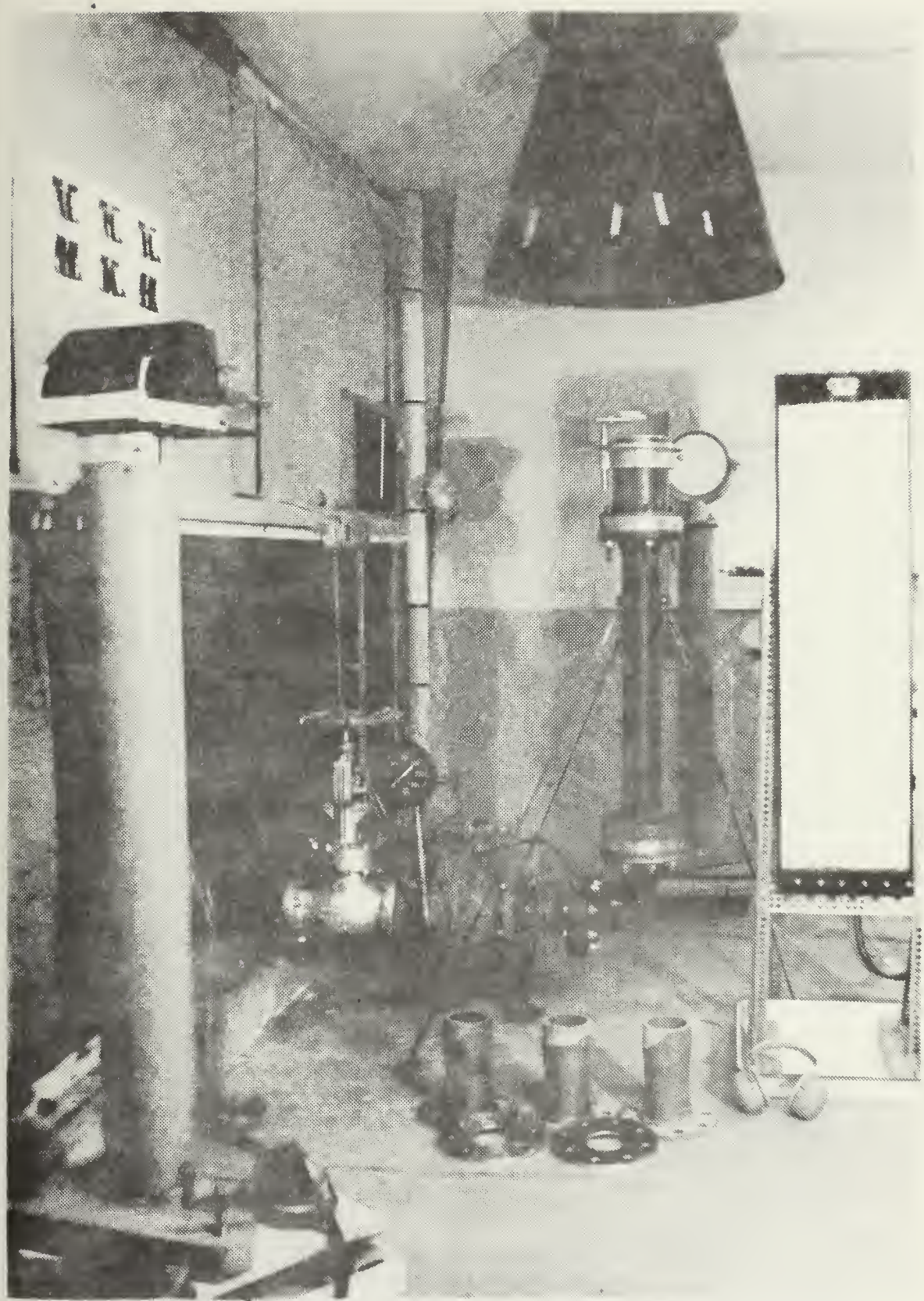

Figure 11. Photograph of Free Jet Experimental Facility

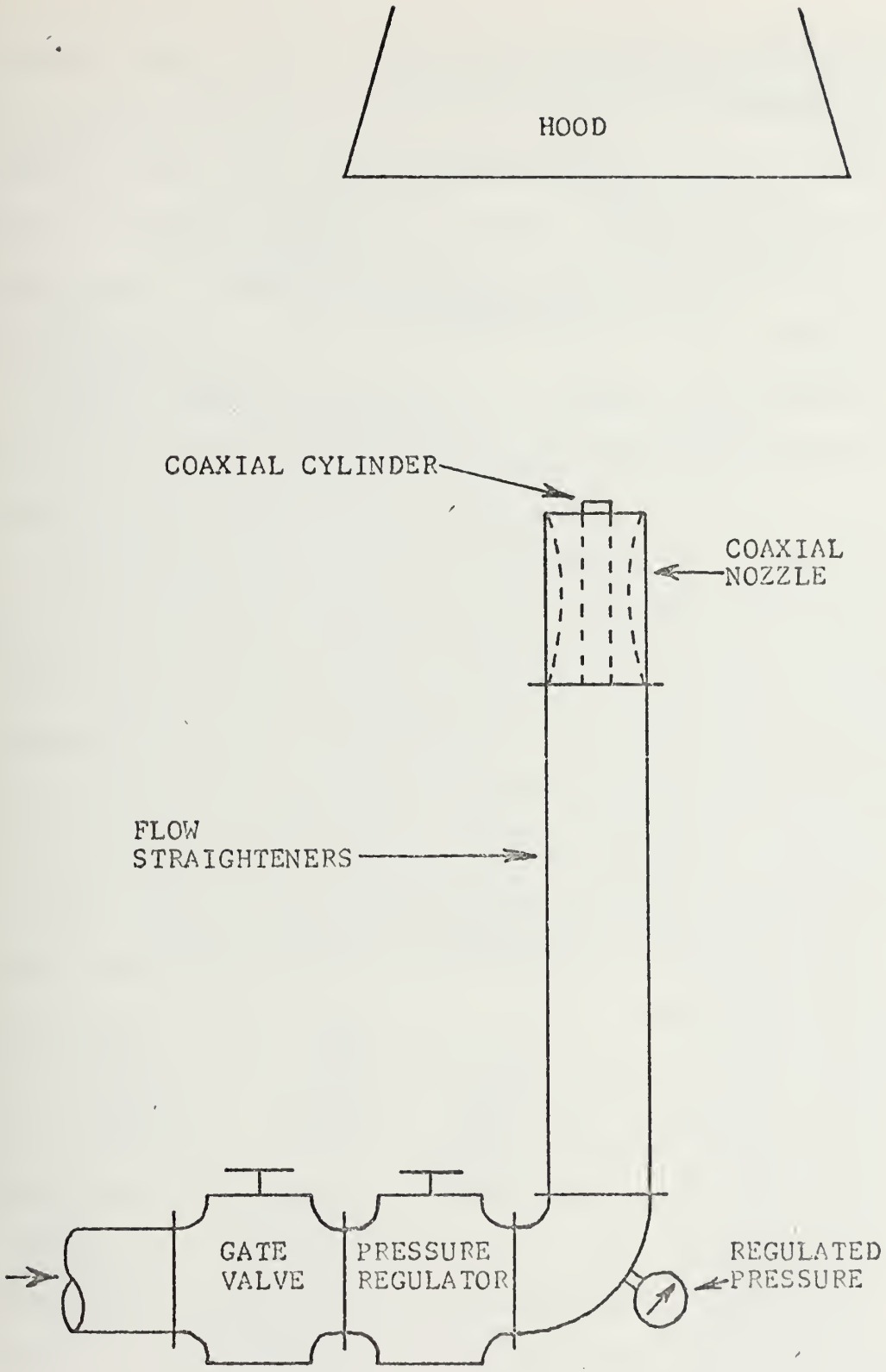

Figure 12. Schematic Diagram of Free Jet Experimental Facility

nozzles, Fig. 13, was the only new hardware innovation. The technique of casting employed a wax plug contoured to the desired shape with an aluminum template. This plug was turned slightly undersize and then restored to size using a thin coat of automotive body plastic. After melting the wax from the cast nozzle, the plastic peeled away from the epoxy to leave a smooth nozzle wall. Without this plastic, the heat generated by the epoxy had softened the wax and caused some irregularity in the nozzle wall.

The location of the zone of combustion to be simulated by the nozzle was estimated using an empirical formula for penetration depth of a jet normal to a supersonic free-stream [Ref. 30]. For Mach 2.0 flow, internal pressures from 300 to 500 psia were computed to provide penetration to 2½ inches with various orifice diameters. Thus it was assumed that external burning at 5 inches from the projectile centerline would be practical. Assuming a fuel rich propellant exhaust, ARC-168, with an available heating value of 7200 BTU/lb and 0.6 lb/sec flow rate, it was found using one dimensional theory that the flow should be deflected about 4½° for a distance of 15 inches, or three diameters, downstream. This computation used the integral methods of reference 5 which gave a perturbation velocity normal to the flow of -163 feet per second. The resulting flow angle tangent was -163/2058, which gave a computed flow angle of -4.54 degrees along the inner streamline of the heat zone.

Figure 13.Coaxial Epoxy Nozzle. Insert Showing Spacers.

These estimated values for the heat zone were taken as the upper limit and were used to form a test matrix and for subsequent nozzle design. Several different nozzle contours were computed by the method of characteristics for 4½° streamline deflection at a radius equal to a cylinder diameter from the centerline and with different assumed lengths for the combustion zone. The test matrix included using spacers, Fig. 13 insert, with each nozzle so that the first full compression waves impinged ahead of, at, or behind the base of the cylinder. Pressures were measured along the base and side of a stationary centerline cylinder, Fig. 13, using mercury manometers. Attempts to carry out experiments with a spinning cylinder were unsuccessful due to faulty air bearing design (Appendix I). Time did not permit correction of this difficulty.

The differences in the flow field with the stationary cylinder and different nozzles can be seen in Fig. 14. The photograph of the uniform flow nozzle in Fig. 14a used a horizontal knife edge and the expansion fan at the base appears dark. The base pressure ratio was 0.635. In Fig. 14b the vertical knife edge was positioned to make a positive density gradient from the centerline to the right appear brighter. The flow with compression, Fig. 14c, had an expansion fan at the base but achieved a higher base pressure ratio of 1.065 due to compression upstream of the base as well as along the shear layer. The compression upstream of the base increased the pressure right before the expansion

Figure 14a.
Uniform Flow,
Horizontal
Knife Edge

Figure 14b.
Uniform Flow,
Vertical
Knife Edge

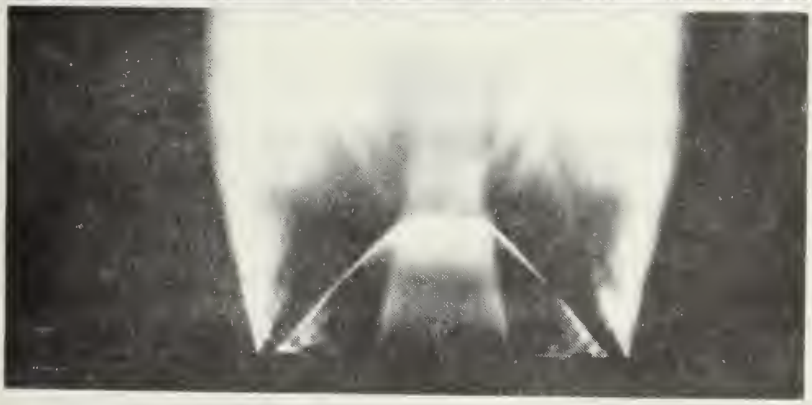

Figure 14c.
Compression Flow,
Horizontal
Knife Edge

Figure 14. Schlieren Photographs at Mach 2.0 Showing Uniform Flow and Flow With Compression

fan.so that it was greater than p_∞, thus the flow was near ambient pressure after passing through the expansion fan. Some test results using the stationary cylinder are given in Table I. Except for the nozzle with w/r = 4.34, these tests indicate that compression applied upstream of the base, z/r = -0.5, is less efficient at increasing base pressure than compression applied at the base, or slightly downstream. The nozzle with w/r = 4.34 had a strong shock wave at the exit, due to compression waves reflected from the cylinder [Ref. 15], which, with z/r = -0.5, impinged on the base flow region ahead of the critical point. In turn, increased pressure across the shock wave was impressed on the subsonic flow in the recirculating zone and gave a higher base pressure. The shock wave observed with this experimental nozzle would not be expected with uniform external burning.

In Table I the experimental base pressure ratios, p_b/p_∞, are shown as the upper number in each box for the various test positions, z/r, of each nozzle, w/r. The cylinder radius is r, the axial location where the first full strength compression wave impinges on the body or shear layer is z (z=0 at the base) and w is the length of the heat zone. The corresponding Reynolds number, Re_b, is shown below each value of z/r. The lower number shown in each box is the computed specific impulse for the assumed projectile flight condition at 23,000 feet. The uniform flow nozzle, with w/r = 0.0, was taken as the reference pressure ratio to compute the

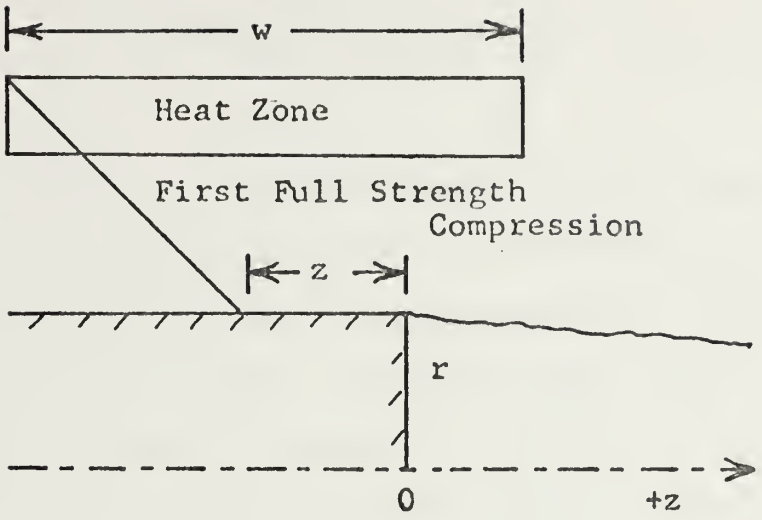

Sketch to Table I

z/r →	-0.5	0.0	0.5	1.0
Re_b X 10^6 →	8.55	7.80	7.05	6.29
w/r ↓				
0.0	0.62	0.61	0.60	0.60
0.72	0.759 227	0.893 460	0.993 639	----
1.84	0.96 216	1.055 283	1.074 302	----
3.91	1.078 137	1.175 169	1.160 167	1.129 158
4.34	1.20 156	1.14 143	1.085 131	----

Table I. Base Pressure Ratio and Specific Impulse With Simulated Heat Addition

base pressure force created by the other nozzles. The fuel flow rate was taken proportional to (w/r)/(6.0), since 6.0 was the combustion zone length assumed for the fuel flow of 0.6 lb/sec.

Once Mach number and operating pressure and temperature are selected, the remaining variable controlling Reynolds number is the length or scale of the apparatus. The free jet facility of Figure 11 has sufficient mass flow to permit duplication of Reynolds number at 23,000 feet altitude provided the cylinder has sufficient length. Consequently the nominal Reynolds number was chosen as $15.7X10^6$ for 23,000 feet to match capability of the facility.

When the design of the spinning cylinder was initiated it became apparent that a long cylinder had problems in regard to shaft whip or the first vibrational mode in bending. A shorter cylinder reduced the Reynolds numbers to the values shown in Table I. Conditions at a higher altitude were simulated, or else conditions for a short projectile at 23,000 feet were duplicated.

Two cylinders could have been designed. Each cylinder would have required a separate family of nozzles. A choice was made to use a short cylinder for both stationary and spinning tests.

Variation in z/r as shown in the sketch with Table I changes Reynolds number slightly. The variation in Re_b in Table I is due to this fact.

IV. NUMERICAL INVESTIGATION

The computer program for this numerical investigation was written to calculate either two-dimensional planar or axisymmetric problems. The program used the method of characteristics where the axisymmetric term in Eqns. (5) and (6), $r_b(\sin\mu\sin\theta)/r$, was deleted for two-dimensional planar flow. Similarly, the effect of radius in the mass flux calculation, at the base and along the shear layer, was deleted or retained as required. The characteristic mesh, Fig. 15, was computed from the body or shear layer upstream through the heat zone, if present, to a reference freestream Mach line (i.e., backwards along a right running ξ characteristic). The error from the reference condition was used to correct ν on the body, since θ was given, or θ along the shear layer since ν was computed from the Crocco-Lees theory. Each body or shear layer point was iterated until the error at the upstream boundary condition was less than 10^{-3} radians. At each point in the characteristic mesh, the value of μ was determined for the resulting value of ν by the method given in Appendix H. In retrospect, this method of characteristics computation could be made more efficient if one could devise a scheme which works with arbitrary points along the body or shear layer and increments the characteristic mesh along the reference freestream Mach line. Then only one calculation would be required along each characteristic, rather that the

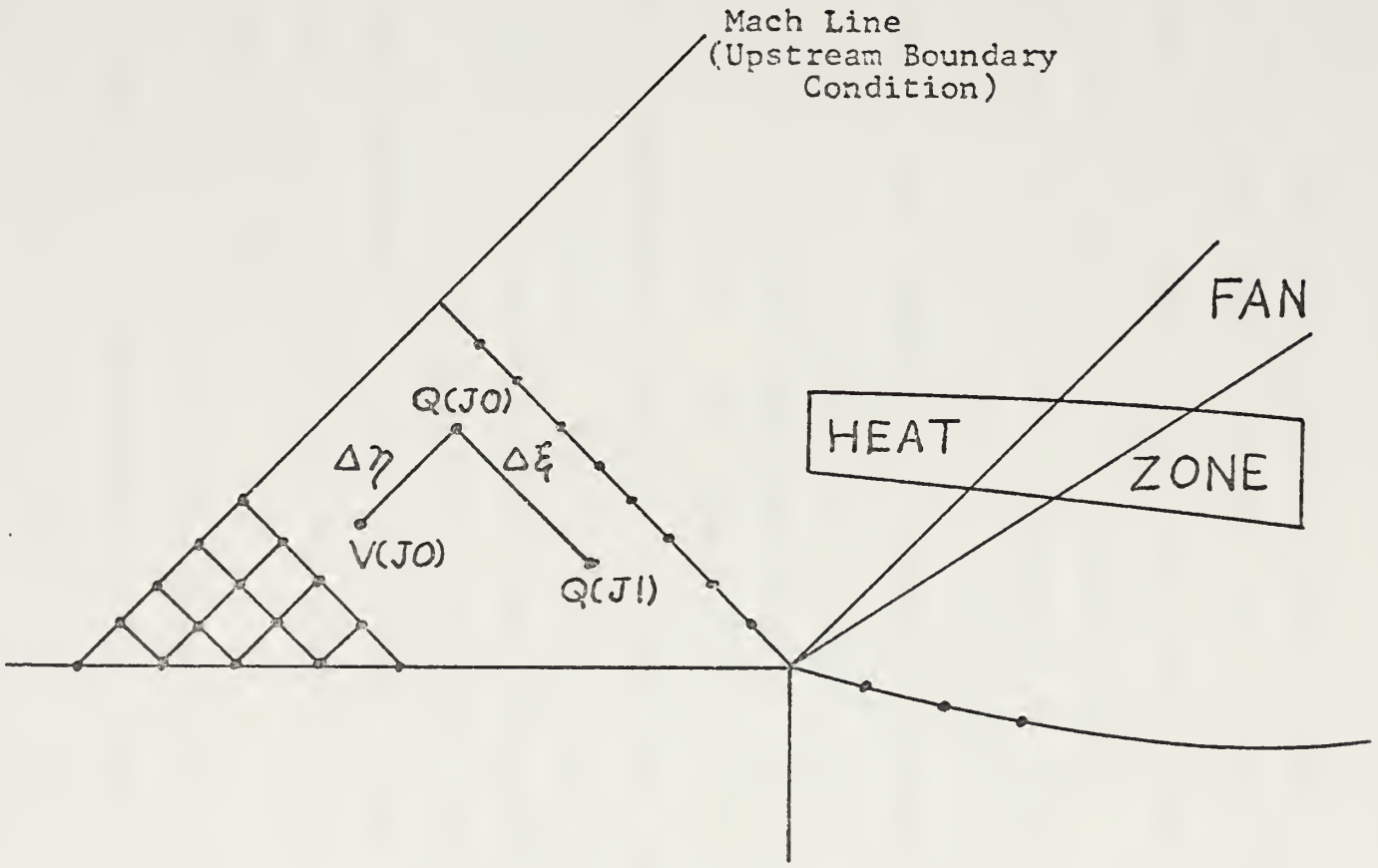

Figure 15. Characteristic Mesh

iterative scheme used in the present method. This approach was considered, but it was not clear how one would formulate the calculation for the corner or the shear layer mass influx (Appendix E).

The flow field was calculated along the body to the base at which point all computed values along the last characteristic were stored. These values were used to reset the flow field for each iteration of the straddle method.

The Crocco-Lees theory was formulated in terms of w_e instead of Mach number, where w_e is the velocity at the edge of the shear layer divided by the freestream stagnation speed of sound, $w_e = U/a_s$. To start the straddle method a value of w_e was chosen for the downstream side of the expansion fan which was too large. The expansion fan was divided into ten parts; downstream of the fan the computation proceeded toward the critical point. Each new point along the shear layer, computed by the Crocco-Lees theory (Appendixes C, E and F), required several iterations along the characteristic to the upstream Mach line boundary condition, where the flow angle error after each iteration was used to correct the shear layer flow angle.

Integration in the F - w_e plane followed the first path shown in Fig. 16. It can be seen that this path falls to the right of the path passing through the saddle point singularity, x, and, as the value of F was decreased, the slope, dF/dw_e, became negative at 1'. This occurred when the denominator used to form dF/dw_e became positive [Ref. 8], i.e. both the numerator and denominator of dF/dw_e were

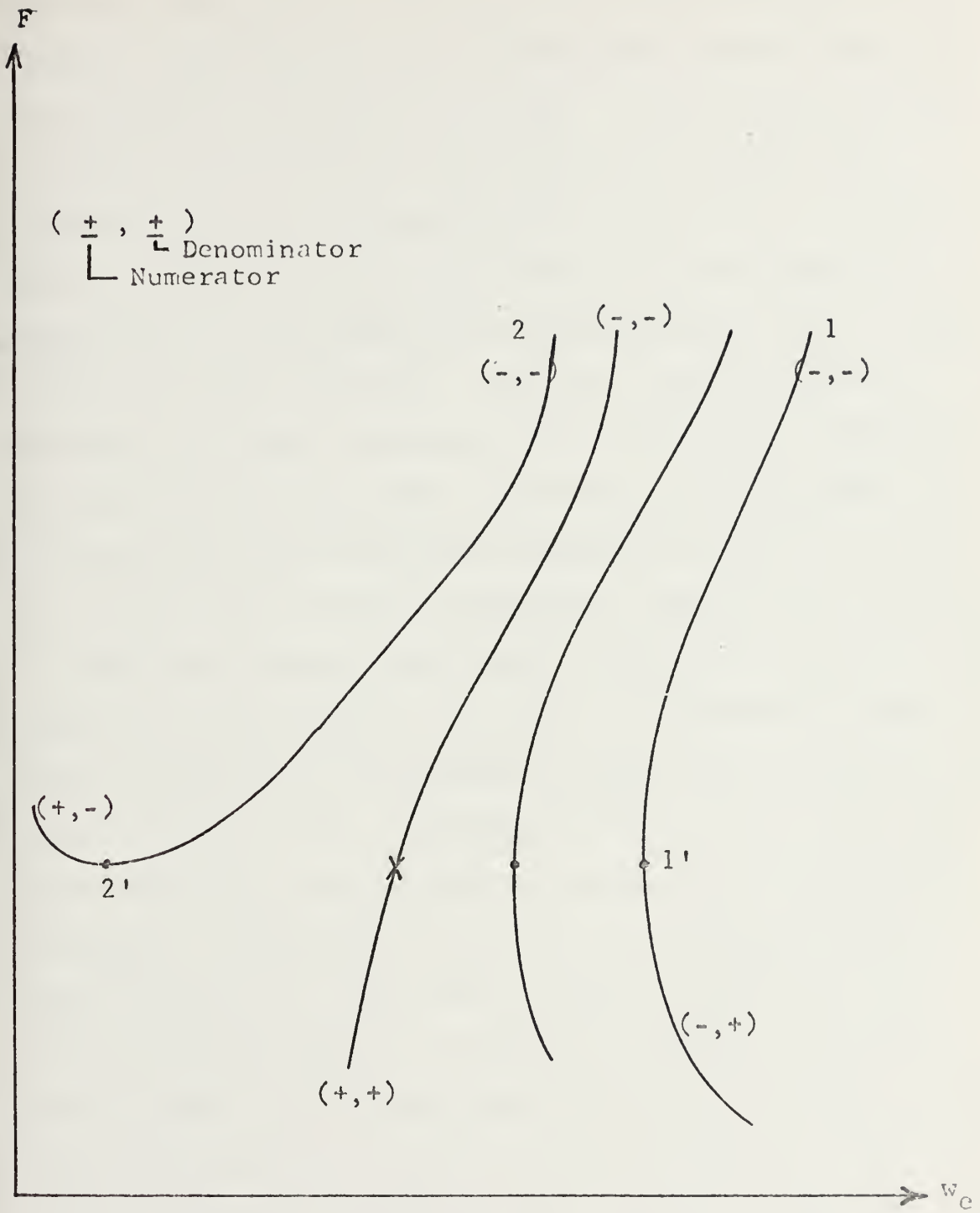

Figure 16. Integration in the F - w_e Plane

negative from 1 to 1'. This transition from positive to negative slope with positive denominator occurred when the initial guess for w_c was too large. By systematically decreasing the initial guess for w_e, say by tenths, one eventually has the integration path from 2 to 2', which is similar to the previous case, except that the negative slope at 2' is associated with the numerator, used to form dF/dw_e, becoming positive. Thus, the last two initial guesses for w_e have straddled the saddle point singularity. The interval between these two values may be divided, say in hundredths, and the process repeated to find two values of w_c which more closely straddle the saddle point singularity.

The heat zone was specified to start and stop at certain values of axial position, z, and to lie between an inner and outer streamline. The quantity $r_b q/Uc_p T$ was assigned a constant numerical value, between 0.15 and 0.175, within the zone, which gave the desired -4½° deflection to the inner streamline. External to the heat zone $r_b q/Uc_p T$ was zero. Before deflection, the inner and outer streamlines have values of approximately 2.0 and 3.0, maximum body radius, respectively. These values were chosen to match the rate of compression increase used in the nozzle design. As the computation proceeded downstream, the values of radius and flow angle for the inner and outer streamlines were computed to insure realistic boundaries for the heat zone.

When a sufficient amount of properly located heat was added to the external flow, the base pressure ratio was

computed to be greater than 1. It is interesting to note that for this condition the method of characteristics routine generated a compression fan at the base, rather than the usual expansion fan. The compression fan calculation mathematically folds the flow field on itself [Ref. 31]. This of course is physically impossible and is replaced in real flow by an oblique shock. For values of p_b/p_∞ = 1.5 at Mach 2.0, the loss of total pressure due to the oblique shock is less than 1%, which corresponds to an entropy increase, $\Delta S/R$, of 0.01. This resulted in an error of less than 0.18° in the turning angle, which was neglected. There is also the possibility of boundary layer separation upstream of the base for values of p_b/p_∞ greater than one [Ref. 7]. This effect was not considered in the calculations. The computer program is discussed in Appendix J.

V. DISCUSSION OF RESULTS

The computed values of p_b/p_∞ versus Re_b, shown in Fig. 9, were based on the apparent transition Reynolds numbers from the uniform flow nozzle experiments. These were $Re_{tr} = 1.95X10^6$ and $Re_{trt} = 7.8X10^6$. The curves display the same general features and approximate values found from experiment [Ref. 32-35]. It should be noted in Fig. 9 that for both the two dimensional planar and axisymmetric flow the maximum value of p_b/p_∞ occurred below Re_{tr} and the minimum value of p_b/p_∞ occurred below Re_{trt}.

A slightly different choice of transition Reynolds numbers, $Re_{tr} = 1.5X10^6$ and $Re_{trt} = 6.0X10^6$, resulted in the curve of p_b/p_∞ versus Reynolds number shown in Fig. 17. One may compare the curves of p_b/p_∞ in Fig. 9 and Fig. 17 with the experimental curves shown in Fig. 18. While the curves are by no means identical, they do agree in having the same general shape. Figure 19 shows additional experimental data to compare with Fig. 9. The locations of maximum and minimum computed p_b/p_∞ are controlled by the choice of values for Re_{tr} and Re_{trt}. The ratio of ¼ for Re_{tr}/Re_{trt} used in these computations was based on information in reference 8. This ratio is an approximation which varies considerably for different bodies, depending on their shape and surface condition. The maximum value of p_b/p_∞ was controlled by the choice of k_L, while the choice of k_T controlled the second

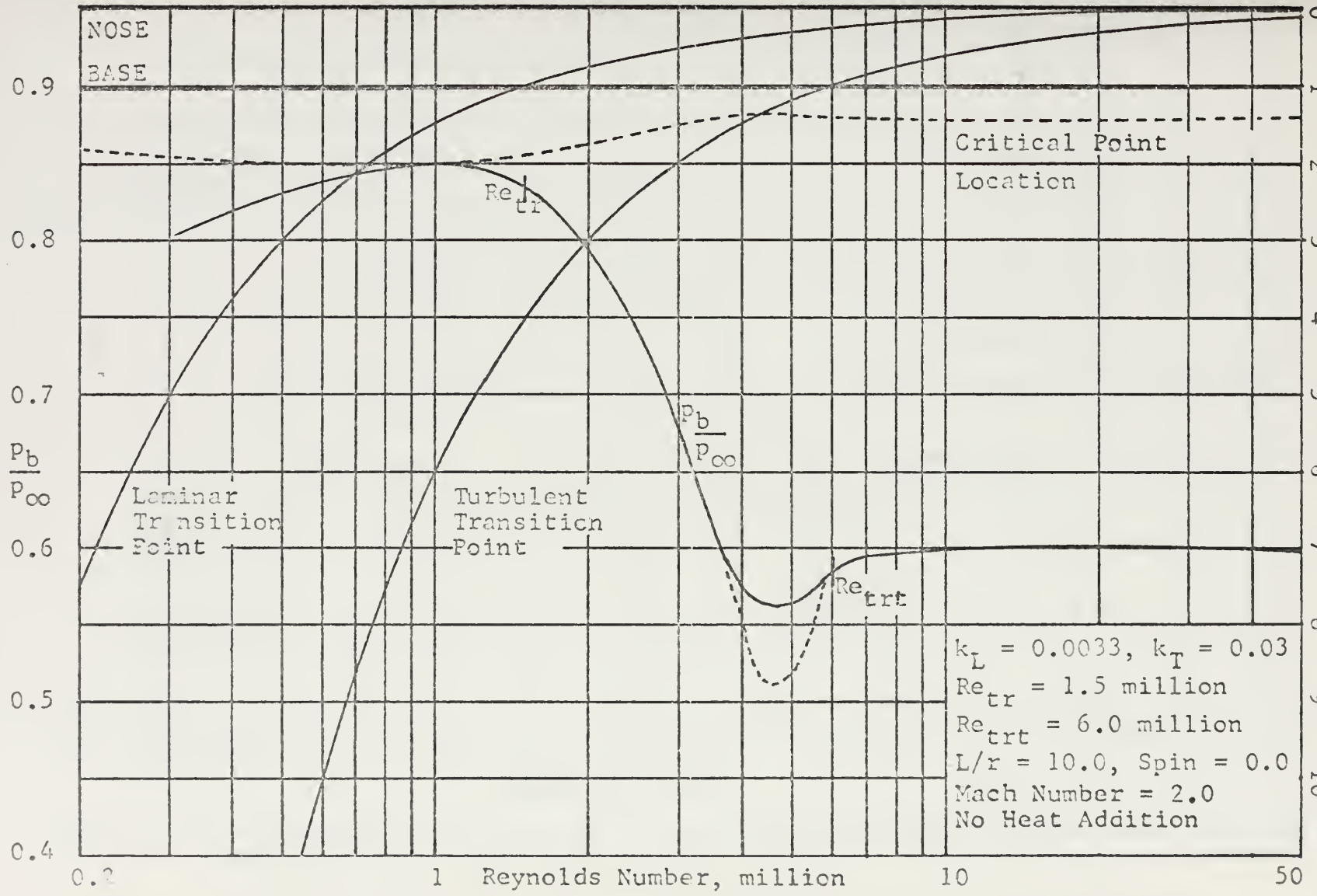

Figure 17. Computed Values of p_b/p_∞, Transition Points and Critical Point

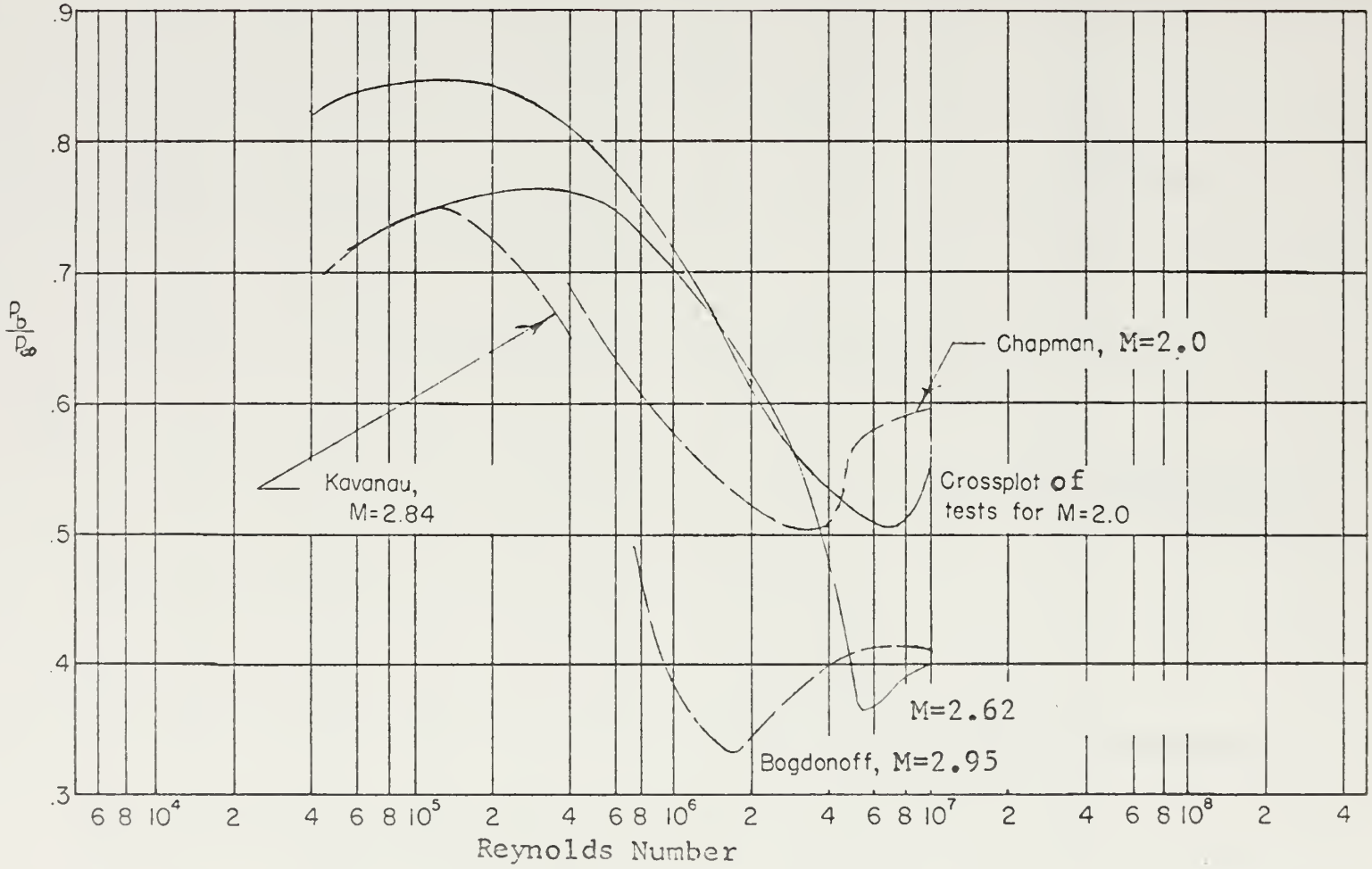

Figure 18. Experimental Values of p_b/p_∞ vs. Reynolds Number Without Heat Addition, from Ref. 32.

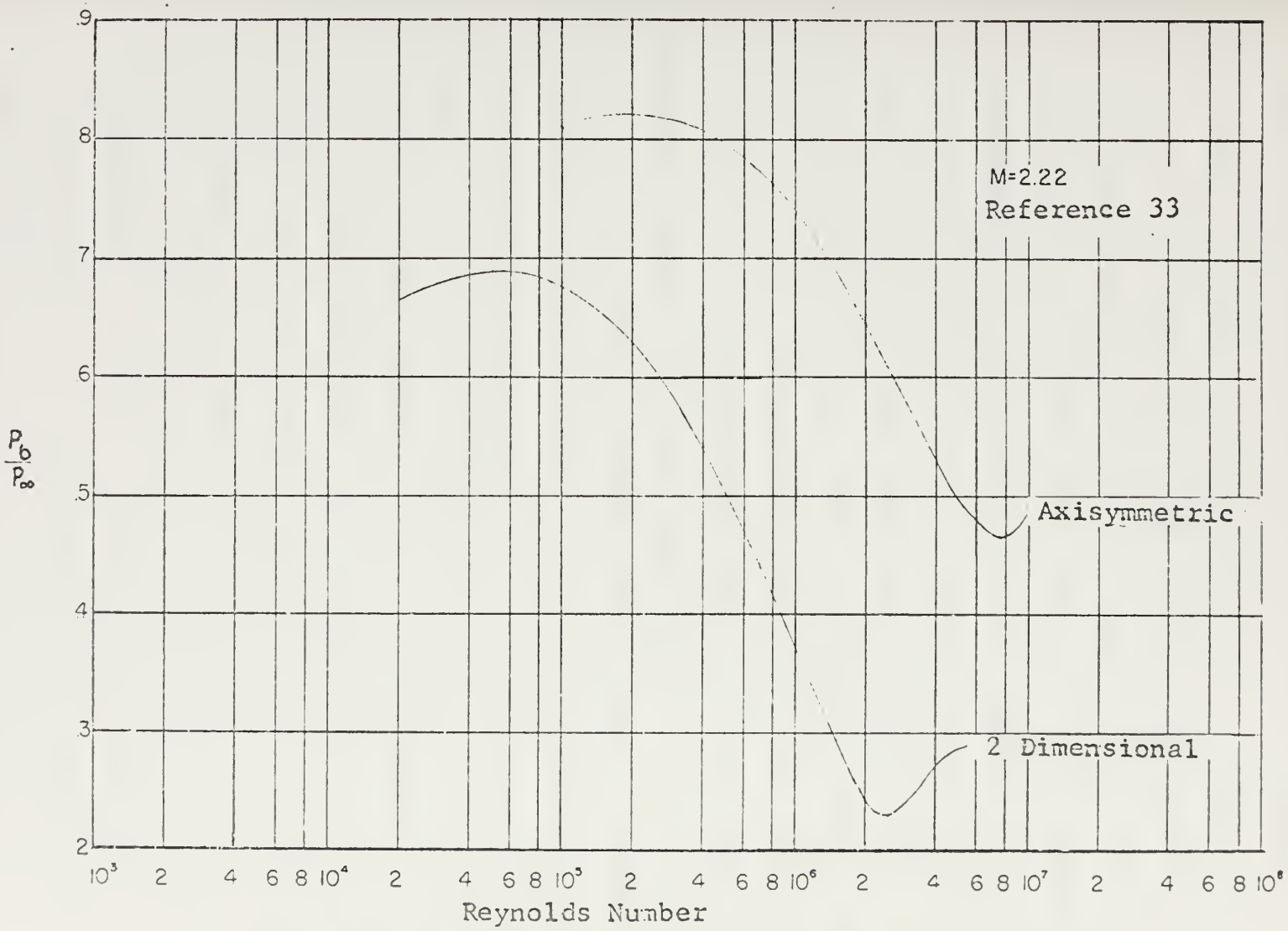

Figure 19. Experimental Values of p_b/p_∞ vs. Reynolds Number Without Heat Addition

maximum value of p_b/p_∞ to the right of Re_{trt}. The slight decrease of p_b/p_∞ to the right of this second maximum is in agreement with the r/δ sensitivity curve of Fig. 8, since increasing Re decreases δ and therefore increases r/δ.

Three additional curves are shown in Fig. 17; these are transition and critical point locations. The laminar and turbulent transition points are found simply by dividing base Reynolds number into Re_{tr} and Re_{trt}. The critical point location was taken from calculation with the Crocco-Lees equations along the shear layer where dF/dw_e changed signs; it is the singularity in Fig. 16 which was discussed in Section IV. In going from small to large values of Reynolds number, the shear layer between the critical point and the base gradually changes from completely laminar to completely turbulent as the laminar and turbulent transition points move upstream to the base and then onto the body. Where this occurs, the shear layer mixing coefficient, k, gradually changes from k_L to k_T. Increasing from some small value of Reynolds number, the thickness of the laminar boundary layer at the base decreases until the laminar transition point reaches the base and moves onto the body. As the boundary layer at the base transitions to turbulent its thickness increases. The thickness continues to increase as the turbulent transition point moves forward along the body, reaching a maximum when the transition point is near the nose of the body. Beyond this point, the thickness decreases.

In Fig. 17, the value of p_b/p_∞ starts to decrease slightly before reaching Re_{tr}, while the laminar transition point is still on the shear layer and the base boundary layer is laminar. Although the boundary layer thickness is still decreasing at this point and in turn should provide an increase in p_b/p_∞, the value of k along part of the shear layer (between the laminar transition point and the critical point) starts to increase from k_L to k_T and consequently dominates the overall change in p_b/p_∞ with Reynolds number.

The mechanism responsible for the abrupt minimum value of p_b/p_∞ in Fig. 18 was not clear. However, this minimum was calculated and is shown in Fig. 17 as a dashed line. From the sensitivity curve in Fig. 8, it appeared that k would be most likely quantity responsible. In numerical experiments this abrupt minimum was calculated by assuming additional mixing. The additional mixing was assumed to have a normal distribution about Re_{trt}, i.e. $k = k_T(1+(e^{-x^2/2})/(2\pi)^{\frac{1}{2}})$. The argument, x, was adjusted so that the additional mixing fell to about ten percent of its maximum value in $2X10^6$ either side of Re_{trt}. This additional mixing was not used in any other calculations since it was not understood and was not clearly observed in the experimental data reported later in this section.

Calculations were made for external heat addition in two dimensional planar flow to compare with Strahle's previously reported calculations [Ref. 7]. The values of $Re_{tr} = 1.95X10^6$ and $Re_{trt} = 7.8X10^6$ were assumed and a

Reynolds number of $Re_b = 20.0X10^6$ gave the same value of δ/r used by Strahle. The Mach number was M = 2.3. The heat addition zone was started at the same point, z/r = 0.4, and assigned the same length, w/r = 3.0, but to avoid subsonic flow with the method of characteristics it was necessary to increase the height of the heat zone from the value of $0.2r_b$ used by Strahle to a value of one base radius. The values of $Q = r_b q/Uc_p T$ were reduced accordingly to provide the same total heat addition based on the rectangular heat zone used by Strahle, i.e. $Q = 0.2\eta/\tan\mu$. The results in Table II show good agreement at the low intensity of heat addition, but only fair agreement at the higher intensities with the method of characteristics program showing higher values of p_b/p_∞. Although the non linearity included in the method of characteristics calculation may be responsible for part of the higher base pressure ratio, the main cause was attributed to expansion of the heat zone. This effect was included in the bounding streamline calculation for the heat zone in the method of characteristics program and resulted in a greater amount of total heat added than in the linearized theory calculations.

Linearized Theory[7]		Method of Characteristics	
η	p_b/p_∞	Q	p_b/p_∞
0.0	0.420	0.0	0.410
0.4	0.657	0.167	0.669
0.8	0.900	0.334	1.075
1.2	1.158	0.5	1.45 ± 0.02

Table II. Comparison of Calculated Base Pressure Ratio with External Heat Addition, Two Dimensional Planar Flow and Mach Number of 2.3.

Both experimental and calculated results are shown in Fig. 20 for a Mach number of 2.0. The value of p_b/p_∞ = 0.6314 at Re_b = 10.4 was the average of nine runs with the uniform flow nozzle. The probable error about this average was ± 0.004, with a maximum observed deviation of - 0.0104. In comparing the experimental values of Fig. 20 and Table I with early test results using the free jet, variations as high as 7% in p_b/p_∞ were found for similar runs. These variations were attributed to problems, such as mechanical alignment during nozzle installation or leaks in the manometer tubing, which were found and corrected during subsequent testing.

Early test data were rejected and were not reported herein. As experience was gained with operation of the facility, the 7% variations were narrowed to less than 3½%.

Cylinder wall temperatures were also recorded during these nine runs using a thermocouple imbedded in the wall, 1½ inches from the base. These temperatures ranged from 5°F to 35°F. A plot of p_b/p_∞ versus temperature showed no correlation scatter in p_b/p_∞ due to temperature was less than 1.4%. Since the stagnation temperatures of the air supply were not recorded, they could not be compared with the cylinder wall temperatures.

The values of $Re_{tr} = 1.95X10^6$ and $Re_{trt} = 7.8X10^6$ were assumed for the computed values of p_b/p_∞ shown in Fig. 20 as triangles. The experimental values of p_b/p_∞ for the

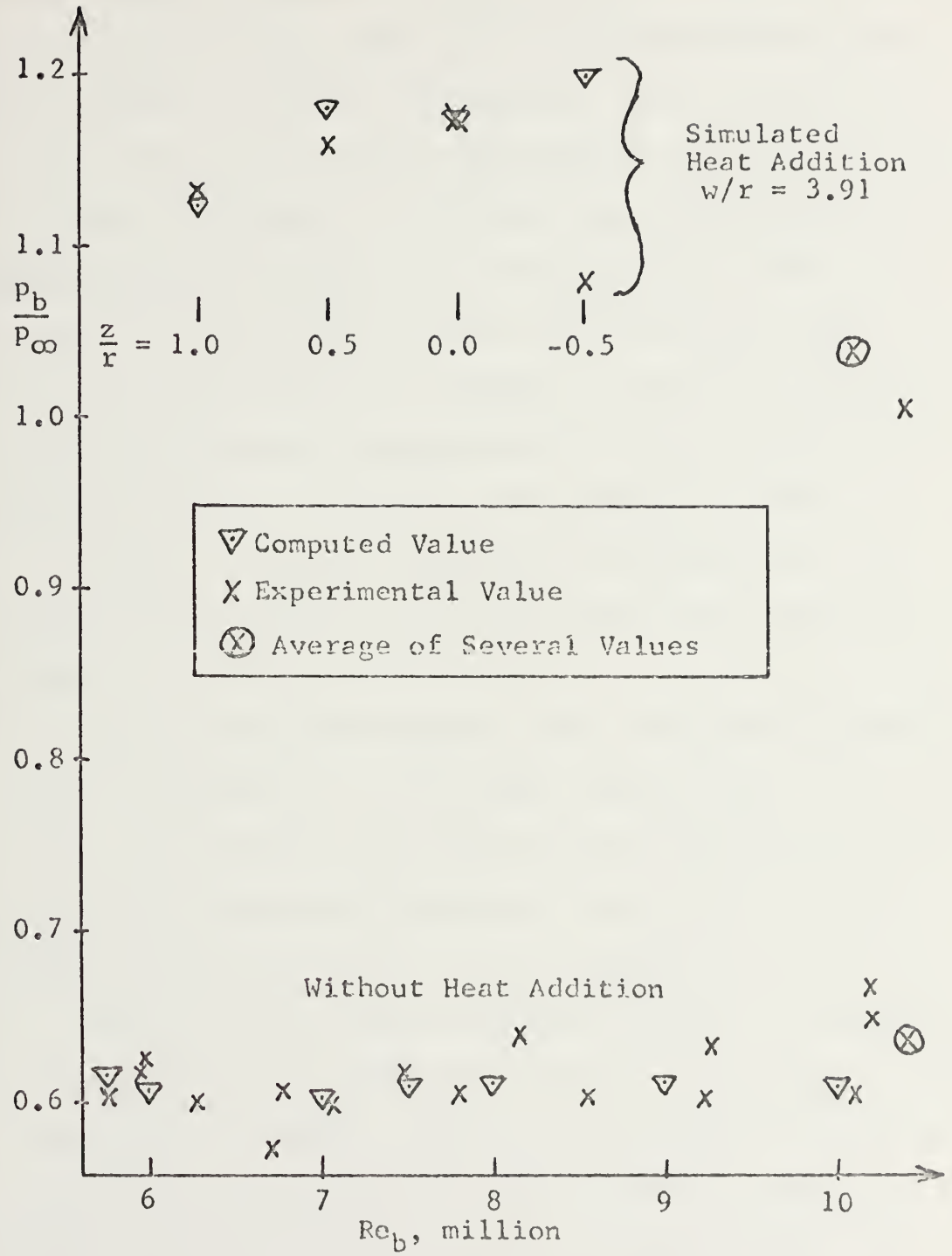

Figure 20. Comparison of Experimental and Computed Values of Base Pressure Ratio vs. Reynolds Number at Mach 2.0 Without and With Simulated Heat Addition

uniform flow nozzle without heat addition showed good agreement with the computed values. Three of the four experimental values of p_b/p_∞ with w/r = 3.91 compression agreed with the computed values. The observed value of p_b/p_∞ with z/r = -0.5 was less than the computed value. This difference was attributed to an adverse pressure gradient along the cylinder wall that was not considered in the calculation. In view of this result, base pressure ratios computed by the program given in Appendix J should be considered with caution if the full compression due to external burning impinges ahead of the base on the projectile body.

Figure 21 shows a comparison of experimental [Ref. 26] and computed values of base pressure ratio resulting from spin.

In the Crocco-Lees model there are several input parameters including M_∞, k_L, k_T, Re_{tr}, Re_{trt} and F - κ relationship. A procedure for predicting the influence of spin on p_b/p_∞ was discussed previously at the end of Section II. This procedure was used for the computed values in Fig. 21.

Choice of the input parameters remains. Preliminary calculations were conducted with M_∞ = 2.86, $Re_{tr} = 1.95X10^6$ and $Re_{trt} = 4.6X10^6$. Values of p_b/p_∞ had the correct trends relative to experimental values. However, the calculated p_b/p_∞ for $Re_b = 2.6X10^6$ and zero spin was about 0.54. To decrease the calculated p_b/p_∞, the Mach number was arbitrarily increased to 3.0. For $Re_b = 2.6X10^6$, zero spin and M_∞ = 3.0, the calculated and observed p_b/p_∞ values agree. In

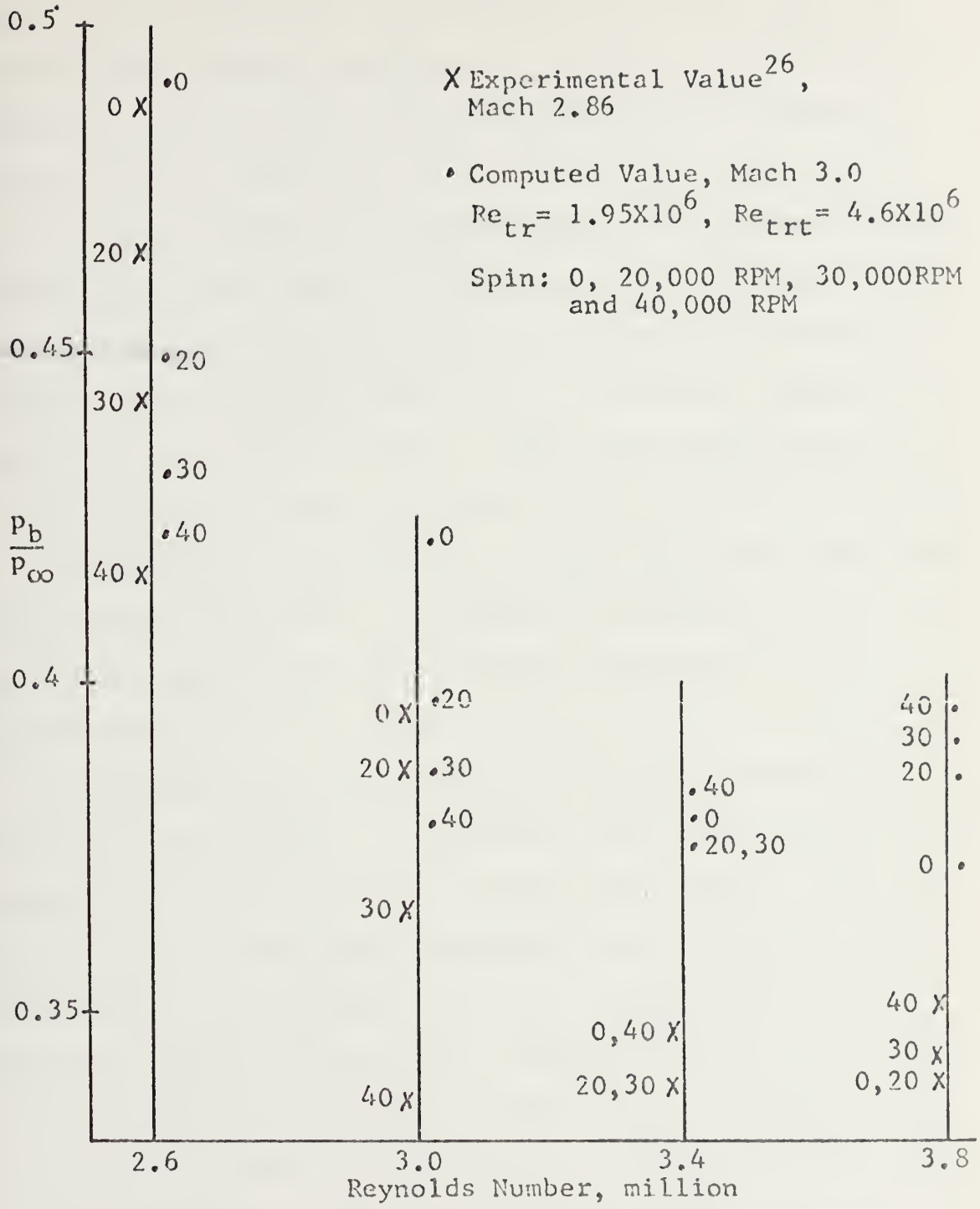

Figure 21. Comparison of Experimental[26] and Computed Values of Base Pressure Ratio vs. Reynolds Number With Spin

retrospect, additional calculations should have been conducted with increased mixing, i.e. larger k_T, while retaining correct $M_\infty = 2.86$. In fact, spin should increase k_T as discussed in Section II.

A better procedure for calculating the influence of spin might be to use a shift in transition Reynolds number coupled with a $k_{spin} = k(1+(r\omega/U))$, as discussed by Smithey, Naber, Caswell and Fuhs [Ref. 15]. The dashed segment of p_b/p_∞ vs. Re_b curve in Fig. 17 shows the influence of increased mixing (larger k_T) in the vicinity of minimum p_b/p_∞.

The computed values shown in Fig. 21 required four hours time on the IBM 360/67. In view of the computing time, the procedure suggested in the preceding paragraph was not accomplished.

To provide some estimate of the optimum location for external heat addition, a fixed fuel flow was assumed to be burned in zones of different length and location. The initial radius of the inner streamline was 2.0 and the outer streamline initial radius was 3.0. The heat zone were assigned integer values from 1 through 6 for w/r. The zone with w/r = 1.0 was assigned a value of $Q = r_b q/Uc_p T = 0.2$. This value was decreased by 1/(w/r) for the other five zones. The heat zones were positioned along the axial axis starting with compression at the base and moving downstream in integer values of radius. The results of two of these computations are shown as the two lower curves in Fig. 22. The

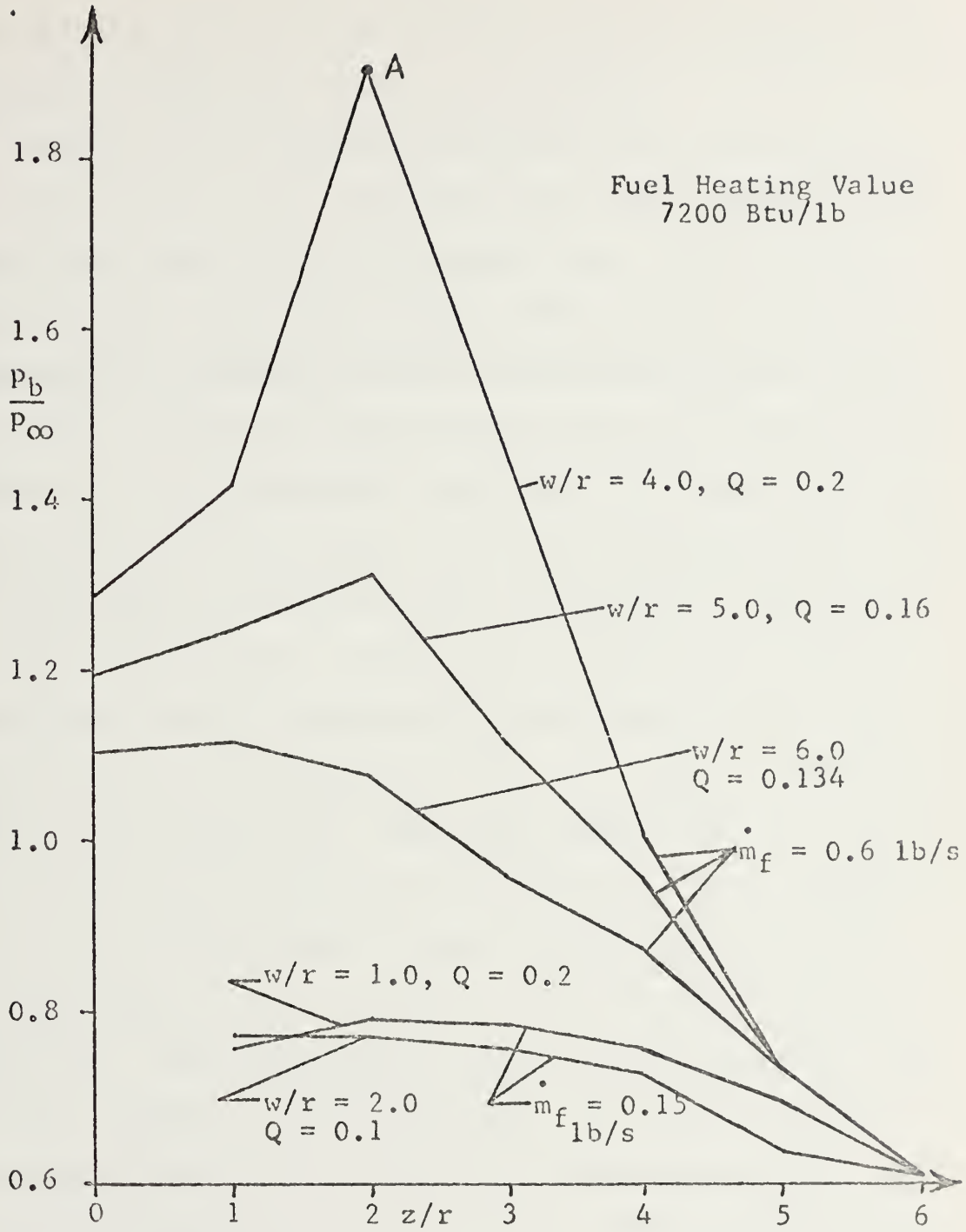

Figure 22. Computed Values of Base Pressure Ratio at a Mach Number of 2.0 With External Burning

gain in p_b/p_∞ for $\dot{m}$ = 0.15 lb/sec is seen to be fairly insensitive to heat zone size and placement.

Another set of similar calculations were made based on Q = 0.8 at w/r = 1.0. This value of Q corresponded to the design fuel flow rate of 0.6 pounds per second at 23,000 feet altitude. The first three values of w/r, 1.0,2.0 or 3.0 would not compute because the external flow was driven to a sonic condition by the base pressure rise and the heat addition. This condition is analogous of thermal choking; however, in two dimensional flow both streamtube area change and heat addition drive the flow toward sonic conditions. The last three values of w/r = 4.0, 5.0 and 6.0, did not experience subsonic conditions in the external flow and their values of base pressure ratio are shown as the upper three curves in Fig. 22. The high value of p_b/p_∞ = 1.91 for the w/r = 4.0 curve was not expected. This represents a factor of six increase in base pressure over the two bottom curves in Fig. 22 with a factor of four increase in fuel flow. The combustion for this flight condition, Fig. 23, was assumed to start at (z/r) = -1.2 and the initial compression was on the shear layer, downstream of the base, with full compression at z/r = +2.0. There is some error in the calculation introduced by neglecting vorticity and by the compression fan at the base, rather than the oblique shock. See Shaprio [Ref. 31] for a discussion of compression fans. Assuming as much as a 1° error in the flow angle, far exceeding the estimate given in Section IV, the value of

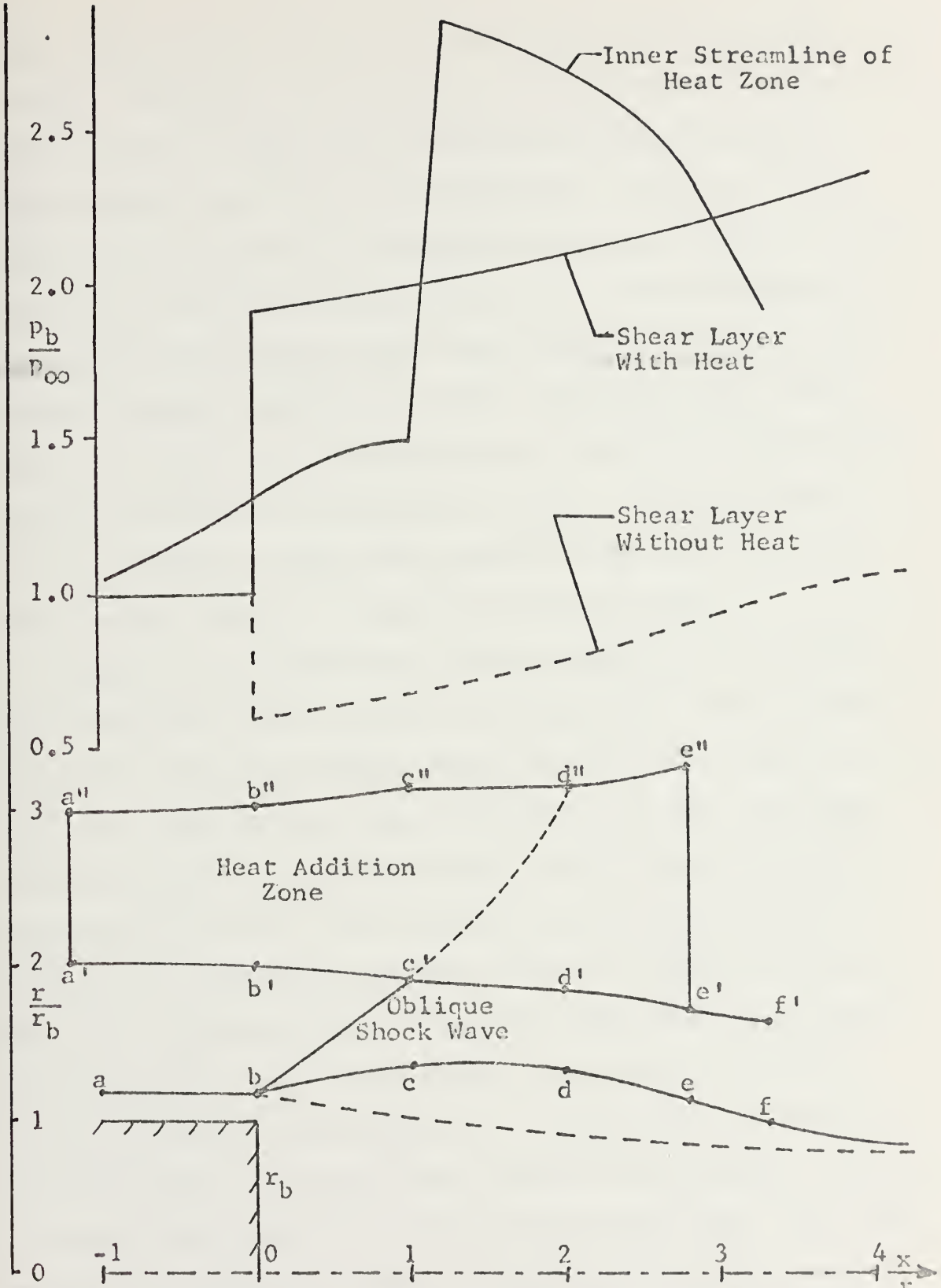

Figure 23. Comparison of Calculated Base Flow With And Without Heat Addition at Mach 2.0

p_b/p_∞^* remains at 1.8 and gives specific impulse of 230 seconds. With w/r = 4.0 and z/r = 2.0, part of the compression due to combustion was applied along the shear layer downstream of the critical point. With z/r = 1.0 more of the compression was applied upstream of the critical point, but the base pressure was less. The variation of p_b/p_∞ with z/r indicates that the location of dp/ds (due to the external compression waves) along the shear layer may be an important consideration in achieving high values of base pressure with external burning. This hypothesis and the condition where the external flow with heat addition becomes subsonic require additional study.

Figure 23 provides some details regarding the optimum flow condition shown in Fig. 22 as point A. The heat zone and shear layer have been plotted in the lower half of Fig. 23. The boundary layer thickness has been included as well as the oblique shock wave which forms when p_b/p_∞ is greater than one. For comparison, the shear layer without heat addition has been shown as a dashed curve in Fig. 23. Pressure ratios along the shear layer have been plotted in the upper half of Fig. 23; again, the dashed curve is without heat addition. In both cases, with and without heat, the shear layer pressure ratio shows a gradual increase with distance downstream from the base. The pressure ratio along the inner streamline of the heat zone (points a' through e') has also been plotted along with the shear layer pressure ratios (points a through f). This

streamline experiences an abrupt increase in pressure ratio where it intersects the oblique shock wave at c'; then, its pressure ratio starts to decrease with a corresponding increase in Mach number, indicating that the flow along the inner streamline accelerates downstream of the oblique shock wave. The calculation along the shear layer was terminated before reaching a maximum pressure ratio due to the saddle point singularity, Fig. 4, since the straddle method employed in the computer program had established the required base pressure ratio within ± ½%.

Additional calculations with the computer program given in Appendix J would improve the accuracy of p_b/p_∞ and would take values for the shear layer slightly closer to the critical point, but, since the critical point is a saddle point singularity, would not be expected to calculate through the critical point. Calculation "through" the critical point, using the straddle method, would require changes in the program to restrict the values allowed for dF/dw_e and force the calculation across the singularity. Additional study is required to include this change and provide the capability of calculating the entire base flow field.

To verify the existence of an oblique shock wave at the base, which was calculated in Fig. 23, one may consider the field of compression waves impinging on the shear layer as being concentrated into a single oblique shock wave impinging on the shear layer. This simplified condition, shown in Fig. 24, has been studied experimentally by Korst

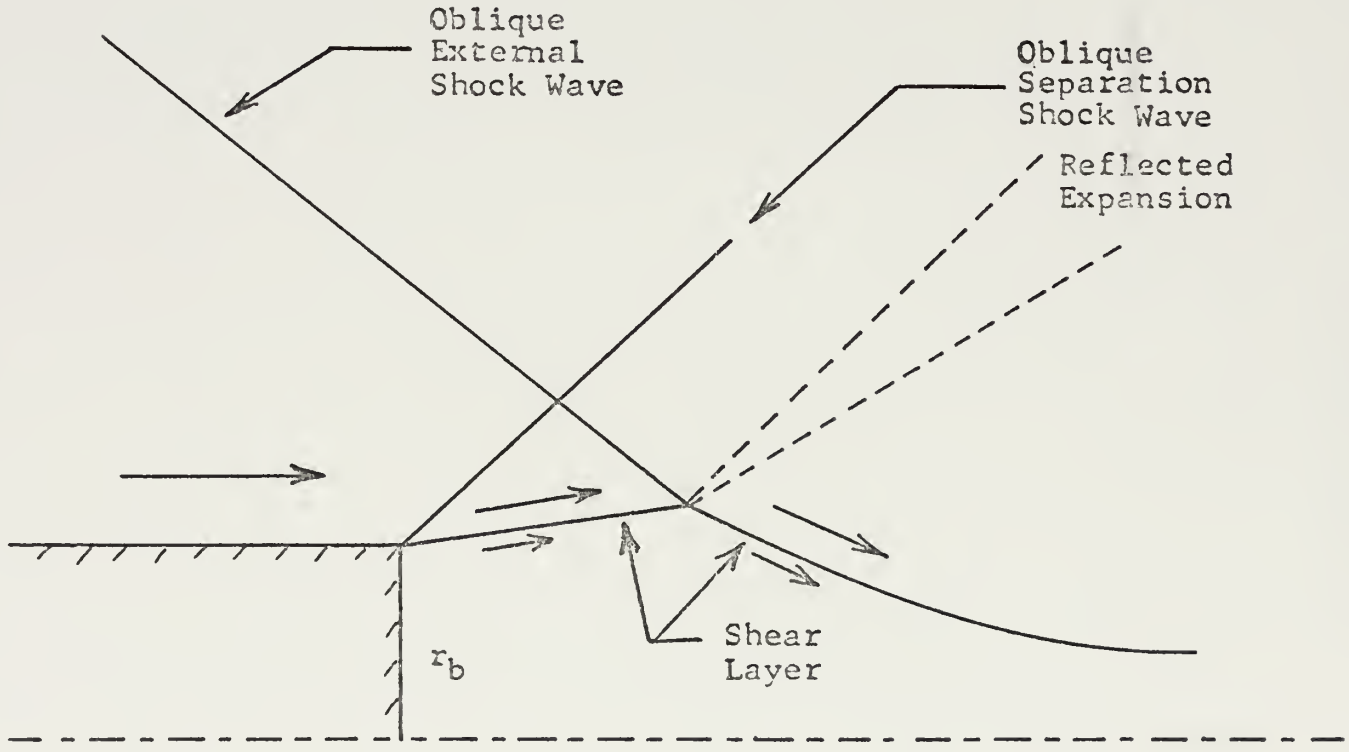

Figure 24. Schematic Diagram of Resulting Base Flow When an External Shock Wave Impinges on the Shear Layer

[Ref. 36] and was found to create an oblique shock wave at the base. Thus, the calculated shear layer profile and pressure ratios in Fig. 23 are in agreement with experimental results from the simplified condition.

VI. CONCLUSIONS

With the method of characteristics and the Crocco-Lees base flow model, one can accurately predict the base pressure ratio of a two dimensional or axisymmetric body with moderate external burning for various Mach and Reynolds numbers. The correct values for the two transition Reynolds numbers are essential for accurate base pressure ratio calculation of a particular body and should be obtained from experiment. The effect of projectile spin can be included approximately by dividing the transition Reynolds numbers with one plus the spin number.

Net thrust can be produced by external burning. Placing the combustion zone well forward of the base to give full compression on the body was found by experiment to produce a decrease in thrust. For maximum projectile thrust with supersonic external flow the computed heat zone placement was found to start 1.2 base radii upstream of the base and extend 4.0 base radii downstream. The zone started with an inner and outer streamline of 2.0 and 3.0 base radii respectively and received a fuel flow of 0.6 pounds per second of fuel rich propellant exhaust, ARC-168. It appeared higher values of base pressure would be possible with the same fuel flow rate by decreasing the length of the combustion zone still further. The flow field could not be computed with this heat distribution because of the resulting

subsonic flow and requires additional study to determine any further advantage or limits under these conditions. Experiments with actual combustion should be conducted to determine the feasibility of the desired combustion placement and to measure the resulting base pressure.

The rate of pressure increase along the shear layer due to the heat zone placement appeared to influence the computed value of base pressure ratio. This effect requires additional study to determine its significance in achieving higher values of base pressure ratio with external burning. Experimental studies are needed to determine any variation of the empirical F - κ relation when external pressure waves impinge on the shear layer.

APPENDIX A: DERIVATION OF THE CHARACTERISTIC EQUATIONS WITH HEAT ADDITION

Equations (1) through (4) govern steady compressible flow with heat addition [Ref. 18]. These equations neglect heat conduction, viscosity and body forces. In natural coordinates, Fig. 1, $\bar{U} = w\bar{s}$. The continuity equation, Eqn. (1), may be written

$$(2\pi r)^{\alpha} \rho w \Delta n = \text{constant} \tag{1A}$$

where $\alpha = 0$ for two dimensional planar flow and $\alpha = 1$ for axisymmetric flow. The momentum equation, Eqn. (2), may be written for the two unit vector directions, $\bar{s}$ and $\bar{n}$,

$$\left(\rho w \frac{\partial w}{\partial s} + \frac{\partial p}{\partial s} \right)\bar{s} = 0 \tag{2A}$$

$$\left(\rho w^2 \frac{\partial \theta}{\partial s} + \frac{\partial p}{\partial n} \right)\bar{n} = 0 \ . \tag{3A}$$

The energy equation, Eqn. (3), becomes

$$w\frac{\partial}{\partial s} \left(h + \frac{1}{2} w^2\right) = q = w \frac{\partial h_0}{\partial s} \tag{4A}$$

where the total enthalpy, $h_0 = h + \frac{1}{2}w^2$, has been used. The thermodynamic relation for entropy, S, may be written

$$T\nabla S = \nabla h - \frac{1}{\rho} \nabla p \tag{5A}$$

$$T\frac{\partial S}{\partial s} = - \left(w\frac{\partial w}{\partial s} + \frac{1}{\rho} \frac{\partial p}{\partial s}\right) + \frac{\partial h_0}{\partial s} \tag{6A}$$

$$T\frac{\partial S}{\partial n} = - \left(w\frac{\partial w}{\partial n} + \frac{1}{\rho} \frac{\partial p}{\partial n}\right) + \frac{\partial h_0}{\partial n} \ . \tag{7A}$$

Using Eqn. (3A) into (7A)

$$\frac{1}{w}\frac{\partial w}{\partial n} - \frac{\partial \theta}{\partial s} = -\frac{T}{w^2}\frac{\partial S}{\partial n} + \frac{1}{w^2}\frac{\partial h_0}{\partial n} \quad . \tag{8A}$$

Forming the logarithmic derivative of Eqn. (1A) in the s direction

$$\frac{\alpha}{r}\sin\theta + \frac{1}{\rho}\frac{\partial \rho}{\partial s} + \frac{1}{w}\frac{\partial w}{\partial s} + \frac{\partial \theta}{\partial n} = 0 \tag{9A}$$

where the relations $\partial r/\partial s = \sin\theta$ and $[1/\Delta n][\partial \Delta n/\partial s] = \partial\theta/\partial n$ have been used. Forming the logarithmic derivative of Eqn. (4) in the s direction

$$\frac{1}{p}\frac{\partial p}{\partial s} = \frac{1}{\rho}\frac{\partial \rho}{\partial s} + \frac{1}{T}\frac{\partial T}{\partial s} \quad . \tag{10A}$$

Substituting Eqns. (2A) and (10A) into (9A)

$$\frac{\alpha}{r}\sin\theta + \left(\frac{1}{w} - \frac{w}{RT}\right)\frac{\partial w}{\partial s} - \frac{1}{T}\frac{\partial T}{\partial s} + \frac{\partial \theta}{\partial n} = 0. \tag{11A}$$

From Eqn. (4A)

$$\frac{q}{w} = c_p\frac{\partial T}{\partial s} + w\frac{\partial w}{\partial s} \tag{12A}$$

where the enthalpy has been written in terms of a constant c_p, $h = c_pT$. Substituting Eqn. (12A) into (11A)

$$\left(\frac{1}{w} - \frac{w}{RT} + \frac{w}{c_pT}\right)\frac{\partial w}{\partial s} + \frac{\partial \theta}{\partial n} - \frac{q}{wc_pT} + \frac{\alpha\sin\theta}{r} = 0. \tag{13A}$$

Combining terms, and using the Mach angle relation $\cot^2\mu = M^2 - 1$, Eqn. (13A) becomes

$$\frac{\cot^2\mu}{w}\frac{\partial w}{\partial s} - \frac{\partial \theta}{\partial n} = \frac{\alpha\sin\theta}{r} - \frac{q}{wc_pT} \quad . \tag{14A}$$

The Prandtl-Meyer Angle, ν, is defined by the relation

$$d\nu = \frac{\cot\mu}{w}\, dw \ . \tag{15A}$$

Using Eqn. (15A) into (14A) and multiplying by tan μ

$$\frac{\partial \nu}{\partial s} - \tan\mu \frac{\partial \theta}{\partial n} = \tan\mu \left\{ \frac{\alpha \sin\theta}{r} - \frac{q}{wc_p T} \right\} . \tag{16A}$$

Similarly, Eqn. (15A) into (8A) becomes

$$\tan\mu \frac{\partial \nu}{\partial n} - \frac{\partial \theta}{\partial s} = - \frac{T}{w^2} \frac{\partial S}{\partial n} + \frac{1}{w^2} \frac{\partial h_0}{\partial n} \ . \tag{17A}$$

Adding Eqns. (16A) and (17A)

$$\left(\frac{\partial}{\partial s} + \tan\mu \frac{\partial}{\partial n} \right)(\nu - \theta) = \tan\mu \left\{ \frac{\alpha \sin\theta}{r} - \frac{q}{wc_p T} \right\} - \frac{1}{w^2} \left\{ T \frac{\partial S}{\partial n} - \frac{\partial h_0}{\partial n} \right\} . \tag{18A}$$

Subtracting Eqn. (17A) from (16A)

$$\left(\frac{\partial}{\partial s} - \tan\mu \frac{\partial}{\partial n} \right)(\nu + \theta) = \tan\mu \left\{ \frac{\alpha \sin\theta}{r} - \frac{q}{wc_p T} \right\} + \frac{1}{w^2} \left\{ T \frac{\partial S}{\partial n} - \frac{\partial h_0}{\partial n} \right\} . \tag{19A}$$

Now, in the characteristic coordinate system

$$\sec\mu \frac{\partial (\quad)}{\partial \eta} = \left(\frac{\partial}{\partial s} + \tan\mu \frac{\partial}{\partial n} \right)(\quad) \tag{20A}$$

and

$$\sec\mu \frac{\partial (\quad)}{\partial \xi} = \left(\frac{\partial}{\partial s} - \tan\mu \frac{\partial}{\partial n} \right)(\quad) \ . \tag{21A}$$

With this, Eqns. (18A) and (19A) become

$$\frac{\partial(\nu - \theta)}{\partial\eta} = \sin\mu \left\{ \frac{\alpha\sin\theta}{r} - \frac{q}{wc_pT} \right\} - \frac{\cos\mu}{w^2} \left\{ T\frac{\partial S}{\partial n} - \frac{\partial h_0}{\partial n} \right\} \tag{22A}$$

and

$$\frac{\partial(\nu + \theta)}{\partial\xi} = \sin\mu \left\{ \frac{\alpha\sin\theta}{r} - \frac{q}{wc_pT} \right\} + \frac{\cos\mu}{w^2} \left\{ T\frac{\partial S}{\partial n} - \frac{\partial h_0}{\partial n} \right\}. \tag{23A}$$

Eqns. (22A) and (23A) are the characteristic equations, with heat addition, governing the two dimensional planar, $\alpha = 0$, or axisymmetric, $\alpha = 1$, flow. These equations are dimensional, having the dimension of reciprocal length.

APPENDIX B: DERIVATION OF CONDITION FOR IRROTATIONALITY WITH HEAT ADDITION

The equations required for this derivation are momentum with no viscosity or body force,

$$\frac{D\bar{U}}{Dt} = -\frac{1}{\rho}\nabla p \tag{1B}$$

where $\bar{U}$ is velocity, ρ is density, and p is static pressure; energy with heat addition, but without viscosity, body force, or conduction,

$$\frac{D(h + \frac{1}{2}\bar{U}\cdot\bar{U})}{Dt} = q + \frac{1}{\rho}\frac{\partial p}{\partial t} \tag{2B}$$

where h is enthalpy, and q is time rate of heat addition per unit mass; the second law of thermodynamics

$$T\nabla S = \nabla h - \frac{1}{\rho}\nabla p \tag{3B}$$

where S is specific entropy; and the vector identity

$$\bar{U}\cdot\nabla\bar{U} = \nabla(\tfrac{1}{2}\bar{U}\cdot\bar{U}) - \bar{U}\times(\nabla\times\bar{U}). \tag{4B}$$

Combining Eqns. (1B), (3B) and (4B)

$$\frac{\partial\bar{U}}{\partial t} + \nabla(\frac{1}{2}\bar{U}\cdot\bar{U}) - \bar{U}\times(\nabla\times\bar{U}) = T\nabla S - \nabla h . \tag{5B}$$

Introducing the definition for total enthalpy, $h_0 = h + \frac{1}{2}\bar{U}\cdot\bar{U}$, into Eqn. (5B), one obtains Croccos's Theorem

$$T\nabla S + \bar{U}\times(\nabla\times\bar{U}) = \nabla h_0 + \frac{\partial\bar{U}}{\partial t} . \tag{6B}$$

Let $\nabla\times\bar{U} = \bar{\Omega}$ and take the curl of Eqn. (6B),

$$\frac{D\bar{\Omega}}{Dt} = \nabla T\times\nabla S + \bar{\Omega}\cdot\nabla\bar{U} - \bar{\Omega}\nabla\cdot\bar{U} \tag{7B}$$

since $\nabla\cdot\overline{\Omega} = \nabla\cdot(\nabla X\overline{U}) = 0$ and the curl of a gradient is zero. Eqn. (7B) describes the total rate of change of vorticity, $\overline{\Omega}$.

Now assume that $\overline{\Omega} = 0$ prior to and during heat addition. Eqn. (7B) becomes

$$\frac{D\overline{\Omega}}{Dt} = \nabla T X \nabla S = 0. \tag{8B}$$

Then, Eqn. (8B) is the condition which must be satisfied during heat addition if the flow is to remain irrotational; that is, the temperature gradient must be parallel to the entropy gradient. Referring to Eqn. (3B) and assuming $h = c_p T$, where c_p is constant, the condition for irrotationality may be stated in terms of pressure; that is, the temperature gradient must be parallel to the pressure gradient.

In the case of steady flow, the irrotationality condition may be given in terms of heat per unit mass which has been added, Q. In Eqn. (2B) let $q = \overline{U}\cdot\nabla Q$, and, using the total enthalpy $h_0 = h + \frac{1}{2}\overline{U}\cdot\overline{U}$,

$$\overline{U}\cdot\nabla(h_0 - Q) = 0. \tag{9B}$$

Then along any streamline

$$h_0 - Q = h_{0_\infty} \tag{10B}$$

where it is assumed that the upstream conditions, before heat is added, i.e. $Q = 0$, are uniform [Ref. 19]. With these assumptions one may take the gradient of Eqn. (10B)

$$\nabla(h_0 - Q) = 0 \tag{11B}$$

since h_{0_∞} is constant. Using the steady form of Eqn. (6B), with $\bar{\Omega} = 0$, and Eqn. (11B)

$$\nabla S = \frac{1}{T} \nabla h_0 = \frac{1}{T} \nabla Q. \tag{12B}$$

Also, from Eqn. (11B), one may write

$$\nabla Q = \nabla(h + \tfrac{1}{2}\bar{U}\cdot\bar{U}) = c_p \nabla T + \nabla(\tfrac{1}{2}\bar{U}\cdot\bar{U}). \tag{13B}$$

Combining Eqns. (12B) and (13B) in (8B)

$$\frac{1}{c_p} \left\{ \nabla Q - \nabla(\tfrac{1}{2}\bar{U}\cdot\bar{U}) \right\} \times \frac{1}{T} \nabla Q = 0. \tag{14B}$$

Since $(\nabla Q)\times(\nabla Q) = 0$, Eqn. (14B) reduces to

$$(\nabla Q)\times\nabla(\tfrac{1}{2}\bar{U}\cdot\bar{U}) = 0. \tag{15B}$$

Eqn. (15B) is the condition which must be satisfied to preserve irrotationality in steady flow with heat addition; that is, the gradient of heat added must be parallel to the gradient of kinetic energy.

If the gradient of heat added is a small perturbation, as is the case of linearized flow, then the irrotationality condition in Eqn. (15B) is automatically satisfied. To show this let $Q = h_\infty Q'$, where $|Q'| << 1$, and $\bar{U} = U_\infty(\bar{i} + \frac{\bar{U}'}{U_\infty})$, where $\bar{U}'\cdot\bar{U}' << 1$, then, substituting in Eqn. (15B),

$$\nabla Q \times \nabla(\tfrac{1}{2}\bar{U}\cdot\bar{U}) = h_\infty \nabla Q' \times \nabla(U_\infty \bar{i}\cdot\bar{U}' + \tfrac{1}{2}\bar{U}\cdot\bar{U}') \tag{16B}$$

is of second and third order perturbation.

This condition may be applied to Eqns. (24A) and (25A), Appendix A, and neglect the vorticity term

$$\frac{1}{w} \left\{ T\frac{\partial S}{\partial n} - \frac{\partial h_0}{\partial n} \right\},$$

thus simplifying the method of characteristics calculation. First of all, if the heat zone is started in a region of uniform flow along a line normal to the streamlines, and if the heat is added uniformly in a zone bounded by two streamlines, then the condition of Eqn. (15B) will be approximately satisfied within the zone since the gradient of heat added will be approximately parallel to the gradient of kinetic energy. Second, if the first condition is not satisfied (i.e., along the streamline boundaries of the heat zone where there is a jump in Q normal to the streamline), the vorticity may still be neglected if the heat added is a small perturbation, that is

$$q = \bar{U}\cdot\nabla Q = h_\infty \bar{U}\cdot\nabla Q'. \tag{17B}$$

Then the heat term used in Eqns. (24A) and (25A) must be

$$\frac{q}{wc_pT} = \frac{h_\infty w(\partial Q'/\partial s)}{wc_pT} \doteq \frac{\partial Q'}{\partial s} << 1/r_b. \tag{18B}$$

This condition is satisfied for the heat zone boundary, where $r_b q/wc_pT$ is taken as 0.171 to get - 4½° deflection of the inner heat zone streamline.

APPENDIX C: BRIEF DEVELOPMENT OF CROCCO-LEES BASE FLOW FORMULATION [Refs. 1,8,13]

The mass flux, $\bar{m}$, in the base flow is given by the integral

$$\bar{m} = \int_0^{\delta} (2\pi r)^{\alpha} \rho u dr \tag{1C}$$

where δ is the viscous flow thickness, r is radius, ρ is density, u is axial component of velocity, α equals zero for two dimensional planar flow and α equals one for axisymmetric flow. The momentum flux is

$$I = \int_0^{\delta} (2\pi r)^{\alpha} \rho u^2 dr \ . \tag{2C}$$

For the base flow, where there is no wall drag, the momentum equation becomes

$$\frac{dI}{dx} = u_e \frac{d\bar{m}}{dx} - (\pi\delta)^{\alpha} \delta \frac{dp}{dx} \tag{3C}$$

where u_e is the external axial component of velocity, dp/dx is the static pressure gradient and, assuming small angles,

$$\frac{d\bar{m}}{dx} = (2\pi\delta)^{\alpha} \rho_e u_e \left(\frac{d\delta}{dx} - \theta_e \right). \tag{4C}$$

A major point of the Crocco-Lees theory is that

$$\frac{d\delta}{dx} - \theta_e = k \tag{5C}$$

where k is a non dimensional mixing coefficient which must be specified. The value for k is approximately 0.0033 for laminar mixing and 0.03 for turbulent mixing.

A mean velocity is defined by

$$u_1 = I/\bar{m} \tag{6C}$$

and a velocity ratio by

$$\kappa = u_1/u_e. \tag{7C}$$

The mean density, ρ_1, is defined by the equation

$$\bar{m} = (\pi\delta)^{\alpha}\, \delta\rho_1 u_1 . \tag{8C}$$

It is assumed that the stagnation temperature is constant throughout the flow and that the lateral pressure gradient, dp/dr, is zero. Knowing the pressure, $p = p_e$, and ρ_1, a mean temperature, T_1, can be defined

$$T_1 = p_e/\rho_1 R. \tag{9C}$$

Introducing the displacement thickness, δ^*, and momentum thickness, δ^{**}, of ordinary boundary layer theory

$$\delta^{*(1+\alpha)} = \int_0^{\delta} (2r)^{\alpha}\left(1 - \frac{\rho u}{\rho_e u_e}\right)dr = \delta^{(1+\alpha)} - \frac{\bar{m}}{\rho_e u_e \pi^{\alpha}} \tag{10C}$$

and

$$\delta^{**(1+\alpha)} = \int_0^{\delta} (2r)^{\alpha} \frac{\rho u}{\rho_e u_e}\left(1 - \frac{u}{u_e}\right)dr$$

$$= \delta^{(1+\alpha)} - \delta^{*(1+\alpha)} - \frac{I}{\rho_e u_e^2 \pi^{\alpha}} . \tag{11C}$$

Noting that $\kappa = I/\bar{m}u_e$ and using Eqns. (10C) and (11C), one has

$$\kappa = \frac{\delta^{(1+\alpha)} - \delta^{*(1+\alpha)} - \delta^{**(1+\alpha)}}{\delta^{(1+\alpha)} - \delta^{*(1+\alpha)}} . \qquad (12C)$$

On application of the Stewartson transformation [Refs. 8,13] one finds δ, δ^*, and δ^{**} in Eqn. (12C) are replaced by the incompressible quantities δ_i, δ_i^* and δ_i^{**}. Thus, within the restrictions of the Stewartson transformation, any compressible laminar base flow can be related to a corresponding incompressible laminar flow. It is assumed this also applies in the turbulent case. The ratio of mean temperature, T_1, to stagnation temperature, T_s, may be written

$$\frac{T_1}{T_s} = f - \frac{\gamma-1}{2} w_1^2 \qquad (13C)$$

where

$$f = \frac{\kappa \delta_i^{(1+\alpha)}}{\delta_i^{(1+\alpha)} - \delta_i^{*(1+\alpha)}} \qquad (14C)$$

$w_1 = u_1/a_s$, and a_s is the stagnation speed of sound. It has been found more convenient to work with the quantity $F \geq 0$,

$$F + 1 = f/\kappa^2 . \qquad (15C)$$

Experimental data [Ref. 8] has shown a relationship between F and κ which can be expressed by the polynomial

$$\kappa = 1.0 - 0.4F + 0.16F^2 - 0.01185F^3 . \qquad (16C)$$

For $F \geq 1.5$, $\kappa = 0.72$ and $d\kappa/dF = 0.0$.

From Eqn. (8C) one may write an expression for mass flux

$$m = \bar{m}a_s = \frac{\gamma(\pi\delta)^{\alpha}\ \delta\ p_e w_e}{\kappa[F + 1 - \frac{\gamma-1}{2} w_e^2]} \tag{17C}$$

Using this and Eqns. (3C), (4C) and (5C) one may form a single ordinary differential equation

$$\frac{dF}{dw_e} = (\frac{\gamma+1}{2} w_e^2 - 1)(1 - \frac{\gamma-1}{2} w_e^2) + \frac{F\left[\gamma w_e^2 - \frac{\kappa F}{1-\kappa} + \frac{1 - \frac{\gamma-1}{2} w_e^2}{1-\kappa} \frac{\theta_e}{k}\right]}{w_e(1-\frac{\gamma-1}{2}w_e^2)\left\{\left[\frac{1 - \frac{\gamma-1}{2} w_e^2}{\kappa\ (1-\kappa)} \frac{\theta_e}{k} - \kappa \frac{F}{(1-\kappa)}\right] (d\kappa/dF) - 1\right\}} \tag{18C}$$

Eqn. (18C) has a saddle point singularity, [Refs. 1,8], also called the critical point, which, in integrated form, determines the one unique solution describing the given base flow condition. In two dimensional planar flow without external heat addition, where θ_e is known from w_e by the Prandtl-Meyer relation, one may start at the critical point, where both the numerator and denominator of Eqn. (18C) are zero, and integrated toward the base [Ref. 8]. In flow with external heat addition, and in axisymmetric flow, θ_e is not known as a function of w_e; thus, in these cases, one must start integration of Eqn. (18C) at the base and concurrently solve the external flow field, by the method of characteristics or linearized theory, for the values of θ_e along the shear layer. This process is one of trial and error described in section IV as the straddle method.

APPENDIX D: CALCULATION OF BOUNDARY LAYER MASS FLUX AT THE BASE

The boundary layer is assumed to be adiabatic, have constant pressure across its thickness, δ, and have a velocity profile $(u/u_e) = (y/\delta)^{1/n}$, where u_e is the external flow velocity and n is an integer [Ref. 24]; $1 \leq n \leq 7$, for laminar to turbulent flow. The boundary layer mass flux at the base is given by the integral

$$\bar{m}_b = \int_{r_b}^{r_b+\delta} (2\pi r)^{\alpha} \rho u dr \qquad (1D)$$

where α is zero for two dimensional planar flow, or one for axisymmetric flow, ρ is density and r_b is the base radius or half-height. Using the equation of state, $p = \rho RT$, and the above assumptions, Eqn. (1D) becomes

$$\bar{m}_b = \frac{p_e}{R} \int_{r_b}^{r_b+\delta} \frac{(2\pi r)^{\alpha} u_e \left(\frac{r-r_b}{\delta}\right)^{1/n} dr}{T_T - \frac{u_e^2}{2c_p}\left(\frac{r-r_b}{\delta}\right)^{2/n}} \qquad (2D)$$

where p_c is the external pressure. Defining w_e as u_e/a_s, where a_s is the stagnation speed of sound, Eqn. (2D) becomes

$$m_b = \bar{m}_b a_s = \gamma \delta p_e w_c (2\pi\delta)^{\alpha} \int_{r_b}^{r_b+\delta} \frac{\left(\frac{r-r_b}{\delta}\right)^{1/n} \left(\frac{r}{\delta}\right)^{\alpha} \left(\frac{dr}{\delta}\right)}{1 - \frac{\gamma-1}{2} w_c^2 \left(\frac{r-r_b}{\delta}\right)^{2/n}} \qquad (3D)$$

Then

$$M_b = \frac{m_b}{\gamma \delta p_e w_e (2\pi\delta)^\alpha} = \int_0^1 \frac{X^{1/n} \left(X + \frac{r_b}{\delta}\right)^\alpha dx}{1 - B^2 X^{2/n}} \tag{4D}$$

where $x = (r - r_b)/\delta$ and $B^2 = \frac{\gamma - 1}{2} w_e^2$.

If $\alpha = 0$ and $x = z^n$, Eqn. (4D) becomes

$$I_{2D} = n \int_0^1 \frac{z^n dz}{1 - B^2 z^2} \ . \tag{5D}$$

This may be integrated. For n odd, Eqn. (5D) gives

$$I_{2D_{ODD}} = n \left\{ \frac{1}{2B^{n+1}} \ln\left(\frac{1}{1-B^2}\right) - \sum_{j=1}^{(n-1)/2} \frac{1}{[n+1-2j]B^{2j}} \right\}$$

where the summation is omitted if n = 1. For n even, Eqn. (5D) gives

$$I_{2D_{EVN}} = n \left\{ \frac{1}{2B^{n+1}} \ln\left(\frac{1+B}{1-B}\right) - \sum_{j=1}^{n/2} \frac{1}{[n + 1 - 2j]B^{2j}} \right\} \tag{7D}$$

If $\alpha = 1$ and $x = z^n$, Eqn. (4D) becomes

$$I_{AXI} = n \int_0^1 \frac{z^{2n} dz}{1 - B^2 z^2} + \frac{r_b}{\delta} n \int_0^1 \frac{z^n dz}{1 - B^2 z^2} \tag{8D}$$

The second integral in Eqn. (8D) is the same as Eqn. (5D), which is evaluated in Eqns. (6D) and (7D). Integrating the first integral, Eqn. (8D) becomes

$$I_{AXI} = n \left\{ \frac{1}{2B^{2n+1}} \ln \left(\frac{1+B}{1-B}\right) - \sum_{j=1}^{n} \frac{1}{[2(n-j)+1]B^{2j}} \right\}$$

$$+ \frac{r_b}{\delta} I_{2D}. \qquad (9D)$$

The results of Eqns. (6D), (7D) and (9D) are used with Eqn. (4D) to evaluate $m_{b_{2D}}$ or $m_{b_{AXI}}$. This boundary layer mass flux at the base, before the corner expansion, m_b, is set equal to the mass flux after the corner expansion, m_b', expressed in terms of the Crocco-Lees formulation, Appendix C.

$$m_{b_{2D}} = \gamma\delta p_e w_e I_{2D} = m'_{b_{2D}} = \frac{\gamma\delta' p_e' w_e'}{\kappa'[F'+1-\frac{\gamma-1}{2}w_e'^2]} \qquad (10D)$$

Taking $\kappa' = 0.72$ and the value of w_e' assumed from the straddle method, one solves Eqn. (10D) for the value of F' which starts the integration along the shear layer. Similarly, in the axisymmetric case,

$$m_{b_{AXI}} = 2\pi\gamma\delta^2 p_e w_e I_{AXI} = m'_{b_{AXI}} = \frac{\pi\gamma\delta'^2 p_e' w_e'}{\kappa'[F'+1-\frac{\gamma-1}{2}w_e'^2]} \qquad (11D)$$

APPENDIX E: MASS FLUX CALCULATION ALONG THE SHEAR LAYER

From Appendix C, Eqn. (17C), the mass flux, m, may be written

$$m = \frac{\gamma(\pi\delta)^{\alpha}\ \delta\ p_c w_c}{\kappa[F+1-\frac{\gamma-1}{2}\ w_e^2]} \tag{1E}$$

where $\alpha = 0$ for the two dimensional planar flow and $\alpha = 1$ for axisymmetric flow. One may evaluate Eqn. (1E) at two adjacent points along the shear layer, m_i and m_{i+1}, and solve for the distance between these two points, dx, by using the additional relations [Ref. 1,8].

$$\frac{d\delta}{dx} = \theta + k \tag{2E}$$

and

$$\frac{dm}{dx} = (2\pi\delta)^{\alpha}\ \rho_e w_e\ a_s^2\ \left(\frac{d\delta}{dx} - \theta\right). \tag{3E}$$

Assuming small angles, Eqn. (2E) states that the rate of change of the shear layer height or radius, $d\delta/dx$, is equal to the flow angle θ plus some constant, k. Then the rate of change of mass flux, dm/dx, given by Eqn. (3E), is the mass entrained by the shear layer from the external flow.

To compute m_{i+1}, one increments F_i with ΔF_i, say $\Delta F_i = 0.1F_i$ with the condition $\Delta F \geq 0.08$,

$$F_{i+1} = F_i + \Delta F_i. \tag{4E}$$

Then

$$w_{c_{i+1}} = w_{c_i} + \Delta F_i/(dF/dw_c) \tag{5E}$$

where dF/dw_e is computed from Eqn. (18C). The value for κ_{i+1} is computed from an empirical relation using F_{i+1}, given by Eqn. (16C), with $\kappa_{i+1} = 0.72$ if $F_{i+1} \geq 1.5$. The isentropic relation between static and total pressure, in terms of γ and w_e, is used to evaluate p_e at i and i+1. Average values between i and i+1 are used to evaluate $d\delta/dx$ and dm/dx, where the isentropic relation between static and total density must be used with the latter. Since

$$m_{i+1} = m_i + (dm/dx)dx \tag{4E}$$

and

$$\delta_{i+1} = \delta_i + (d\delta/dx)dx \ . \tag{5E}$$

One may solve directly for the value of dx, in the two dimensional planar case, which corresponds to the increment ΔF_i

$$dx_{i_{2D}} = \delta_i \left(\frac{m_i}{\delta_i} - \frac{m_{i+1}}{\delta_{i+1}} \right) / \left(\frac{d\delta}{dx} - \frac{dm}{dx} \right). \tag{6E}$$

For the axisymmetric case

$$dx_{i_{AXI}} = \frac{1}{2} \left(dx_{i_{2D}} - \frac{1}{\delta_i} \frac{d\delta}{dx} dx^2_{i_{AXI}} \right). \tag{7E}$$

Eqn. (7E) may be iterated several times, as long as $dx_{i_{AXI}} \leq 1$, to determine the correct value of $dx_{i_{AXI}}$.

APPENDIX F: CALCULATION OF BOUNDARY LAYER THICKNESS AND MIXING COEFFICIENT

The laminar boundary layer thickness, δ_L, was computed at point x from the compressible Blasius solution [Ref. 8]

$$\delta_L = (5.0 + 1.2(\gamma-1)M^2)x/(Re_x)^{\frac{1}{2}} \tag{1F}$$

where x is the distance along the surface from the leading edge and Re_x is the Reynolds number based on this distance. If the base Reynolds number, Re_b, is less than the transition Reynolds number, Re_{tr}, then the boundary layer at the base is completely laminar and its thickness was computed from Eqn. (1F), with x taken as the body length.

If the base Reynolds number, Re_b, is greater than the transition Reynolds number, Re_{tr}, the boundary layer will be partly or completely turbulent. The turbulent thickness, δ_T, was computed from [Ref. 8]

$$\delta_T = \frac{0.037x}{(Re_x)^{1/5}}(C_{fM}/C_{fi})(\delta/\delta^{**}) \tag{2F}$$

C_{fi} is von Karman's incompressible turbulent skin friction coefficient given by [Ref. 24]

$$(0.242)/(C_{fi})^{\frac{1}{2}} = \log_{10}(Re_x C_{fi}) \tag{3F}$$

and C_{fM} is van Driest's compressible turbulent skin friction coefficient given by [Ref. 24]

$$\frac{0.242(1-B^2)^{\frac{1}{2}}}{(B^2 C_{fM})^{\frac{1}{2}}}\sin^{-1}B = \log_{10}(Re_x C_{fM}) + 1.26\log_{10}(1-B^2) \tag{4F}$$

where B^2 is $(\gamma-1)w_e^2/2$. Equations (3F) and (4F) must be solved by iteration. The quantity δ/δ^{**} (Appendix C) may be evaluated for the two dimensional 1/7th profile using the same assumptions employed in Appendix D. Briefly

$$\delta^{**} = \int_{r_b}^{r_b+\delta} \frac{(\rho u)}{(\rho_e u_e)} \left(1 - \frac{u}{u_e} \right) dr \qquad (5F)$$

$$\frac{\delta^{**}}{\delta} = \left(1-\frac{\gamma-1}{2}w_e^2\right) \int_{r_b}^{r_b+\delta} \frac{\left(\frac{r-r_b}{\delta}\right)^{1/7} - \left(\frac{r-r_b}{\delta}\right)^{2/7}}{\left(1-\frac{\gamma-1}{2}w_e^2\left(\frac{r-r_b}{\delta}\right)^{2/7}\right)} (dr/\delta) \qquad (6F)$$

$$\frac{\delta^{**}}{\delta} = 7(1-B^2)\left(\frac{1}{2B^8}\ln\left(\frac{1}{1-B^2}\right) - \sum_{j=1}^{3} \frac{1}{(8-2j)B^{2j}} - \frac{1}{2B^9}\ln\left(\frac{1+B}{1-B}\right) + \sum_{j=1}^{4} \frac{1}{(9-2j)B^{2j}}\right). \qquad (7F)$$

Since the actual transition process is more or less probabilistic in nature, it was assumed that the transition from laminar to turbulent flow can be described by the integrated normal distribution. It was necessary to assume a turbulent transition Reynolds number, Re_{trt}, for this purpose, where Re_{trt} is approximately four times Re_{tr}. The transition computation was made with the error function, erf, which is exactly related to the integrated normal distribution. The argument of the error function was formed in terms of base distance from the initial transition point, and was weighted

so its value was -0.96 at Re_{tr} and 0.96 at Re_{trt}. A numerical span, S, of 4.0 takes the integrated normal distribution from 0.02 to 0.98. Formulating these conditions in terms of body radius, r,

$$Z_{tr} = (Re_{tr}/Re_b - 1.0)(L/r) \tag{8F}$$

is the transition point on the body measured from the base, and

$$Z_{trt} = (Re_{trt}/Re_b - 1.0)(L/r) \tag{9F}$$

is the turbulent transition point. Note that Z_{trt} will lie downstream of the base if $Re_{trt} > Re_b$. Forming the average,

$$Z_{trav} = \tfrac{1}{2}(Z_{tr} + Z_{trt}) \tag{10F}$$

is the distance from the base to the center of the transition zone. If Z_{trav} is zero, the integral of the cumulative distribution must be 0.5. The value of erf at this point will be 0.0, and the cumulative distribution integral, I_{CD}, is

$$I_{CD} = \tfrac{1}{2}(1 + erf). \tag{11F}$$

The values of erf at the base, ERF_b, range from - 1.0 to + 1.0. In terms of Z

$$ERF_b = erf\left(\frac{S}{2^{\frac{1}{2}}} \frac{Z_{trav}}{(Z_{trt} - Z_{tr})}\right) \tag{12F}$$

Then, when $Re_b > Re_{tr}$, δ_{BASE} is given by

$$\delta_{BASE} = \tfrac{1}{2}\delta_L(1 + ERF_b) + \tfrac{1}{2}\delta_T(1 - ERF_b). \tag{13F}$$

In Eqn. (13F), ERF_b will be positive if Re_b is less than $\frac{1}{2}(Re_{tr} + Re_{trt})$, thus as Re_b ranges from Re_{tr} to Re_{trt}, the contribution of δ_L will range from 0.99 to 0.01 and the contribution of δ_T will range from 0.01 to 0.99. The value for n used to compute the velocity profile at the base (see Appendix D) is formed exactly as Eqn. (13F)

$$n_{BASE} = \tfrac{1}{2}(1 + ERF_b) + \frac{7}{2}(1 - ERF_b) \qquad (14F)$$

since n ranges from 1 to 7.

When the transition zone lies along the shear layer, one must compute a transition value for the mixing coefficient, k, at the point being considered, x_{BL}. The distance x_{BL} is measured from the base in terms of r. To carry out this calculation, the value of erf at x_{BL}, ERF_{BL}, is written, as in Eqn. (12F), in terms of Z

$$ERF_{BL} = erf\left(\frac{S}{2^{\frac{1}{2}}} \frac{(Z_{trav} - x_{BL})}{(Z_{trt} - Z_{tr})}\right). \qquad (15F)$$

Note that Eqn. (15F) reduces to (12F) since x_{BL} is zero at the base. Using Eqn. (15F), the value for the coefficient, k_{BL}, is formed in a similar manner from the laminar and turbulent mixing coefficients, k_L and k_T,

$$k_{BL} = \tfrac{1}{2}k_L(1 + ERF_{BL}) + \tfrac{1}{2}k_T(1 - ERF_{BL}). \qquad (16F)$$

In Eqn. (16F), the value of ERF_{BL} will be positive if Z_{trav} is downstream of x_{BL}, and vice versa.

APPENDIX G: DERIVATION OF LINEARIZED STEADY FLOW EQUATION WITH HEAT ADDITION

The equations, (1) - (4), are required for this derivation.

$$\nabla\cdot(\rho\bar{U}) = 0 \tag{1G}$$

$$\rho\bar{U}\cdot\nabla\bar{U} = -\nabla p \tag{2G}$$

$$\bar{U}\cdot\nabla(h + \tfrac{1}{2}\bar{U}\cdot\bar{U}) = q \tag{3G}$$

$$p = \rho RT \tag{4G}$$

Forming the directional derivative, $\bar{U}\cdot\nabla$, of Eqn. (4G)

$$\bar{U}\cdot\nabla p = \rho R\bar{U}\cdot\nabla T + RT\bar{U}\cdot\nabla\rho. \tag{5G}$$

Substituting Eqn. (1G) into (5G)

$$\rho R\bar{U}\cdot\nabla T = \bar{U}\cdot\nabla p + \rho RT\nabla\cdot\bar{U} \tag{6G}$$

Substituting $\bar{U}\cdot$ of Eqn. (2G) in (6G)

$$R\bar{U}\cdot\nabla T = -\bar{U}\cdot\nabla(\tfrac{1}{2}\bar{U}\cdot\bar{U}) + RT\nabla\cdot\bar{U} \tag{7G}$$

Assuming c_p is constant, using $h = c_pT$ and $c_p = \gamma R/(\gamma-1)$, substitute $\gamma/(\gamma-1)$ times Eqn. (7G) into (3G)

$$\nabla\cdot\bar{U} - \frac{1}{a^2}\,\bar{U}\cdot\nabla(\tfrac{1}{2}\bar{U}\cdot\bar{U}) = q/c_pT. \tag{8G}$$

Let $T = T_\infty(1 + T')$, $q = h_\infty q'$, $\bar{U} = U_\infty\bar{i} + \nabla\phi$.

With this, Eqn. (8G) becomes

$$\nabla^2\phi - \frac{(U_\infty T + \nabla\phi)\cdot\nabla}{a_\infty^2\,(1 + T')}\,(\tfrac{1}{2}U_\infty^2 + U_\infty\phi_x + \tfrac{1}{2}\nabla\phi\cdot\nabla\phi) = q'/(1 + T') \tag{9G}$$

Retaining only first order terms, Eqn. (9G) becomes

$$\nabla^2\phi - M_\infty^2 \phi_{xx} = q'. \tag{10G}$$

This is the linearized steady flow equation, with heat addition for irrotation subsonic or supersonic flow.

APPENDIX H: DETERMINATION OF THE MACH ANGLE

This appendix derives a numerical procedure for determining the Mach angle, μ, for a given value of the Prandtl-Meyer angle, ν

The Prandtl-Meyer angle may be written [Ref. 18]

$$\nu = \frac{1}{g} \tan^{-1}(g(M^2-1)^{\frac{1}{2}}) - \tan^{-1}(M^2-1)^{\frac{1}{2}} \tag{1H}$$

where M is the Mach Number, $1 \leq M \leq \infty$,

$$g = ((\gamma-1)/(\gamma+1))^{\frac{1}{2}} \tag{2H}$$

and γ is the specific heat ratio. Let

$$\mu + \varepsilon = \pi/2 \tag{3H}$$

where μ is the Mach angle defined by

$$\sin \mu = 1/M. \tag{4H}$$

From Eqns. (3H) and (4H)

$$(M^2-1)^{\frac{1}{2}} = \tan\varepsilon. \tag{5H}$$

Using equation (5H), equation (1H) may be written

$$\tan g(\nu+\varepsilon) = g\tan\varepsilon. \tag{6H}$$

In Eqn. (6H), the relation between ν and ε is still implicit. For $\gamma = 5/3$, $g = \frac{1}{2}$ and Eqn. (6H) can be reduced to the explicit form

$$\tan^3 \frac{\varepsilon}{2} = \tan\frac{\nu}{2} . \tag{7H}$$

Thus, using Eqns. (3H) and (7H), the simple relation may be written when $\gamma = 5/3$

$$\mu = \frac{\pi}{2} - 2\tan^{-1}\left(\left(\tan\frac{\nu}{2}\right)^{1/3}\right). \tag{8H}$$

This analytical result [Ref. 37] was first given in terms of M, rather than μ, along with a more complicated expression when $\gamma = 5/4$. There are no analytical expressions, $\mu = \mu(\nu,\gamma)$, for other values of γ, consequently, μ must be determined from tables, or numerically, in all other cases.

Equation (6H) may be written in a form for iteration which always converges to the correct value of ε

$$\varepsilon_{i+1} = \tan^{-1}\left(\frac{1}{g}\tan g(\nu+\varepsilon_i)\right) \tag{9H}$$

for $0 \leq \varepsilon_i \leq \pi/2$ and $0 \leq \nu \leq \nu_{max}$. The value ν_{max} is given by Eqn. (1H) for M infinite

$$\nu_{max} = \frac{\pi}{2}\left(\left((\gamma+1)/(\gamma-1)\right)^{\frac{1}{2}} - 1\right). \tag{10H}$$

One may start the iteration of Eqn. (9H) with an approximation for ε_1 given by Eqn. (7H)

$$\varepsilon_1 = 2\tan^{-1}\left(\left(\tan\frac{\nu}{2}\right)^{1/3}\right). \tag{11H}$$

This approximation fails for large values of ν since it may give a value $\varepsilon_1 > \pi/2$. When this occurs, set $\varepsilon_1 = \pi/2$ to start the iteration with Eqn. (9H).

While Eqn. (9H) will always converge to the correct value of ε, its convergence is slow and, after two or three iteration, should be replaced by a method utilizing the derivatives. In effect, Eqn. (9H) is used to find an approximation of ε which lies in the range of convergence of a faster method.

One method which provides rapid convergence may be written from Eqn. (6H) by using a Taylor's series expansion for the separate sides about ε_i and solving for $\Delta\varepsilon$. Let

$$f_{1_i} = \text{tang}(\nu+\varepsilon_i) \tag{12H}$$

$$f_{2_i} = g\tan\varepsilon_i \tag{13H}$$

then

$$\Delta\varepsilon_{j+1} = (f_{1_i} - f_{2_i} + \frac{\Delta\varepsilon_j^2}{2!}(f_{1_i}'' - f_{2_i}'') + \frac{\Delta\varepsilon_j^3}{3!}\cdot (f_{1_i}''' - f_{2_i}''')+\cdots)/(f_{2_i}' - f_{1_i}') \tag{14H}$$

where $\Delta\varepsilon_1 = 0$ starts the iteration in Eqn. (14H). The advantage of this form lies in the fact that the derivatives may be written in terms of the values of f_{1_i} and f_{2_i}, i.e. f_{1_i}' and f_{2_i}' involve the $\sec^2 x$, which can be written as $1 + \tan^2 x$, etc. Thus the derivatives may be included with only two numerical evaluations by the computer of the tangent functions in Eqns. (12H) and (13H). Depending on the number of derivatives included, two or three iterations with Eqn. (14H) should be sufficient. Then, of course,

$$\varepsilon_{i+1} = \varepsilon_i + \Delta\varepsilon_{j+1} \tag{15H}$$

is used to evaluate $f_{1_{i+1}}$ and $f_{2_{i+1}}$, etc. For $\gamma = 1.4$ and including the fourth derivative, the above procedure will provide twelve place accuracy for ε in two iterations. With the required value for ε, μ can be written using Eqn. (3H).

This method was used in the computer program discussed in Appendix J.

APPENDIX I: SPINNING CYLINDER DESIGN

The spinning cylinder was designed to be compatible with the coaxial free jet fixtures, nozzles and spacers used for the nonspinning investigation [Ref. 29]. The spinning cylinder and its support assembly had the same external dimensions as the stationary cylinder design, 1.282-inch diameter and 9.95-inch length, to insure similar test results without spin. The cylinder was driven by an internal impulse turbine. The design speed of 48,000 revolutions per minute, to match the spin number of 0.1595, was not achieved. This was due in part to physical interference during the fabrication process which reduced the tangential component of the turbine jet to less than one-half the desired value. The maximum speed achieved, without nozzle flow, was 18,000 revolutions per minute.

The spinning cylinder was made of Plexiglas, to reduce rotating mass, and was glued to a metal endcap which formed the cylinder base. The endcap was driven through a shaft which screwed into the internal turbine. The shaft also carried thrust loads, from an internal air bearing surface on the turbine face, to react with pressure and friction forces due to the nozzle flow. This part of the design was deficient in that the loads due to nozzle flow caused the turbine face to rub and stopped the cylinder. Time did not permit modification to correct this deficiency.

The spinning cylinder was positioned radially by 24 air bearing pads provided along the outer surface of the support cylinder. High pressure air was supplied to these pads through orifices formed by drilling into supply tubes soldered into the walls of the support cylinder, Fig. 11. The bearing air exhausted through ports to the inside of the support cylinder where it mixed with turbine exhaust and flowed out the bottom.

The base pressure on the spinning cylinder was measured by a total pressure probe, positioned on centerline next to the base, and a mercury manometer. The cylinder speed was determined through a photo diode and a pulse counter. The photo diode was illuminated by a laser beam reflecting from the metal endcap and half of the endcap was painted black to generate one pulse per revolution.

Figure 11. Disassembled View of Spinning Cylinder.

APPENDIX J: COMPUTER PROGRAM

The FORTRAN computer program, included at the end of this appendix, required 150K for compile, 110K for link and 80K for execution. It was written to compute base pressure ratio, within approximately 0.5 percent, by applying the equations and methods discussed in this thesis. In view of the empirical information and approximations employed in many of the equations, computation to greater accuracy did not appear warranted. Using an IBM 360 computer, computation of the base pressure ratio for one flight condition required approximately two minutes for the fully turbulent shear layer without heat addition. The addition of heat upstream of the base and low Reynolds number, which involved a long laminar shear layer, increased the size of the characteristic mesh and resulted in computation times as high as ten minutes.

The flight condition was specified before making a computer run. This included choosing the Mach number, card 80, and the base Reynolds number, card 140. The two no spin transition Reynolds numbers, cards 120 and 130, were choosen for the particular body to provide agreement with available experimental data. The ratio of body radius to body length was specified on card 150. The spin number, rw/U, was given on card 131. The ratio of specific heats for air was set at 1.4 on card 200. Card 180 and 190 were interchanged for two dimensional planar flow. For flow without heat addition,

card 90 was set to zero, card 60 to ISTRT = 90, and card 100 to ZSTRT = 20.0.

Several additional considerations were required to compute the flight condition with external burning. The starting values for the radii of the heat zone inner and outer streamlines were specified on cards 420 and 430. The axial positions to start and stop heat addition were given on cards 100 and 110, with reference to the base. The value for Q, card 90, was specified to obtain a desired - 4½° deflection of the inner heat zone streamline, however, this value could have been specified by assuming various fuel flow rates and heating values. Finally, the value for ISTRT, card 60, was set low enough (minimum value of 1) to place the Mach line boundary condition well upstream of the outer compression waves generated by the heat zone. The values of selected quantities were printed, to monitor the progress of the computation, in addition to the required values for the base pressure ratio.

A simplified flow diagram is shown in Fig. 1J. It is intended to show the basic sections of the computer program and computational details have been omitted.

In the computer program the group of IF STATEMENTS which examine the mesh point for heat addition can introduce a slight error at two corners of the heat zone. The amount of heat assigned between two points is proportional to the element of length along the characteristic in the heat zone. The IF condition is checked in radial position against the

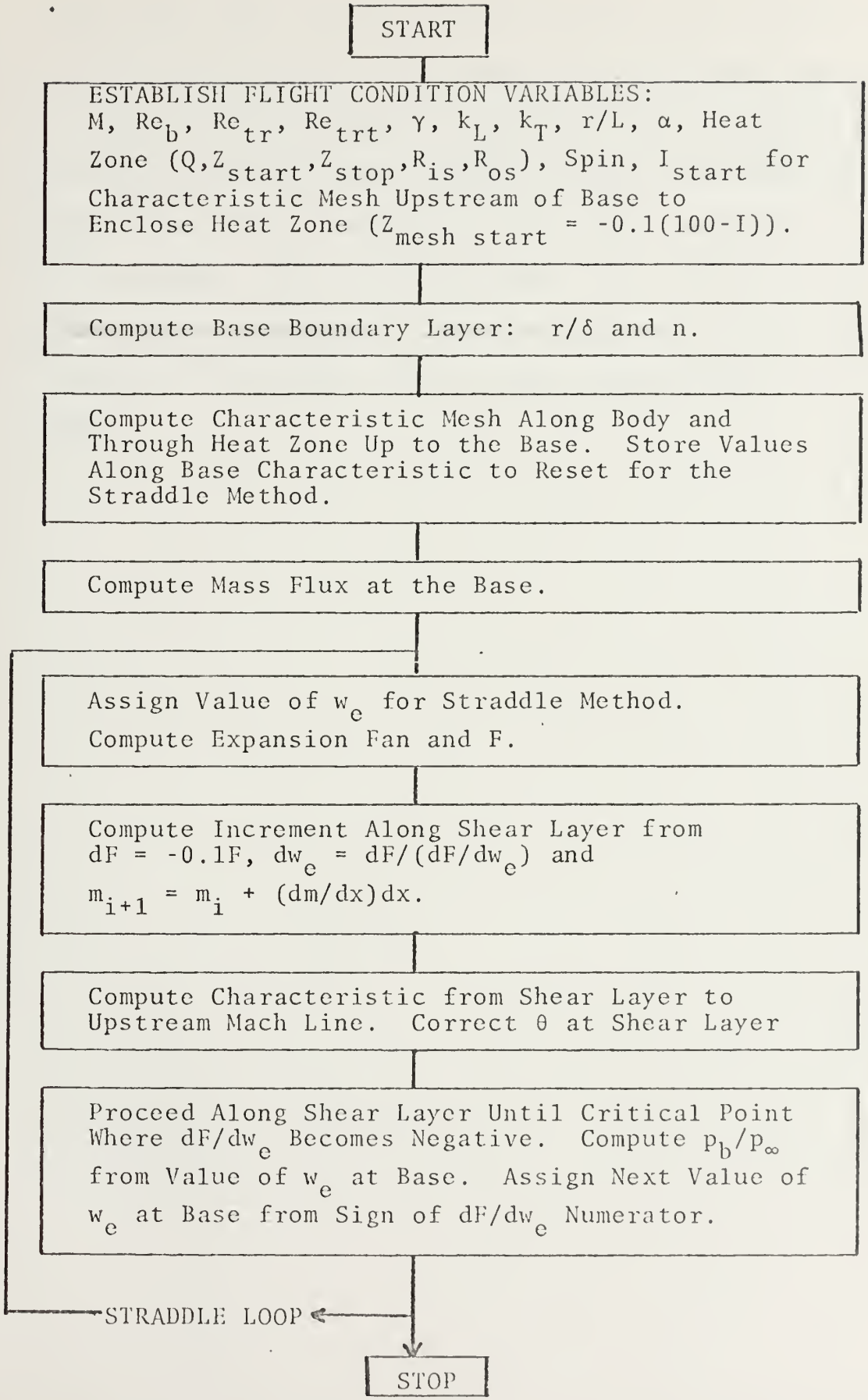
START
ESTABLISH FLIGHT CONDITION VARIABLES: M, Re_b, Re_{tr}, Re_{trt}, γ, k_L, k_T, r/L, α, Heat Zone ($Q, Z_{start}, Z_{stop}, R_{is}, R_{os}$), Spin, I_{start} for Characteristic Mesh Upstream of Base to Enclose Heat Zone ($Z_{mesh\ start} = -0.1(100-I)$).
Compute Base Boundary Layer: r/δ and n.
Compute Characteristic Mesh Along Body and Through Heat Zone Up to the Base. Store Values Along Base Characteristic to Reset for the Straddle Method.
Compute Mass Flux at the Base.
Assign Value of w_e for Straddle Method.
Compute Expansion Fan and F.
Compute Increment Along Shear Layer from $dF = -0.1F$, $dw_e = dF/(dF/dw_e)$ and $m_{i+1} = m_i + (dm/dx)dx$.
Compute Characteristic from Shear Layer to Upstream Mach Line. Correct θ at Shear Layer
Proceed Along Shear Layer Until Critical Point Where dF/dw_e Becomes Negative. Compute p_b/p_∞ from Value of w_e at Base. Assign Next Value of w_e at Base from Sign of dF/dw_e Numerator.
STRADDLE LOOP
STOP

Figure 1J. Simplified Flow Diagram for External Burning Assisted Projectile (EBAP) Computer Program.

inner and outer streamlines of the heat zone, and in axial position against the start and end of the heat zone. Thus a right running element at the lower left or upper right corner of the heat zone could be outside the zone, but still pass the IF condition tests and be assigned ¼ value for heating. This error is small with a small characteristic mesh and is neglected. The same applies to a left running element at the upper left or lower right corner of the heat zone.

```
C       EBAP PROGRAM                                                                    EBAP   10
        DIMENSION QR(200), QZ(200), QT(200), QUN(200), QUM(200), QACH(200)EBAP   20
       1, QDEG(202), BL(200), VR(200), VZ(200), VT(200), VUN(200), VUM(200EBAP   30
       2), VACH(200), RSR(100), RSZ(100), RST(100), RSUN(100), RSUM(100), EBAP   40
       3RSACH(100)                                                                      EBAP   50
        ISTRT=90                                                                        EBAP   60
        V=1.95                                                                          EBAP   70
        ACHO=2.0                                                                        EBAP   80
        Q=0.0                                                                           EBAP   90
        ZSTRT=20.0                                                                      EBAP  100
        WBYH=4.0                                                                        EBAP  101
        ZSTOP=ZSTRT+WBYH                                                                EBAP  110
        RETN=1.95                                                                       EBAP  120
        RETNT=4.0*RETN                                                                  EBAP  130
        SPIN=0.06                                                                       EBAP  131
        RETR=RETN/(1.0+SPIN)                                                            EBAP  132
        RETRT=RETNT/(1.0+SPIN)                                                          EBAP  133
        REL=15.29086                                                                    EBAP  140
        RBYL=0.1                                                                        EBAP  150
        BKL1=0.0033                                                                     EBAP  160
        BKT=0.03                                                                        EBAP  170
        IXA=0                                                                           EBAP  180
        IXA=1                                                                           EBAP  190
        G=1.4                                                                           EBAP  200
        SPAND=4.0                                                                       EBAP  210
        VSTRT=V                                                                         EBAP  220
        PIBY2=1.570796                                                                  EBAP  230
        TENLG=ALOG(10.0)                                                                EBAP  240
        SQ2RT=SQRT(2.0)                                                                 EBAP  250
        AK1=0.72                                                                        EBAP  260
        TH00=-0.000001                                                                  EBAP  270
        TH01=0.000001                                                                   EBAP  280
        TH10=1000.0*TH01                                                                EBAP  290
        UM00=ARSIN(1.0/ACH0)                                                            EBAP  300
        G1=0.5*(G-1.0)                                                                  EBAP  310
        G2=G/(G-1.0)                                                                    EBAP  320
        G3=SQRT((G+1.0)/(G-1.0))                                                        EBAP  330
        G4=0.5*(G+1.0)                                                                  EBAP  340
        G6=1.0/(G-1.0)                                                                  EBAP  350
        G7=1.0/G3                                                                       EBAP  360
        UMMAX=PIBY2*(G3-1.0)-0.00029                                                    EBAP  370
        SHOCK=9.999991                                                                  EBAP  380
        C13=0.333333                                                                    EBAP  390
C       START LOOP ON REYNOLDS NUMBER, REL                                              EBAP  400
        DO 1052 IREL=1,1                                                                EBAP  410
        RIS=2.0                                                                         EBAP  420
        RCS=3.0                                                                         EBAP  430
        REL6=1000.0*1000.0*REL                                                          EBAP  440
```

```
      BKL=BKL1*SQRT(RETR/REL)                                                    EBAP  450
      ZTR=(RETR/REL-1.0)/RBYL                                                    EBAP  460
      ZTRT=(RETRT/REL-1.0)/RBYL                                                  EBAP  470
      ZTRAV=0.5*(ZTR+ZTRT)                                                       EBAP  480
      XCONV=(SPAND/(ZTRT-ZTR))/SQ2RT                                             EBAP  490
      ACH=ACH0                                                                   EBAP  500
      ACH2=ACH*ACH                                                               EBAP  510
      G5=SQRT(ACH2-1.0)                                                          EBAP  520
      UNOO=G3*ATAN(G5/G3)-ATAN(G5)                                               EBAP  530
      W2=ACH2/(1.0+G1*ACH2)                                                      EBAP  540
      W=SQRT(W2)                                                                 EBAP  550
      NBL=1                                                                      EBAP  560
      RBYBL=200.0*RBYL*(SQRT(REL))/(1.0+0.48*G1*ACH2)                            EBAP  570
      IF (ZTR.GE.0.0) GO TO 1004                                                 EBAP  580
      BLERF=0.5*ERF(ZTRAV*XCONV)                                                 EBAP  590
      BETA2=G1*W2                                                                EBAP  600
      BETA=SQRT(BETA2)                                                           EBAP  610
      BLTKS=1.0/(BETA2**4)                                                       EBAP  620
      BLTKS=BLTKS*(1.0+0.5*(ALOG(1.0/(1.0-BETA2))-(1.0/BETA)*ALOG((1.0+BEBAP  630
     1ETA)/(1.0-BETA))))                                                         EBAP  640
C     LOOP FOR PART OF BL (MOMENTUM THKNESS)/(THKNESS)                           EBAP  650
      DO 1001 J=1,3                                                              EBAP  660
      BLTKS=BLTKS+(1.0/(9.0-2.0*J)-1.0/(8.0-2.0*J))/(BETA2**J)                   EBAP  670
 1001 CONTINUE                                                                   EBAP  680
C     COMPUTE BL (MOMENTUM THKNESS)/(THKNESS), BLTKS                             EBAP  690
      BLTKS=7.0*(1.0-BETA2)*BLTKS                                                EBAP  700
      BETAL=1.26*(ALOG(1.0-BETA2))/TENLG                                         EBAP  710
      BETAA=(0.242/BETA)*(ARSIN(BETA))*SQRT(1.0-BETA2)                           EBAP  720
      CFI=0.003                                                                  EBAP  730
C     SOLVE INCOMPRESSIBLE FRICTION COEFFICIENT, CFI                             EBAP  740
      DO 1002 J=1,5                                                              EBAP  750
      CFFI=(ALOG(CFI*REL6))/TENLG-0.242/SQRT(CFI)                                EBAP  760
      DCFFI=1.0/(CFI*TENLG)+(0.121/CFI)/SQRT(CFI)                                EBAP  770
      CFI=CFI-CFFI/DCFFI                                                         EBAP  780
 1002 CONTINUE                                                                   EBAP  790
C     ESTIMATE COMPRESSIBLE FRICTION COEFFICIENT, CFC                            EBAP  800
      CFC=CFI*(1.0-0.08*ACH0)                                                    EBAP  810
C     SOLVE FOR CFC                                                              EBAP  820
      DO 1003 J=1,5                                                              EBAP  830
      CFFC=(ALOG(CFC*REL6))/TENLG+BETAL-BETAA/SQRT(CFC)                          EBAP  840
      DCFFC=1.0/(CFC*TENLG)+(0.5*BETAA/CFC)/SQRT(CFC)                            EBAP  850
      CFC=CFC-CFFC/DCFFC                                                         EBAP  860
 1003 CONTINUE                                                                   EBAP  870
C     COMPUTE (RADIUS)/(TURB BL THKNESS), RBYBT                                  EBAP  880
      RBYBT=270.5*RBYL*((10.0*REL)**0.2)*(CFI/CFC)*BLTKS                         EBAP  890
      RBYBL=RBYBL*(0.5+BLERF)+RBYBT*(0.5-BLERF)                                  EBAP  900
      NBL=1.2*(0.5+BLERF)+7.2*(0.5-BLERF)                                        EBAP  910
 1004 CONTINUE                                                                   EBAP  920
```

```
      TIS=THOO                                                          EBAP 930
      TIDEG=57.3*TIS                                                    EBAP 940
      TCS=THOO                                                          EBAP 950
      P=(1.0-G1*W2)**G2                                                 EBAP 960
      PCO=P                                                             EBAP 970
      P7=P                                                              EBAP 980
      MSTBT=98                                                          EBAP 990
      BTR=1.0                                                           EBAP1000
C     BTR IS BL(100)/BL(ISTRT) WHEN BOATTAIL IS PRESENT                 EBAP1010
      DW=-0.1                                                           EBAP1020
      ISTP1=ISTRT+1                                                     EBAP1030
      BL(ISTRT)=1.0+1.0/RBYBL                                           EBAP1040
      DZ=0.1                                                            EBAP1050
      DZC=DZ*(100-MSTBT)                                                EBAP1060
      DZC2=DZC*DZC                                                      EBAP1070
      BTC=(1.0/BTR-1.0)/DZC2                                            EBAP1080
      VR(ISTRT)=BL(ISTRT)                                               EBAP1090
      QR(ISTRT)=VR(ISTRT)                                               EBAP1100
      VZ(ISTRT)=-DZ*(100-ISTRT)                                         EBAP1110
      QZ(ISTRT)=VZ(ISTRT)                                               EBAP1120
      VT(ISTRT)=THOO                                                    EBAP1130
      QT(ISTRT)=THOO                                                    EBAP1140
      VUN(ISTRT)=UNOO                                                   EBAP1150
      QUN(ISTRT)=UNOO                                                   EBAP1160
      VUM(ISTRT)=UMOO                                                   EBAP1170
      QUM(ISTRT)=UMOO                                                   EBAP1180
      VACH(ISTRT)=ACHO                                                  EBAP1190
      QACH(ISTRT)=ACHO                                                  EBAP1200
      ZIS=VZ(ISTRT)+(RIS-VR(ISTRT))/TAN(UMOO+THOO)                      EBAP1210
      ZOS=VZ(ISTRT)+(ROS-VR(ISTRT))/TAN(UMOO+THOO)                      EBAP1220
      BTDRG=0.0                                                         EBAP1230
      M=ISTRT                                                           EBAP1240
      QDEG(M)=0.0                                                       EBAP1250
      WRITE (6,1053) M,VR(M),VZ(M),VT(M),VACH(M),VT(ISTRT),QDEG(M),BTDRGEBAP1260
      PMCOR=0.0                                                         EBAP1270
C     START INCREMENTING CHARACTERISTIC MESH ALONG BODY                 EBAP1280
      DO 1016 M=ISTP1,100                                               EBAP1290
      M7=M-1                                                            EBAP1300
      MM100=M-ISTRT                                                     EBAP1310
      MM99=MM100+1                                                      EBAP1320
      MMID=ISTRT+(M-ISTRT)/2                                            EBAP1330
      DZB=DZ*(M-MSTBT)                                                  EBAP1340
      BL(M)=BL(ISTRT)/(1.0+BTC*DZB*DZB)                                 EBAP1350
      IF (M.LE.MSTBT) BL(M)=BL(ISTRT)                                   EBAP1360
      QR(M)=BL(M)                                                       EBAP1370
      QZ(M)=-DZ*(100-M)                                                 EBAP1380
      SLP=-2.0*BTC*DZB*BL(M)*BL(M)/BL(ISTRT)                            EBAP1390
      SLP=THOO                                                          EBAP1400
```

```
C       REMOVE SLP=THOO WHEN PROVIDING BOATTAIL SHAPE                          EBAP1410
        IF (M.LE.MSTBT) SLP=THOO                                               EBAP1420
        QT(M)=ATAN(SLP)                                                        EBAP1430
        QUN(M)=VUN(M7)+VT(M7)-QT(M)+PMCOR                                      EBAP1440
        ABFN1=1.0                                                              EBAP1450
        ABFT1=1.0                                                              EBAP1460
        UNCMP=2.0                                                              EBAP1470
        JXCOR=0                                                                EBAP1471
C       WORK BACKWARDS ALONG RIGHT RUNNING CHARACTERISTIC FROM BODY TO          EBAP1480
C       UPSTREAM MACH LINE BC                                                  EBAP1481
        DO 1013 JX=1,12                                                        EBAP1490
        UNI=QUN(M)                                                             EBAP1500
        IF (UNI.LT.THO1) WRITE (6,1054) M,M,M,M,JX,UNI,QTUNM,QTUNP             EBAP1510
        IF (UNI.LT.THO1) UNI=THO1                                              EBAP1520
        IF (UNI.GE.UNMAX) WRITE (6,1054) M,M,M,M,JX,UNI,QTUNM,QTUNP            EBAP1530
        IF (UNI.GE.UNMAX) UNI=UNMAX+THOO                                       EBAP1540
        GE=2.0*ATAN((TAN(G7*UNI))**C13)                                        EBAP1550
        IF (GE.GT.PIBY2) GE=PIBY2                                              EBAP1560
        GE=ATAN(G3*TAN(G7*(UNI+GE)))                                           EBAP1570
        GE=ATAN(G3*TAN(G7*(UNI+GE)))                                           EBAP1580
C       COMPUTE MACH ANGLE COMPLIMENT ON BODY                                  EBAP1590
        DO 1005 JY=1,2                                                         EBAP1600
        G10=TAN(G7*(UNI+GE))                                                   EBAP1610
        G20=G7*TAN(GE)                                                         EBAP1620
        G11=G7*(1.0+G10*G10)                                                   EBAP1630
        G21=G7+G3*G20*G20                                                      EBAP1640
        G12=G7*G10*G11*2.0                                                     EBAP1650
        G22=G3*G20*G21*2.0                                                     EBAP1660
        G13=G7*(G11*G11+G10*G12)*2.0                                           EBAP1670
        G23=G3*(G21*G21+G20*G22)*2.0                                           EBAP1680
        G14=G7*(G12*(2.0*G11+G12)+G10*G13)*2.0                                 EBAP1690
        G24=G3*(G22*(2.0*G21+G22)+G20*G23)*2.0                                 EBAP1700
        G30=G10-G20                                                            EBAP1710
        G31=G21-G11                                                            EBAP1720
        G32=(G12-G22)/(2.0*G31)                                                EBAP1730
        G33=(G13-G23)/(6.0*G31)                                                EBAP1740
        G34=(G14-G24)/(24.0*G31)                                               EBAP1750
        DGE1=G30/G31                                                           EBAP1760
        DGE=DGE1                                                               EBAP1770
        DGE=DGE1+DGE*DGE*(G32+DGE*(G33+DGE*G34))                               EBAP1780
        DGE=DGE1+DGE*DGE*(G32+DGE*(G33+DGE*G34))                               EBAP1790
        GE=GE+DGE                                                              EBAP1800
 1005   CONTINUE                                                               EBAP1810
C       MACH ANGLE ON BODY                                                     EBAP1820
        QUM(M)=PIBY2-GE                                                        EBAP1830
        QMACH(M)=1.0/(SIN(QUM(M)))                                             EBAP1840
C       COMPUTE EACH CHARACTERISTIC POINT                                      EBAP1850
        DO 1011 J=1,MM100                                                      EBAP1860
```

```
      JO=M-J                                                                    EBAP1870
      J1=JO+1                                                                   EBAP1880
      VUMVT=TAN(VUM(JO)+VT(JO))                                                 EBAP1890
      QUMQT=TAN(QUM(J1)-QT(J1))                                                 EBAP1900
      RITAN=TAN(TIS)                                                            EBAP1910
      ROTAN=TAN(TOS)                                                            EBAP1920
      TJO=VUMVT+TAN(QUM(JO)+QT(JO))                                             EBAP1930
      TJ1=QUMQT+TAN(QUM(JO)-QT(JO))                                             EBAP1940
      QZ(JO)=(2.0*(QR(J1)-VR(JO))+TJO*VZ(JO)+TJ1*QZ(J1))/(TJO+TJ1)              EBAP1950
      QR(JO)=VR(JO)+0.5*TJO*(QZ(JO)-VZ(JO))                                     EBAP1960
      DETA=SQRT((QR(JO)-VR(JO))**2+(QZ(JO)-VZ(JO))**2)                          EBAP1970
      DXI=SQRT((QR(JO)-QR(J1))**2+(QZ(J1)-QZ(JO))**2)                           EBAP1980
      ZINT=(QR(JO)-RIS+RITAN*ZIS+TJ1*QZ(JO))/(RITAN+TJ1)                        EBAP1990
      RINT=RIS+(ZINT-ZIS)*RITAN                                                 EBAP2000
      ZOTR=(QR(JO)-ROS+ROTAN*ZOS+TJ1*QZ(JO))/(ROTAN+TJ1)                        EBAP2010
      ROTR=ROS+(ZOTR-ZOS)*ROTAN                                                 EBAP2020
      ZINV=(RIS-QR(JO)+TJO*QZ(JO)-RITAN*ZIS)/(TJO-RITAN)                        EBAP2030
      RINV=RIS+(ZINV-ZIS)*RITAN                                                 EBAP2040
      ZOTV=(ROS-QR(JO)+TJO*QZ(JO)-ROTAN*ZOS)/(TJO-ROTAN)                        EBAP2050
      ROTV=ROS+(ZOTV-ZOS)*ROTAN                                                 EBAP2060
      RAVG=0.5*(VR(JO)+QR(JO))                                                  EBAP2070
      UMAVG=0.5*(VUM(JO)+QUM(JO))                                               EBAP2080
      THAVG=0.5*(VT(JO)+QT(JO))                                                 EBAP2090
      GEAT=0.0                                                                  EBAP2100
      IF (QZ(JO).LT.ZSTRT) GO TO 1006                                           EBAP2110
      IF (VZ(JO).GT.ZSTOP) GO TO 1006                                           EBAP2120
      IF (QR(JO).LT.RINV) GO TO 1006                                            EBAP2130
      IF (VR(JO).GT.ROTV) GO TO 1006                                            EBAP2140
      GEAT=1.0                                                                  EBAP2150
      IF (VZ(JO).LT.ZSTRT) GEAT=GEAT*(QZ(JO)-ZSTRT)/(QZ(JO)-VZ(JO))            EBAP2160
      IF (QZ(JO).GT.ZSTOP) GEAT=GEAT*(ZSTOP-VZ(JO))/(QZ(JO)-VZ(JO))            EBAP2170
      IF (VR(JO).LT.RINV) GEAT=GEAT*(QR(JO)-RINV)/(QR(JO)-VR(JO))               EBAP2180
      IF (QR(JO).GT.ROTV) GEAT=GEAT*(ROTV-VR(JO))/(QR(JO)-VR(JO))               EBAP2190
 1006 CONTINUE                                                                  EBAP2200
      QTUNM=VT(JO)-VUN(JO)-(SIN(UMAVG))*(IXA*(SIN(THAVG))/RAVG-Q*GEAT)*DEBAP2210
     1ETA                                                                       EBAP2220
      RAVG=0.5*(QR(JO)+QR(J1))                                                  EBAP2230
      UMAVG=0.5*(QUM(JO)+QUM(J1))                                               EBAP2240
      THAVG=0.5*(QT(JO)+QT(J1))                                                 EBAP2250
      ACHAV=0.5*(QACH(JO)+QACH(J1))                                             EBAP2260
      ACAV2=ACHAV*ACHAV                                                         EBAP2270
      HEAT=0.0                                                                  EBAP2280
      IF (QZ(J1).LT.ZSTRT) GO TO 1007                                           EBAP2290
      IF (QZ(JO).GT.ZSTOP) GO TO 1007                                           EBAP2300
      IF (QR(JO).LT.RINT) GO TO 1007                                            EBAP2310
      IF (QR(J1).GT.ROTR) GO TO 1007                                            EBAP2320
      HEAT=1.0                                                                  EBAP2330
      IF (QZ(JO).LT.ZSTRT) HEAT=HEAT*(QZ(J1)-ZSTRT)/(QZ(J1)-QZ(JO))             EBAP2340
```

```
      IF (QZ(J1).GT.ZSTOP) HEAT=HEAT*(ZSTOP-QZ(J0))/(QZ(J1)-QZ(J0))      EBAP2350
      IF (QR(J1).LT.RINT) HEAT=HEAT*(QR(J0)-RINT)/(QR(J0)-QR(J1))        EBAP2360
      IF (QR(J0).GT.ROTR) HEAT=HEAT*(ROTR-QR(J1))/(QR(J0)-QR(J1))        EBAP2370
 1007 CONTINUE                                                           EBAP2380
      QTUNP=QT(J1)+QUN(J1)-(SIN(UMAVG))*(IXA*(SIN(THAVG))/RAVG-Q*HEAT)*DEBAP2390
     1XI                                                                 EBAP2400
      QT(J0)=0.5*(QTUNM+QTUNP)                                           EBAP2410
      QTABS=ABS(QT(J0))                                                  EBAP2420
      IF (QTABS.LT.TH01) QT(J0)=TH00                                     EBAP2430
      IF (ABFN1.GT.TH10) GO TO 1008                                      EBAP2440
      IF (ABFT1.GT.TH10) GO TO 1008                                      EBAP2441
      IF (QR(J0).LT.RINT) GO TO 1008                                     EBAP2450
      IF (QR(J1).GT.RINT) GO TO 1008                                     EBAP2460
      RIS=RINT                                                           EBAP2470
      ZIS=ZINT                                                           EBAP2480
      TIS=QT(J1)+(QT(J0)-QT(J1))*(RINT-QR(J1))/(QR(J0)-QR(J1))           EBAP2490
      TIDEG=57.3*TIS                                                     EBAP2500
 1008 CONTINUE                                                           EBAP2510
      IF (ABFN1.GT.TH10) GO TO 1009                                      EBAP2520
      IF (ABFT1.GT.TH10) GO TO 1009                                      EBAP2521
      IF (QR(J1).GT.ROTR) GO TO 1009                                     EBAP2530
      IF (QR(J0).LT.ROTR) GO TO 1009                                     EBAP2540
      RCS=ROTR                                                           EBAP2550
      ZCS=ZOTR                                                           EBAP2560
      TCS=QT(J1)+(QT(J0)-QT(J1))*(ROTR-QR(J1))/(QR(J0)-QR(J1))           EBAP2570
 1009 CONTINUE                                                           EBAP2580
      QUN(J0)=0.5*(QTUNP-QTUNM)                                          EBAP2590
      UNI=QUN(J0)                                                        EBAP2600
      IF (UNI.LT.TH01) WRITE (6,1054) J,J,M,M,M,UNI,QTUNM,QTUNP          EBAP2610
      IF (UNI.LT.TH01) UNI=TH01                                          EBAP2620
      IF (UNI.GE.UNMAX) WRITE (6,1054) J,J,M,M,M,UNI,QTUNM,QTUNP         EBAP2630
      IF (UNI.GE.UNMAX) UNI=UNMAX+TH00                                   EBAP2640
      GE=2.0*ATAN((TAN(G7*UNI))**C13)                                    EBAP2650
      IF (GE.GT.PIBY2) GE=PIBY2                                          EBAP2660
      GE=ATAN(G3*TAN(G7*(UNI+GE)))                                       EBAP2670
      GE=ATAN(G3*TAN(G7*(UNI+GE)))                                       EBAP2680
C     COMPUTE MACH ANGLE COMPLIMENT                                      EBAP2690
      DO 1010 JY=1,2                                                     EBAP2700
      G10=TAN(G7*(UNI+GE))                                               EBAP2710
      G20=G7*TAN(GE)                                                     EBAP2720
      G11=G7*(1.0+G10*G10)                                               EBAP2730
      G21=G7+G3*G20*G20                                                  EBAP2740
      G12=G7*G10*G11*2.0                                                 EBAP2750
      G22=G3*G20*G21*2.0                                                 EBAP2760
      G13=G7*(G11*G11+G10*G12)*2.0                                       EBAP2770
      G23=G3*(G21*G21+G20*G22)*2.0                                       EBAP2780
      G14=G7*(G12*(2.0*G11+G12)+G10*G13)*2.0                             EBAP2790
      G24=G3*(G22*(2.0*G21+G22)+G20*G23)*2.0                             EBAP2800
```

```
      G30=G10-G20                                                          EBAP2810
      G31=G21-G11                                                          EBAP2820
      G32=(G12-G22)/(2.0*G31)                                              EBAP2830
      G33=(G13-G23)/(6.0*G31)                                              EBAP2840
      G34=(G14-G24)/(24.0*G31)                                             EBAP2850
      DGE1=G30/G31                                                         EBAP2860
      DGE=DGE1                                                             EBAP2870
      DGE=DGE1+DGE*DGE*(G32+DGE*(G33+DGE*G34))                             EBAP2880
      DGE=DGE1+DGE*DGE*(G32+DGE*(G33+DGE*G34))                             EBAP2890
      GE=GE+DGE                                                            EBAP2900
 1010 CONTINUE                                                             EBAP2910
C     COMPUTE MACH ANGLE AT EACH CHARACTERISTIC POINT                      EBAP2920
      QUM(J0)=PIBY2-GE                                                     EBAP2930
      QACH(J0)=1.0/(SIN(QUM(J0)))                                          EBAP2940
 1011 CONTINUE                                                             EBAP2950
C     DETERMINE FACTOR FOR AND MAKE ERROR CORRECTION                       EBAP2960
      IF (JXCOR.EQ.1) GO TO 1014                                           EBAP2970
      ABDEN=ABS(QUN(ISTRT)-UN00-D1FNU)                                     EBAP2980
      IF (ABDEN.LE.TH10) GO TO 1012                                        EBAP2990
      IF (JX.GT.2) UNCOR=ABS(D2FNU/ABDEN)                                  EBAP3000
      IF (UNCOR.LT.1.0) UNCOR=1.0                                          EBAP3010
      IF (UNCOR.GT.4.0) UNCOR=4.0                                          EBAP3020
      IF (JX.GT.2) UNCMP=(UNCMP*(JX-1)+UNCOR)/JX                           EBAP3030
 1012 CONTINUE                                                             EBAP3040
      IF (JX.GT.6) UNCMP=0.75                                              EBAP3050
      D1FNU=QUN(ISTRT)-UN00                                                EBAP3060
      ABFN1=ABS(D1FNU)                                                     EBAP3061
      D1FTH=QT(ISTRT)-TH00                                                 EBAP3062
      ABFT1=ABS(D1FTH)                                                     EBAP3063
      IF (ABFT1.GT.TH10) GO TO 2014                                        EBAP3064
      IF (ABFN1.LE.TH10) JXCOR=1                                           EBAP3065
      IF (ABFN1.LE.TH10) GO TO 1013                                        EBAP3066
 2014 CONTINUE                                                             EBAP3070
      D2FNU=UNCMP*D1FNU                                                    EBAP3080
      IF (JX.LT.12) QUN(M)=QUN(M)-D2FNU                                    EBAP3090
 1013 CONTINUE                                                             EBAP3100
C     ESTIMATE PRANDTL-MEYER CORRECTION FOR NEXT BODY POINT, COMPUTE       EBAP3110
C     FINAL ERROR OF NU AT BC POINT, COMPUTE BOATTAIL DRAG                 EBAP3111
 1014 CONTINUE                                                             EBAP3120
      PMCOR=QUN(M)+QT(M)-VUN(M7)-VT(M7)                                    EBAP3130
      QDEG(M)=57.3*(QUN(ISTRT)-UN00)                                       EBAP3140
      P=1.0/((1.0+G1*QACH(M)*QACH(M))**G2)                                 EBAP3150
      BTDRG=BTDRG-(2.0*P00-P-P7)*(BL(M7)*BL(M7)-BL(M)*BL(M))               EBAP3160
      P7=P                                                                 EBAP3170
C     RESET FOR NEXT CHARACTERISTIC MESH LINE                              EBAP3180
      DO 1015 J=1,MM100                                                    EBAP3190
      J1=M-J+1                                                             EBAP3200
      VR(J1)=QR(J1)                                                        EBAP3210
```

```
      VZ(J1)=QZ(J1)                                                          EBAP3220
      VT(J1)=QT(J1)                                                          EBAP3230
      VUN(J1)=QUN(J1)                                                        EBAP3240
      VUM(J1)=QUM(J1)                                                        EBAP3250
      VACH(J1)=QACH(J1)                                                      EBAP3260
 1015 CONTINUE                                                               EBAP3270
C     COMPUTE FINAL VALUE OF THETA AT BC POINT                               EBAP3280
      QTDEG=57.3*QT(ISTRT)                                                   EBAP3290
      WRITE (6,1055) JX,UNCMP,VZ(M),QTDEG,P,QDEG(M),RIS,TIDEG                EBAP3300
 1016 CONTINUE                                                               EBAP3310
C     COMPUTE BTDRG BASED ON P TOTAL OF 1, R OF 1, NEGLECT BL THKNESS        EBAP3320
      BTDRG=PIBY2*BTDRG                                                      EBAP3330
C     STORE RESET VALUES FOR BASE CHARACTERISTIC MESH LINE                   EBAP3340
      DO 1017 MRS=ISTRT,100                                                  EBAP3350
      RSR(MRS)=VR(MRS)                                                       EBAP3360
      RSZ(MRS)=VZ(MRS)                                                       EBAP3370
      RST(MRS)=VT(MRS)                                                       EBAP3380
      RSUM(MRS)=VUM(MRS)                                                     EBAP3390
      RSUN(MRS)=VUN(MRS)                                                     EBAP3400
      RSACH(MRS)=VACH(MRS)                                                   EBAP3410
 1017 CONTINUE                                                               EBAP3420
C     STORE RESET VALUES FOR HEAT ZONE                                       EBAP3430
      RSRIS=RIS                                                              EBAP3440
      RSROS=ROS                                                              EBAP3450
      RSZIS=ZIS                                                              EBAP3460
      RSZOS=ZOS                                                              EBAP3470
      RSTIS=TIS                                                              EBAP3480
      RSTOS=TOS                                                              EBAP3490
      NCK1=NBL/2                                                             EBAP3500
      NCK2=(NBL+1)/2                                                         EBAP3510
      NCK3=(NBL-1)/2                                                         EBAP3520
      RBYBL=BTR*RBYBL                                                        EBAP3530
      W2=1.0/(G1+1.0/(RSACH(100)*RSACH(100)))                                EBAP3540
      BETA2=G1*W2                                                            EBAP3550
      BETA=SQRT(BETA2)                                                       EBAP3560
      BMO=(0.5/(BETA**(2*NBL+1)))*ALOG((1.0+BETA)/(1.0-BETA))                EBAP3570
C     COMPUTE BL MASS FLUX AT BASE                                           EBAP3580
      DO 1018 J=1,NBL                                                        EBAP3590
      BMO=BMO-0.5/((NBL+0.5-J)*(BETA2**J))                                   EBAP3600
 1018 CONTINUE                                                               EBAP3610
C     DETERMINE IF BL VEL PROFILE EXPONENT IS ODD OR EVEN                    EBAP3620
      IF (NCK2.GT.NCK1) GO TO 1020                                           EBAP3630
      BMEVN=(0.5/(BETA**(NBL+1)))*ALOG((1.0+BETA)/(1.0-BETA))                EBAP3640
C     COMPUTE EVEN CONTRIBUTION                                              EBAP3650
      DO 1019 J=1,NCK1                                                       EBAP3660
      BMEVN=BMEVN-0.5/((NCK1+0.5-J)*(BETA2**J))                              EBAP3670
 1019 CONTINUE                                                               EBAP3680
C     COMPUTE EVEN BL MASS FLUX AT BASE                                      EBAP3690
```

```
      BMASS=NBL*(IXA*BMO+RBYBL*BMEVN)                                    EBAP3700
      GO TO 1023                                                         EBAP3710
 1020 CONTINUE                                                           EBAP3720
      BMODD=(0.5/(BETA**(NBL+1)))*ALOG(1.0/(1.0-BETA2))                  EBAP3730
      IF (NBL.EQ.1) GO TO 1022                                           EBAP3740
C     COMPUTE ODD CONTRIBUTION                                           EBAP3750
      DO 1021 J=1,NCK3                                                   EBAP3760
      BMODD=BMODD-0.5/((NCK2-J)*(BETA2**J))                              EBAP3770
 1021 CONTINUE                                                           EBAP3780
C     COMPUTE ODD BL MASS FLUX AT BASE                                   EBAP3790
 1022 CONTINUE                                                           EBAP3800
      BMASS=NBL*(IXA*BMO+RBYBL*BMODD)                                    EBAP3810
 1023 CONTINUE                                                           EBAP3820
      CNST=(IXA+RBYBL)*(1.0+RBYBL)/(AK1*P*W*BMASS)                       EBAP3830
C     CNST USED TO DETERMINE F AT BASE                                   EBAP3840
      DO 1024 I=101,111                                                  EBAP3850
      BL(I)=BL(100)                                                      EBAP3860
 1024 CONTINUE                                                           EBAP3870
C     INITIAL RADIUS OF EXPANSION CORNER FAN SET                         EBAP3880
      W=V                                                                EBAP3890
      W0=W                                                               EBAP3900
      W2=W*W                                                             EBAP3910
      WRITE (6,1056) G,BKL1,BKT,Q,ZSTRT,ZSTOP,NBL                        EBAP3920
      WRITE (6,1056) REL,RETR,RETRT,RBYL,ACH0,RIS,IXA                    EBAP3930
C     LOOP FOR INCREASING CLOSENESS OF STRADDLE                          EBAP3940
      DO 1050 L=1,4                                                      EBAP3950
      LL1=(L+1)/2                                                        EBAP3960
C     LOOP UNTIL SADDLE POINT IS STRADDLED                               EBAP3970
      DO 1048 N=1,11                                                     EBAP3980
C     RESET  CHARACTERISTIC MESH LINE AFTER EACH INTEGRATION             EBAP3990
      DO 1025 MRS=ISTRT,100                                              EBAP4000
      VR(MRS)=RSR(MRS)                                                   EBAP4010
      VZ(MRS)=RSZ(MRS)                                                   EBAP4020
      VT(MRS)=RST(MRS)                                                   EBAP4030
      VUN(MRS)=RSUN(MRS)                                                 EBAP4040
      VUM(MRS)=RSUM(MRS)                                                 EBAP4050
      VACH(MRS)=RSACH(MRS)                                               EBAP4060
 1025 CONTINUE                                                           EBAP4070
C     RESET HEAT ZONE AFTER EACH INTEGRATION                             EBAP4080
      RIS=RSRIS                                                          EBAP4090
      ROS=RSROS                                                          EBAP4100
      ZIS=RSZIS                                                          EBAP4110
      ZOS=RSZOS                                                          EBAP4120
      TIS=RSTIS                                                          EBAP4130
      TOS=RSTOS                                                          EBAP4140
      XBL=0.0                                                            EBAP4150
C     SET COORDINATES OF EXPANSION CORNER                                EBAP4160
      DO 1026 I=100,111                                                  EBAP4170
```

```
      VR(I)=BL(100)                                                          EBAP4180
      VZ(I)=XBL                                                              EBAP4190
 1026 CONTINUE                                                               EBAP4200
C     COMPUTE P RATIO AND F DOWNSTREAM OF FAN                                EBAP4210
      P=(1.0-G1*W2)**G2                                                      EBAP4220
      F=CNST*P*W-1.0+G1*W2                                                   EBAP4230
      WCO=WO                                                                 EBAP4240
      WO=W                                                                   EBAP4250
      WO2=W2                                                                 EBAP4260
      FO=F                                                                   EBAP4270
      PO=P                                                                   EBAP4280
      PMCOR=0.0                                                              EBAP4290
C     INCREMENT CHARACTERISTIC MESH ALONG SHEAR LAYER                        EBAP4300
      DO 1046 M=111,200                                                      EBAP4310
      MMID=(ISTRT+M)/2                                                       EBAP4320
      M7=M-1                                                                 EBAP4330
      MM100=M-ISTRT                                                          EBAP4340
      MM99=MM100+1                                                           EBAP4350
      XBL7=XBL                                                               EBAP4360
      W9=1.0-G1*W2                                                           EBAP4370
      EM2=W2/W9                                                              EBAP4380
      G5=SQRT(EM2-1.0)                                                       EBAP4390
      EM=SQRT(EM2)                                                           EBAP4400
      IF (M.EQ.111) WRITE (6,1057) L,N,M,F,W,BL(111),P,EM                    EBAP4410
      IF (M.EQ.111) MACH(111)=EM                                             EBAP4420
      UM=ARSIN(1.0/EM)                                                       EBAP4430
      IF (M.EQ.111) VUM(111)=UM                                              EBAP4440
      ENU=G3*ATAN(G5/G3)-ATAN(G5)                                            EBAP4450
      IF (M.EQ.111) VUN(111)=ENU                                             EBAP4460
      IF (M.EQ.111) TH=RSUN(100)+RST(100)-ENU                                EBAP4470
      IF (M.EQ.111) VT(111)=TH                                               EBAP4480
      IF (M.EQ.111) GO TO 1027                                               EBAP4490
      TH=TH7+ENU7-ENU+PMCOR                                                  EBAP4500
 1027 CONTINUE                                                               EBAP4510
      QACH(M)=EM                                                             EBAP4520
      QUM(M)=UM                                                              EBAP4530
      QUN(M)=ENU                                                             EBAP4540
      QT(M)=TH                                                               EBAP4550
      IF (M.GT.111) GO TO 1030                                               EBAP4560
      THCMP=(VT(111)-VT(100))/11.0                                           EBAP4570
C     COMPUTE REMAINING VALUES FOR FAN                                       EBAP4580
      DO 1029 I=101,110                                                      EBAP4590
      IM1=I-1                                                                EBAP4600
      VT(I)=VT(IM1)+THCMP                                                    EBAP4610
      VUN(I)=VUN(100)+VT(100)-VT(I)                                          EBAP4620
      UNI=VUN(I)                                                             EBAP4630
      IF (UNI.LT.TH01) WRITE (6,1058) L,N,M,JX,JO,UNI,QTUNM,QTUNP            EBAP4640
      IF (UNI.LT.TH01) UNI=TH01                                              EBAP4650
```

```
      IF (UNI.GE.UNMAX) WRITE (6,1058) L,N,M,JX,JC,UNI,QTUNM,QTUNP      EBAP4660
      IF (UNI.GE.UNMAX) UNI=UNMAX+THOO                                  EBAP4670
      GE=2.0*ATAN((TAN(G7*UNI))**C13)                                   EBAP4680
      IF (GE.GT.PIBY2) GE=PIBY2                                         EBAP4690
      GE=ATAN(G3*TAN(G7*(UNI+GE)))                                      EBAP4700
      GE=ATAN(G3*TAN(G7*(UNI+GE)))                                      EBAP4710
C     COMPUTE MACH ANGLE OF EACH WAVE IN FAN                            EBAP4720
      DO 1028 IX=1,2                                                    EBAP4730
      G10=TAN(G7*(UNI+GE))                                              EBAP4740
      G20=G7*TAN(GE)                                                    EBAP4750
      G11=G7*(1.0+G10*G10)                                              EBAP4760
      G21=G7+G3*G20*G20                                                 EBAP4770
      G12=G7*G10*G11*2.0                                                EBAP4780
      G22=G3*G20*G21*2.0                                                EBAP4790
      G13=G7*(G11*G11+G10*G12)*2.0                                      EBAP4800
      G23=G3*(G21*G21+G20*G22)*2.0                                      EBAP4810
      G14=G7*(G12*(2.0*G11+G12)+G10*G13)*2.0                            EBAP4820
      G24=G3*(G22*(2.0*G21+G22)+G20*G23)*2.0                            EBAP4830
      G30=G10-G20                                                       EBAP4840
      G31=G21-G11                                                       EBAP4850
      G32=(G12-G22)/(2.0*G31)                                           EBAP4860
      G33=(G13-G23)/(6.0*G31)                                           EBAP4870
      G34=(G14-G24)/(24.0*G31)                                          EBAP4880
      DGE1=G30/G31                                                      EBAP4890
      DGE=DGE1                                                          EBAP4900
      DGE=DGE1+DGE*DGE*(G32+DGE*(G33+DGE*G34))                          EBAP4910
      DGE=DGE1+DGE*DGE*(G32+DGE*(G33+DGE*G34))                          EBAP4920
      GE=GE+DGE                                                         EBAP4930
 1028 CONTINUE                                                          EBAP4940
C     SET IN ESTIMATED VALUES FOR NEXT COMPUTATION                      EBAP4950
      VUM(I)=PIBY2-GE                                                   EBAP4960
      VACH(I)=1.0/(SIN(VUM(I)))                                         EBAP4970
      QT(I)=VT(I)                                                       EBAP4980
      QUN(I)=VUN(I)                                                     EBAP4990
      QUM(I)=VUM(I)                                                     EBAP5000
      QACH(I)=VACH(I)                                                   EBAP5010
 1029 CONTINUE                                                          EBAP5020
C     COMPUTE KAPPA                                                     EBAP5030
 1030 CONTINUE                                                          EBAP5040
      AK=1.0-(0.5-(0.29333-0.0563*F)*F)*F                               EBAP5050
      DKDF=-0.5+(0.58667-0.16889*F)*F                                   EBAP5060
      IF (F.GT.1.5) AK=0.72                                             EBAP5070
      IF (F.GT.1.5) DKDF=0.0                                            EBAP5080
      IF (M.EQ.111) GO TO 1044                                          EBAP5090
      WA=0.5*(W+W7)                                                     EBAP5100
      WA2=WA*WA                                                         EBAP5110
      ABFT1=1.0                                                         EBAP5120
      ABFN1=1.0                                                         EBAP5130
```

```
      THCMP=2.0                                                          EBAP5140
      JXCOR=0                                                            EBAP5141
C     WORK BACKWARDS ALONG RIGHT RUNNING CHARACTERISTIC FROM SHEAR       EBAP5150
C     LAYER TO UPSTREAM MACH LINE BC                                     EBAP5151
      DO 1041 JX=1,12                                                    EBAP5160
C     DETERMINE NEXT POINT ON SHEAR  LAYER WITH MASS FLUX COMPUTATION    EBAP5170
      DO 1033 IBK=1,2                                                    EBAP5180
      XBL6=0.5*(XBL7+XBL)                                                EBAP5190
      BLERF=0.5*ERF((ZTRAV-XBL6)*XCONV)                                  EBAP5200
      BK=BKL*(0.5+BLERF)+BKT*(0.5-BLERF)                                 EBAP5210
      X1=((1.0-G1*W2)**G2)*(W/AK)/(F+1.0-G1*W2)                          EBAP5220
      X2=(BL(M7))*((1.0-G1*W72)**G2)*(W7/AK7)/(F7+1.0-G1*W72)            EBAP5230
      X3=BK*WA*((1.0-G1*WA2)**G6)                                        EBAP5240
      TPK=0.5*(TH+TH7)+BK                                                EBAP5250
      DX0=(X2-X1*BL(M7))/(X1*TPK-X3)                                     EBAP5260
      DX=DX0                                                             EBAP5270
      IF (IXA.EQ.0) GO TO 1032                                           EBAP5280
      DX=0.5*DX                                                          EBAP5290
C     COMPUTE DX FOR AXISYMMETRIC                                        EBAP5300
      DO 1031 MM=1,4                                                     EBAP5310
      DX=0.5*(DX0-TPK*DX*DX/BL(M7))                                      EBAP5320
 1031 CONTINUE                                                           EBAP5330
C     CAN SOMETIMES GET NEG DX IF W IS LOW AND LEFT OF SADDLE            EBAP5340
 1032 CONTINUE                                                           EBAP5350
      IF (DX.LE.0.0) ANUM=SHOCK                                          EBAP5360
      IF (DX.LE.0.0) GO TO 1047                                          EBAP5370
      BL(M)=BL(M7)+DX*TPK                                                EBAP5380
      XBL=XBL7+DX                                                        EBAP5390
 1033 CONTINUE                                                           EBAP5400
C     SET MESH POINT POSITION TO SHEAR LAYER POINT                       EBAP5410
      QR(M)=BL(M)                                                        EBAP5420
      QZ(M)=XBL                                                          EBAP5430
C     COMPUTE EACH CHARACTERISTIC POINT                                  EBAP5440
      DO 1039 J=1,MM100                                                  EBAP5450
      JO=M-J                                                             EBAP5460
      J1=JO+1                                                            EBAP5470
      VUMVT=TAN(VUM(JO)+VT(JO))                                          EBAP5480
      QUMQT=TAN(QUM(J1)-QT(J1))                                          EBAP5490
      RITAN=TAN(TIS)                                                     EBAP5500
      RCTAN=TAN(TOS)                                                     EBAP5510
      TJO=VUMVT+TAN(QUM(JO)+QT(JO))                                      EBAP5520
      TJ1=QUMQT+TAN(QUM(JO)-QT(JO))                                      EBAP5530
      QZ(JO)=(2.0*(QR(J1)-VR(JO))+TJO*VZ(JO)+TJ1*QZ(J1))/(TJO+TJ1)       EBAP5540
      QR(JO)=VR(JO)+0.5*TJO*(QZ(JO)-VZ(JO))                              EBAP5550
      DETA=SQRT((QR(JO)-VR(JO))**2+(QZ(JO)-VZ(JO))**2)                   EBAP5560
      DXI=SQRT((QR(JO)-QR(J1))**2+(QZ(J1)-QZ(JO))**2)                    EBAP5570
      ZINT=(QR(JO)-RIS+RITAN*ZIS+TJ1*QZ(JO))/(RITAN+TJ1)                 EBAP5580
      RINT=RIS+(ZINT-ZIS)*RITAN                                          EBAP5590
```

```
      ZCTR=(QR(JO)-ROS+ROTAN*ZOS+TJ1*QZ(JO))/(ROTAN+TJ1)                    EBAP5600
      RCTR=ROS+(ZOTR-ZOS)*ROTAN                                             EBAP5610
      ZINV=(RIS-QR(JO)+TJO*QZ(JO)-RITAN*ZIS)/(TJO-RITAN)                    EBAP5620
      RINV=RIS+(ZINV-ZIS)*RITAN                                             EBAP5630
      ZOTV=(RCS-QR(JO)+TJO*QZ(JO)-ROTAN*ZOS)/(TJO-ROTAN)                    EBAP5640
      RCTV=ROS+(ZOTV-ZOS)*ROTAN                                             EBAP5650
      RAVG=0.5*(VR(JO)+QR(JO))                                              EBAP5660
      UMAVG=0.5*(VUM(JO)+QUM(JO))                                           EBAP5670
      THAVG=0.5*(VT(JO)+QT(JO))                                             EBAP5680
      GEAT=0.0                                                              EBAP5690
      IF (QZ(JO).LT.ZSTRT) GO TO 1034                                       EBAP5700
      IF (VZ(JO).GT.ZSTOP) GO TO 1034                                       EBAP5710
      IF (QR(JO).LT.RINV) GO TO 1034                                        EBAP5720
      IF (VR(JO).GT.ROTV) GO TO 1034                                        EBAP5730
      GEAT=1.0                                                              EBAP5740
      IF (VZ(JO).LT.ZSTRT) GEAT=GEAT*(QZ(JO)-ZSTRT)/(QZ(JO)-VZ(JO))        EBAP5750
      IF (QZ(JO).GT.ZSTOP) GEAT=GEAT*(ZSTOP-VZ(JO))/(QZ(JO)-VZ(JO))        EBAP5760
      IF (VR(JO).LT.RINV) GEAT=GEAT*(QR(JO)-RINV)/(QR(JO)-VR(JO))           EBAP5770
      IF (QR(JO).GT.ROTV) GEAT=GEAT*(ROTV-VR(JO))/(QR(JO)-VR(JO))           EBAP5780
 1034 CONTINUE                                                              EBAP5790
      QTUNM=VT(JO)-VUN(JO)-(SIN(UMAVG))*(IXA*(SIN(THAVG))/RAVG-Q*GEAT)*DE   EBAP5800
     1ETA                                                                   EBAP5810
      RAVG=0.5*(QR(JO)+QR(J1))                                              EBAP5820
      UMAVG=0.5*(QUM(JO)+QUM(J1))                                           EBAP5830
      THAVG=0.5*(QT(JO)+QT(J1))                                             EBAP5840
      HEAT=0.0                                                              EBAP5850
      IF (QZ(J1).LT.ZSTRT) GO TO 1035                                       EBAP5860
      IF (QZ(JO).GT.ZSTOP) GO TO 1035                                       EBAP5870
      IF (QR(JO).LT.RINT) GO TO 1035                                        EBAP5880
      IF (QR(J1).GT.ROTR) GO TO 1035                                        EBAP5890
      HEAT=1.0                                                              EBAP5900
      IF (QZ(JO).LT.ZSTRT) HEAT=HEAT*(QZ(J1)-ZSTRT)/(QZ(J1)-QZ(JO))        EBAP5910
      IF (QZ(J1).GT.ZSTOP) HEAT=HEAT*(ZSTOP-QZ(JO))/(QZ(J1)-QZ(JO))        EBAP5920
      IF (QR(J1).LT.RINT) HEAT=HEAT*(QR(JO)-RINT)/(QR(JO)-QR(J1))           EBAP5930
      IF (QR(JO).GT.ROTR) HEAT=HEAT*(ROTR-QR(J1))/(QR(JO)-QR(J1))           EBAP5940
 1035 CONTINUE                                                              EBAP5950
      QTUNP=QT(J1)+QUN(J1)-(SIN(UMAVG))*(IXA*(SIN(THAVG))/RAVG-Q*HEAT)*DE   EBAP5960
     1XI                                                                    EBAP5970
      QT(JO)=0.5*(QTUNM+QTUNP)                                              EBAP5980
      QTABS=ABS(QT(JO))                                                     EBAP5990
      IF (QTABS.LT.TH01) QT(JO)=TH00                                        EBAP6000
      IF (ABFT1.GT.TH10) GO TO 1036                                         EBAP6010
      IF (ABFN1.GT.TH10) GO TO 1036                                         EBAP6011
      IF (QR(JO).LT.RINT) GO TO 1036                                        EBAP6020
      IF (QR(J1).GT.RINT) GO TO 1036                                        EBAP6030
      RIS=RINT                                                              EBAP6040
      ZIS=ZINT                                                              EBAP6050
      TIS=QT(J1)+(QT(JO)-QT(J1))*(RINT-QR(J1))/(QR(JO)-QR(J1))              EBAP6060
```

```
      ACHIS=QACH(J1)+(QACH(JO)-QACH(J1))*(RINT-QR(J1))/(QR(JO)-QR(J1))   EBAP6061
      PRIS=1.0/(POO*(1.0+G1*ACHIS*ACHIS)**G2)                            EBAP6062
 1036 CONTINUE                                                           EBAP6070
      IF (ABFT1.GT.TH10) GO TO 1037                                      EBAP6080
      IF (ABFN1.GT.TH10) GO TO 1037                                      EBAP6081
      IF (QR(J1).GT.ROTR) GO TO 1037                                     EBAP6090
      IF (QR(JO).LT.ROTR) GO TO 1037                                     EBAP6100
      RCS=ROTR                                                           EBAP6110
      ZCS=ZOTR                                                           EBAP6120
      TOS=QT(J1)+(QT(JO)-QT(J1))*(ROTR-QR(J1))/(QR(JO)-QR(J1))           EBAP6130
      ACHOS=QACH(J1)+(QACH(JO)-QACH(J1))*(ROTR-QR(J1))/(QR(JO)-QR(J1))   EBAP6131
      PROS= 1.0/(POO*(1.0+G1*ACHOS*ACHOS)**G2)                           EBAP6132
 1037 CONTINUE                                                           EBAP6140
      QUN(JO)=0.5*(QTUNP-QTUNM)                                          EBAP6150
      UNI=QUN(JO)                                                        EBAP6160
      IF (UNI.LT.TH01) WRITE (6,1058) M,N,L,JX,JO,UNI,QTUNM,QTUNP        EBAP6170
      IF (UNI.LT.TH01) UNI=TH01                                          EBAP6180
      IF (UNI.GE.UNMAX) WRITE (6,1058) M,N,L,JX,JO,UNI,QTUNM,QTUNP       EBAP6190
      IF (UNI.GE.UNMAX) UNI=UNMAX+TH00                                   EBAP6200
      GE=2.0*ATAN((TAN(G7*UNI))**C13)                                    EBAP6210
      IF (GE.GT.PIBY2) GE=PIBY2                                          EBAP6220
      GE=ATAN(G3*TAN(G7*(UNI+GE)))                                       EBAP6230
      GE=ATAN(G3*TAN(G7*(UNI+GE)))                                       EBAP6240
C     COMPUTE MACH ANGLE COMPLIMENT                                      EBAP6250
      DO 1038 JY=1,2                                                     EBAP6260
      G10=TAN(G7*(UNI+GE))                                               EBAP6270
      G20=G7*TAN(GE)                                                     EBAP6280
      G11=G7*(1.0+G10*G10)                                               EBAP6290
      G21=G7+G3*G20*G20                                                  EBAP6300
      G12=G7*G10*G11*2.0                                                 EBAP6310
      G22=G3*G20*G21*2.0                                                 EBAP6320
      G13=G7*(G11*G11+G10*G12)*2.0                                       EBAP6330
      G23=G3*(G21*G21+G20*G22)*2.0                                       EBAP6340
      G14=G7*(G12*(2.0*G11+G12)+G10*G13)*2.0                             EBAP6350
      G24=G3*(G22*(2.0*G21+G22)+G20*G23)*2.0                             EBAP6360
      G30=G10-G20                                                        EBAP6370
      G31=G21-G11                                                        EBAP6380
      G32=(G12-G22)/(2.0*G31)                                            EBAP6390
      G33=(G13-G23)/(6.0*G31)                                            EBAP6400
      G34=(G14-G24)/(24.0*G31)                                           EBAP6410
      DGE1=G30/G31                                                       EBAP6420
      DGE=DGE1                                                           EBAP6430
      DGE=DGE1+DGE*DGE*(G32+DGE*(G33+DGE*G34))                           EBAP6440
      DGE=DGE1+DGE*DGE*(G32+DGE*(G33+DGE*G34))                           EBAP6450
      GE=GE+DGE                                                          EBAP6460
 1038 CONTINUE                                                           EBAP6470
C     COMPUTE MACH ANGLE AT EACH CHARACTERISTIC POINT                    EBAP6480
      QUN(JO)=PIBY2-GE                                                   EBAP6490
```

```
      QACH(J0)=1.0/(SIN(QUM(J0)))                                                    EBAP6500
 1039 CONTINUE                                                                       EBAP6510
C     DETERMINE FACTOR FOR AND MAKE ERROR CORRECTION                                 EBAP6520
      IF (JXCOR.EQ.1) GO TO 1042                                                     EBAP6530
      ABTEN=ABS(QT(ISTRT)-TH00-D1FTH)                                                EBAP6540
      IF (ABTEN.LE.TH10) GO TO 1040                                                  EBAP6550
      IF (JX.GT.2) THCOR=ABS(D2FTH/ABTEN)                                            EBAP6560
      IF (THCOR.LT.1.0) THCOR=1.0                                                    EBAP6570
      IF (THCOR.GT.4.0) THCOR=4.0                                                    EBAP6580
      IF (JX.GT.2) THCMP=(THCMP*(JX-1)+THCOR)/JX                                     EBAP6590
 1040 CONTINUE                                                                       EBAP6600
      IF (JX.GT.6) THCMP=0.75                                                        EBAP6610
      D1FNU=QUN(ISTRT)-UN00                                                          EBAP6611
      ABFN1=ABS(D1FNU)                                                               EBAP6612
      D1FTH=QT(ISTRT)-TH00                                                           EBAP6620
      ABFT1=ABS(D1FTH)                                                               EBAP6621
      IF (ABFN1.GT.TH10) GO TO 2042                                                  EBAP6622
      IF (ABFT1.LE.TH10) JXCOR=1                                                     EBAP6623
      IF (ABFT1.LE.TH10) GO TO 1041                                                  EBAP6624
 2042 CONTINUE                                                                       EBAP6625
      D2FTH=THCMP*D1FTH                                                              EBAP6630
      IF (JX.LT.12) QT(M)=QT(M)-D2FTH                                                EBAP6650
      TH=QT(M)                                                                       EBAP6660
 1041 CONTINUE                                                                       EBAP6670
C     ESTIMATE PRANDTL-MEYER CORRECTION FOR NEXT SHEAR LAYER POINT                   EBAP6680
 1042 CONTINUE                                                                       EBAP6690
      IF (M.GT.111) PMCOR=QUN(M)+QT(M)-VUN(M7)-VT(M7)                                EBAP6700
      QDEG(M)=57.3*QT(ISTRT)                                                         EBAP6710
      QDENU=57.3*(QUN(ISTRT)-UN00)                                                   EBAP6720
      BLPR=1.0/(P00*((1.0+G1*QACH(M)*QACH(M))**G2))                                  EBAP6730
      IF (L.EQ.1) WRITE (6,1060) JX,N,M,BL(M),QZ(M),QT(M),QDEG(M),QDENU              EBAP6740
      IF (L.EQ.1) WRITE (6,1060) JX,N,M,BLPR,RIS,ZIS,ROS,ZCS                         EBAP6741
      IF (L.EQ.1) WRITE (6,1060) JX,N,M,PRIS,ACHIS,PROS,ACHOS                        EBAP6742
C     RESET FOR NEXT CHARACTERISTIC MESH LINE                                        EBAP6750
      DO 1043 J=1,MM100                                                              EBAP6760
      J1=M-J+1                                                                       EBAP6770
      VR(J1)=QR(J1)                                                                  EBAP6780
      VZ(J1)=QZ(J1)                                                                  EBAP6790
      VT(J1)=QT(J1)                                                                  EBAP6800
      VUN(J1)=QUN(J1)                                                                EBAP6810
      VUM(J1)=QUM(J1)                                                                EBAP6820
      VACH(J1)=QACH(J1)                                                              EBAP6830
 1043 CONTINUE                                                                       EBAP6840
C     CHECK FOR DFDW SIGN CHANGE, RESET FOR NEXT COMPUTATION                         EBAP6850
 1044 CONTINUE                                                                       EBAP6860
      XBL6=0.5*(XBL7+XBL)                                                            EBAP6870
      BLERF=0.5*ERF((ZTRAV-XBL6)*XCONV)                                              EBAP6880
      BK=BKL*(0.5+BLERF)+BKT*(0.5-BLERF)                                             EBAP6890
```

```
      H3=(TH/BK)*W9/(1.0-AK)                                                    EBAP6900
      ANUM=(G4*W2-1.0)*W9+F*(G*W2-F*AK/(1.0-AK)+H3)                             EBAP6910
      DEN=W*W9*(DKDF*(H3/AK-(F/AK)/(1.0-AK))-1.0)                               EBAP6920
      DFDW=ANUM/DEN                                                             EBAP6930
      IF (DFDW.LE.0.0) GO TO 1047                                               EBAP6940
      ENU7=ENU                                                                  EBAP6950
      TH7=TH                                                                    EBAP6960
      F7=F                                                                      EBAP6970
      W7=W                                                                      EBAP6980
      W72=W2                                                                    EBAP6990
      AK7=AK                                                                    EBAP7000
      DFDW7=DFDW                                                                EBAP7010
      DF=0.1*F                                                                  EBAP7020
      IF (F.LT.0.8) DF=0.08                                                     EBAP7030
      F=F-DF                                                                    EBAP7040
C     INCREMENT W TO MATCH F AND APPROX DFDW AT NEXT POINT                      EBAP7050
      DO 1045 J=1,3                                                             EBAP7060
      W=W7-0.5*DF*(1.0/DFDW+1.0/DFDW7)                                          EBAP7070
      IF (W.LE.1.0) W=1.0+TH01                                                  EBAP7080
      W2=W*W                                                                    EBAP7090
      W9=1.0-G1*W2                                                              EBAP7100
      EM2=W2/W9                                                                 EBAP7110
      G5=SQRT(EM2-1.0)                                                          EBAP7120
      ENU=G3*ATAN(G5/G3)-ATAN(G5)                                               EBAP7130
      TH=TH7+ENU7-ENU+PMCOR                                                     EBAP7140
      AK=1.0-(0.5-(0.29333-0.0563*F)*F)*F                                       EBAP7150
      DKDF=-0.5+(0.58667-0.16889*F)*F                                           EBAP7160
      IF (F.GT.1.5) AK=0.72                                                     EBAP7170
      IF (F.GT.1.5) DKDF=0.0                                                    EBAP7180
      XBL6=0.5*(XBL7+XBL)                                                       EBAP7190
      BLERF=0.5*ERF((ZTRAV-XBL6)*XCONV)                                         EBAP7200
      BK=BKL*(0.5+BLERF)+BKT*(0.5-BLERF)                                        EBAP7210
      H3=(TH/BK)*W9/(1.0-AK)                                                    EBAP7220
      ANUM=(G4*W2-1.0)*W9+F*(G*W2-F*AK/(1.0-AK)+H3)                             EBAP7230
      DEN=W*W9*(DKDF*(H3/AK-(F/AK)/(1.0-AK))-1.0)                               EBAP7240
      DFDW=ANUM/DEN                                                             EBAP7250
      IF (DFDW.LE.0.0) GO TO 1047                                               EBAP7260
 1045 CONTINUE                                                                  EBAP7270
C     COMPUTE W FOR NEXT POINT                                                  EBAP7280
      W=W7-0.5*DF*(1.0/DFDW+1.0/DFDW7)                                          EBAP7290
      W2=W*W                                                                    EBAP7300
      IF (W.LE.1.0) WRITE (6,1059) W,W2,W,W2,W,W2                               EBAP7310
      IF (F.LE.0.7) GO TO 1051                                                  EBAP7320
      IF (W.LE.1.0) GO TO 1049                                                  EBAP7330
      IF (W.GT.2.2) GO TO 1047                                                  EBAP7340
 1046 CONTINUE                                                                  EBAP7350
C     COMPUTE DRAG, INCREMENT W FOR NEXT INTEGRATION OF STRADDLE METHOD         EBAP7360
 1047 CONTINUE                                                                  EBAP7370
```

```
      IF (M.GT.111) WRITE (6,1060) L,N,M7,F7,W7,BL(M7),XBL7,ANUM          EBAP7380
      PBYPO=PO/POO                                                       EBAP7390
      BDRAG=2.0*PIBY2*(PO-POO)*BTR*BTR                                   EBAP7400
      TDRAG=BDRAG+BTDRG                                                  EBAP7410
      WRITE (6,1061) PBYPO,BTDRG,BDRAG,TDRAG                             EBAP7420
      IF (ANUM.GT.0.0) GO TO 1049                                        EBAP7430
      W=WO+DW                                                            EBAP7440
      IF (W.LE.1.0) WRITE (6,1059) W,W,W,W,W,W                           EBAP7450
      IF (W.LE.1.0) GO TO 1049                                           EBAP7460
      W2=A*W                                                             EBAP7470
 1048 CONTINUE                                                           EBAP7480
C     STRADDLE CONDITION ACHIEVED, DIVIDE STRADDLE INTERVAL              EBAP7490
 1049 CONTINUE                                                           EBAP7500
      WC=WOO                                                             EBAP7510
      DW=DW/SHOCK                                                        EBAP7520
      W=WO+DW                                                            EBAP7530
      W2=W*W                                                             EBAP7540
 1050 CONTINUE                                                           EBAP7550
 1051 CONTINUE                                                           EBAP7560
      PBYPO=PO/POO                                                       EBAP7570
      BDRAG=2.0*PIBY2*(PO-POO)*BTR*BTR                                   EBAP7580
      TDRAG=BDRAG+BTDRG                                                  EBAP7590
      WRITE(6,1061)PBYPO,BTDRG,BDRAG,TDRAG                               EBAP7600
      V=VSTRT                                                            EBAP7610
 1052 CONTINUE                                                           EBAP7620
 1053 FORMAT(' ',1I12,7E16.7)                                            EBAP7640
 1054 FORMAT(' ',5I12,3E16.7)                                            EBAP7650
 1055 FORMAT(' ',1I12,7E16.7)                                            EBAP7660
 1056 FORMAT(' ',6F16.7,1I12)                                            EBAP7670
 1057 FORMAT(' ',3I12,5E16.7)                                            EBAP7680
 1058 FORMAT(' ',5I12,3E16.7)                                            EBAP7690
 1059 FORMAT(' ',6E16.7)                                                 EBAP7700
 1060 FORMAT(' ',3I12,5E16.7)                                            EBAP7710
 1061 FORMAT(' ',4E16.7)                                                 EBAP7720
      STOP                                                               EBAP7730
      END                                                                EBAP7740
```

LIST OF REFERENCES

1. Fuhs, A. E., Smithey, W., and Naber, M. E., "Axisymmetric Analysis of External Burning Assisted Projectile," 9th JANNAF Combustion Meeting, Vol.II (CPIA Pub. 231, Dec. 1972), pp. 384-416. Inc. many refs.

2. Tsien, H. S., and Beilock, M., "Heat Sources in a Uniform Flow," J. Aero. Sci., 16, p. 756, 1949.

3. Beilock, Milton, "Heat Sources in a Compressible Fluid." Master of Science Thesis, Massachusetts Institute of Technology, 1949.

4. Rues, D., "Concerning the Equivalence Between Heat, Force and Mass Sources," RAE Lib. Trans. No. 1119, July 1965.

5. Fuhs, A. E., "Quasi Area Rule for Heat Addition in Transonic and Supersonic Flight Regimes," Technical Report AFAPL-TR-72-10, Aug. 1972.

6. Strahle, W. C., "Combustion Effects on Base Pressure in Supersonic Flight and Application," IDA Research Paper P-389, Feb. 1968.

7. Strahle, W. C., "Theoretical Consideration of Combustion Effects on Base Pressure in Supersonic Flight," Twelfth Symposium on Combustion, Combustion Institute, Pittsburgh., pp. 1163-1173, 1969.

8. Crocco, L., and Lees, L., "A Mixing Theory for the Interaction Between Dissipative Flows and Nearly Isentropic Streams," J. Aero. Sci., 19, pp. 649-676, 1952.

9. Billig, F. S., "External Burning in Supersonic Streams," The Johns Hopkins University Applied Physics Laboratory, TG-912, May 1967.

10. Serafini, J. I., *et. al.*, "Exploratory Investigation of Static and Base Pressure Increases Resulting from Combustion of Aluminum Borohydride Adjacent to a Body of Revolution in a Supersonic Wind Tunnel," NACA RME57E15, Oct. 2, 1957.

11. Hosack, G. A., O'Learly, R. A., and Schnurstein, R. E., "External Burning Propulsion." 10th JANNAF Combustion Meeting, Vol. IV(CPIA Pub. 243, Dec. 1973) pp. 43-55.

12. Davis, D. D., "Extension of Simplified Mixing Theory to Axially Symmetric Supersonic Wake Flows and Application to Base Pressure Problem for a Body of Revolution," Princenton University, M.Sc. Thesis, 24-V-1952.

13. de Krasinski, J. S. A., "A Study of Axially Symmetrical Base Flow Behind Bodies of Revolution at Superonsic Speeds,"AGARD Conference Proceedings No. 4 on Separated Flows, Part 2, pp. 747-771, May 1966.

14. de Krasinski, J. E., "A Study of Axially Symmetrical Base Flow Behind Bodies of Revolution at Supersonic Speed," London Univeristy, Ph.D. Thesis, Nov. 1964.

15. Smithey, W., Naber, M., Caswell, G., and Fuhs, A. E., "External Burning Assisted Projectile; Theory and Experiment," AIAA/SAE 9th Propulsion Conference, AIAA Paper No. 73-1193, Nov. 1973.

16. Guderley, G., "On the Application of the Theory of Characteristics to Problems of Supersonic Flow," Ministry of Supply, Armament Research Establishment Translation No. 5/49. pp. 12-18.

17. Hosack, G. A., and O'Leary, R. A., "Base Burning Feasibility Investigation," North American Rockwell Rocketdyne, Technical Report No. RK - TR- 70-17, Dec. 1970, pp. 50-65.

18. Liepmann, H. W., and Roshko, A., "Elements of Gasdynamics," John Wiley & Sons, Inc., 1957, pp. 191-193, 284-296, 226-233.

19. Zierep, J., "Ahnlichkeitsgesetze für Profilströmungen mit Wärmezufuhr," Acta Mechanica, Vol. 1, 1965, pp. 60-70.

20. Ashley, H., and Landahl, M., "Aerodynamics of Wings and Bodies," Addison-Wesley, 1965, p. 154.

21. Ludloff, H. F., and Reiche, F., "Linearized Supersonic Flow Through Ducts," J. Appl Physics., Vol. 18, July 1947, pp. 681-682.

22. Mack, C. E. Jr., Ludloff, H. F., and Reiche, F., "Rigorous Solution of Linearized Flow Through Ducts," J.App. Physics, Vol. 18, July 1947, pp. 682-683.

23. Ludloff, H. F., and Reiche, F., "Linearized Treatment of Supersonic Flow Through Ducts," J. Aero.Sci., Vol. 16, Jan. 1949, pp. 5-21.

24. Schlichting, H., "Boundary Layer Theory," McGraw-Hill, Inc., Fourth Ed., 1960, Chapt. XII, also pp. 25, 38, 541, 545.

25. Darling, J. A., and Knott, J., "Effect of Spin on the Aerodynamics of the 20mm Projectile," NOLTR 71-180, Sept. 1971.

26. Lehnert, R., and Hastings, S. M., "Spin Effects on Base Pressure of Cone Cylinders at M=2.86," Naval Ordnance Laboratory, TR 2956, Oct. 1953.

27. Schmidt, L. E., and Murphy, C. H., "Effect of Spin on Aerodynamic Properties of Bodies and Revolution," USA Ballistic Research Laboratories, Memorandum Report No. 715, August 1953.

28. Smithey, W., Naber, M., Caswell, G., and Fuhs, A. E., "An Open Jet Wind Tunnel for External Burning with Spinning Projectiles," AIAA/SAE 9th Propulsion Conference, Nov. 1973, AIAA Paper No. 73-1225.

29. Smithey, W., Naber, M., Caswell, G., and Fuhs, A. E., "External Burning Assisted Projectile - A Progress Report," 10th JANNAF Combustion Meeting Proceedings, Vol. II (CPIA Pub. 243, Dec. 1973) pp. 193-205.

30. Kolpin, M. A., Horn, K. P., and Reicherbach, R. E., "Study of Penetration of a Liquid Injectant into a Supersonic Flow," AIAA Journal, Vol. VI, May 1968, pp. 853-858.

31. Shapiro, A. H., "The Dynamics and Thermodynamics of Compressible Flow," Two Volumes, Ronald Press, 1954, pp. 540, 790-791.

32 van Hise, Vernon, "Investigation of Variation in Base Pressure Over the Reynolds Number Range in Which Wake Transition Occurs for Nonlifting Bodies of Revolution at Mach Numbers from 1.62 to 2.62," NACA Technical Note 3942, January 1957.

33. van Hise, Vernon, "Investigation of Variation in Base Pressure Over the Reynolds Number Range in which Wake Transition Occurs for Two-Dimensional Bodies at Mach Numbers from 1.95 to 2.92," NASA Technical Note D-167, November 1959.

34. Murthy, S. N. B. and Osborn, J. R., "Base Flow Data with and without Injection: Bibliography and Semi-Rational Correlations," USA Ballistics Research Laboratories Contract Report No. 113, August 1973.

35. Chang, P. K., "Separation of Flow," Pergamon Press, Inc., 1970, pp. 543-549.

36. Korst, H. H., "Component Analysis and Synthesis for Fully Separated Flows with Special Consideration of Base Drag by Combustion," Workshop on Aerodynamics of Base Combustion, School of Mechanical Engineering, Purcue University, May 1974.

37. Probstein, R. F., "Inversion of the Prandtl-Meyer Relation for Specific - Heat Ratios of 5/3 and 5/4"; J. Aero Sci., Apr. 1957, pp. 316-317.

INITIAL DISTRIBUTION LIST

		No. Copies
1.	Defense Documentation Center Cameron Station Alexandria, Virginia 22314	2
2.	Library, Code 0212 Naval Postgraduate School Monterey, California 93940	2
3.	Professor A. E. Fuhs Department of Aeronautics Naval Postgraduate School Monterey, California 93940	10
4.	LTjg Gary J. Caswell, USN 399 Troy Aurora, Colorado 80010	1
5.	Dr. Warren Strahle Aerospace Engineering Georgia Institute of Technology Atlanta, Georgia 30332	1
6.	Mr. Dominic J. Monetta Gun Systems Engineering Naval Ordnance Station Indian Head, Maryland 20640	2
7.	Dr. Alan Roberts Gun Systems Engineering Naval Ordnance Station Indian Head, Maryland 20640	5
8.	Dr. Frederick Billig Applied Physics Laboratory Johns Hopkins University 8621 Georgia Avenue Silver Springs, Maryland 20910	1
9.	CDR William Smithey 207 Hillside St., N.W. Lenoir, N. C. 28645	5

10. Dr. James S. Holdhusen — 1
Vice President
FluiDyne Engineering Corporation
5900 Olsen Highway
Minneapolis, Minnesota 55422

11. Mr. Thomas Curran — 1
Chief of Ramjet Technology Branch
Air Force Aero Propulsion Laboratory
Wright Patterson Air Force Base, Ohio 45433

12. LT Noel P. Horn, USN — 1
SMC, Box 1183
Naval Postgraduate School
Monterey, California 93940

13. Dr. Richard Weiss — 1
Air Force Rocket Propulsion Laboratory
Edwards Air Force Base, California

14. Professor John Clarke — 1
Cranfield Institute of Technology
Bedford, ENGLAND

15. Dr. E. G. Broadbent — 1
Royal Aeronautical Establishment
Farnborough, ENGLAND

16. Chairman, Department of Aeronautics — 1
Naval Postgraduate School
Monterey, California 93940

17. Dr. Ing. G. Winterfeld — 1
D F V L R
Institut f. Luftstrahlantriebe
505 Porz-Wahn, Linder Höhe
GERMANY

18. LT M. Naber — 1
RT. 1, Box 1048
Sequim, Washington 98382

19. Dr. Andrew Mark (AMXBR-EB) — 1
Ballistic Research Lab.
Aberdeen Proving Grounds, Maryland 21005

20. LT L. Michael Freeman — 1
ARL/LH
Wright Patterson Air Force Base, Ohio 45433

21. Professor G. W. Zumwalt — 1
6311 Marjorie Lane
Wichita, Kansas 67208

22. Miss Theresa Elmendorf (SARFA-MDS-B) 1
Frankford Arsenal
Bridge & Tacony Streets
Philadelphia, Pennsylvania 19137

23. Dr. Raymond Sedney 1
EBL, Bldg. 120
Ballistic Research Laboratory
Aberdeen Proving Grounds, Maryland 21005

24. Dr. H. H. Tang, A3-253 1
McDonnell Douglas Corp.
5301 Bolsa Avenue
Huntington Beach, California 92647

25. Professor J. A. Schetz 1
Virginia Polytechnic Institute & State University
Blacksburg, Virginia 24061

26. Professor H. Doyle Thompson 1
School of Mechanical Engineering
Purdue University
W. Lafayette, Indiana 47907

27. Mr. Henry Hudgins 1
Bldg. 350
Picatinny Arsenal
Dover, New Jersey 07801

28. Professor H. H. Korst 1
210 MEL
University of Illinois
Urbana, Illinois 61820

29. Dr. J. R. Ward 1
Ballistic Research Laboratory, Bldg. 390
Aberdeen Proving Ground, Maryland 21005

30. Mr. Dan Jones III 1
Code GPA
NWL Dahlgren, Virginia

31. LCDR H. W. Burden 1
Code 57Zt
Naval Postgraduate School
Monterey, California 93940

32 Dr. D. W. Netzer 1
Department of Aeronautics
Naval Postgraduate School
Monterey, California 93940

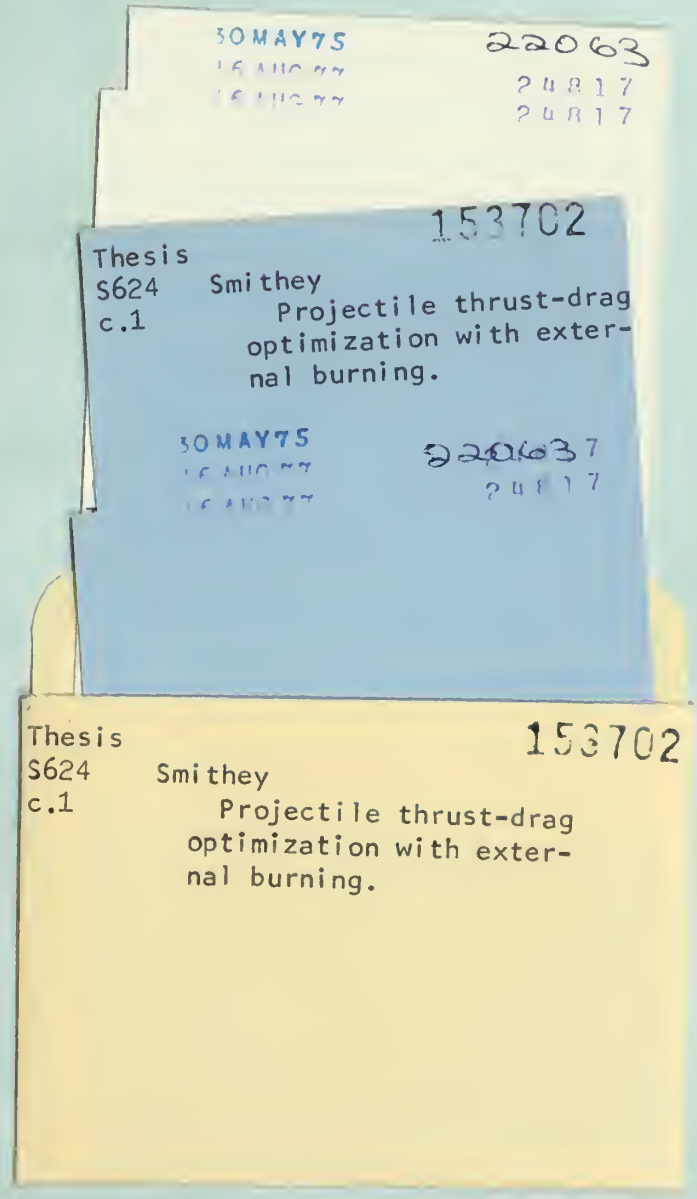
30MAY75
22063
153702
Thesis
S624
c.1
Smithey
Projectile thrust-drag optimization with external burning.
30MAY75
220637
153702
Thesis
S624
c.1
Smithey
Projectile thrust-drag optimization with external burning.

thesS624
Projectile thrust-drag optimization with
3 2768 002 00804 7
DUDLEY KNOX LIBRARY